

# **Modeling and Analysis of Pavement-Vehicle Interaction Dynamics for Pavement Distress Prediction**

**Gamaledine A. M. Elnashar**

**A Thesis  
In the Department  
of  
Mechanical, Industrial and Aerospace Engineering**

**Presented in Partial Fulfilment of the Requirements  
For the Degree of  
Doctor of Philosophy (Mechanical Engineering) at  
Concordia University  
Montreal, Quebec, Canada**

**September 2017**

**© Gamaledine A. M. Elnashar, 2017**

**CONCORDIA UNIVERSITY**  
**SCHOOL OF GRADUATE STUDIES**

This is to certify that the thesis prepared

By: Gamaledidine A. M. Elnashar

Entitled: Modeling and Analysis of Pavement-Vehicle Interaction Dynamics for Pavement Distress Prediction

and submitted in partial fulfillment of the requirements for the degree of

**Doctor of Philosophy in Mechanical Engineering**

complies with the regulations of the University and meets the accepted standards with respect to originality and quality.

Signed by the final examining committee:

_____	Chair
Dr. Thomas Fevens	
_____	External Examiner
Dr. Dan S. Neculescu	
_____	External to Program
Dr. Ashotosh Bagchi	
_____	Examiner
Dr. A. K. Waizuddin Ahmed	
_____	Examiner
Dr. Ion Stiharu	
_____	Thesis Co-supervisor
Dr. Rama B. Bhat	
_____	Thesis Co-supervisor
Dr. Ramin Sedaghati	

Approved by

\_\_\_\_\_  
Dr. Ali Dolabadi, Graduate Program Director

September 22, 2017  
Date of Defence

\_\_\_\_\_  
Dr. Amir Asif, Dean, Faculty of Engineering and Computer Science

# **ABSTRACT**

## **Modeling and Analysis of Pavement-Vehicle Interaction Dynamics for Pavement Distress Prediction**

**Gamaledine A. M. Elnashar, Ph. D.**

**Concordia University, 2017**

Increased road traffic combined with heavy vehicle loads lead to deterioration and distress of pavements and consequently reduces the life span of the paved roads. As a result, large amounts of financial and labor resources are spent every year to improve and maintain road infrastructures around the world. Traditionally, vehicle and pavement dynamics are treated as two separate areas of research. However, they are strongly coupled together through their contact points. Thus, one of the major concerns is to develop a more reliable dynamic pavement-vehicle interaction model to investigate and evaluate accurately both vehicle and pavement responses, and also to examine the pavement distress due to the severity of traffic loads. One of the most important distress modes in pavements is fatigue cracking. Despite the fact that there have been considerable efforts in recent years in fatigue performance evaluation and the design of flexible pavements, there is still a need for further studies in predicting fatigue cracking in terms of damage distribution considering the uncertainty and variability associated with the input parameters of pavement-vehicle interaction and traffic load repetitions.

The main objective of this research study is to carry out an in-depth investigation of the dynamics of the pavement-vehicle interaction and the effect of coupling action on system response, as well as fatigue study of the pavement due to repeated traffic loads. The response of

the pavement-vehicle coupled system supported by a linear visco-elastic foundation has been investigated. The vehicle is modeled as a two-degree-of-freedom quarter-vehicle model, and the pavement-foundation system is described by a simply supported Euler-Bernoulli beam resting on Pasternak foundation, while the tire is coupled to the flexible pavement with a single point contact. Galerkin method has been utilized to develop the governing differential equations of motion. Direct numerical integration approach based on implicit Newmark linear average acceleration technique has been used to solve the governing differential equations in order to evaluate the response of the coupled system. Results have been validated with previous research work and also compared with those of conventional uncoupled system. The effects of different parameters such as vehicle speed, road roughness, soil stiffness and suspension damping on the responses are then investigated. For the fatigue study of flexible pavements, a methodology, for modeling pavement damage and predicting fatigue cracking of flexible pavements is presented. The methodology is based on the combination of deterministic method and stochastic approach using Palmgren-Miner's hypothesis in which Poisson process is employed to characterize the actual repetitions of traffic load. Different models are then presented to estimate the fatigue life of the pavement surface layer. The results are compared and discussed.

## **AKNOWLEDGEMENT**

I would like to express my most sincere gratitude to my supervisors, Professor Rama Bhat and Professor Ramin Sedaghati, for their continuous guidance and generous support, their attention to details, encouragement and valuable suggestions during the course of my Ph.D study. It has been an honor and pleasure to have the opportunity to work with them. I have thoroughly enjoyed working with them and I have learned a lot. I hope that one day I would become as good a supervisor to my students as they have been to me.

I thank all the members of the Department of Mechanical Engineering at Concordia University who helped me in various ways towards the completion of my work, and I want to thank my colleagues and friends for their friendly and continuous support during my study.

I am deeply indebted to my first teacher “my dear mother”, my sisters and entire family members for their unlimited support and strength. My special thanks to my son Rayan and my daughter Rodayna for their endless patience and love, and especially acknowledges the endless support, comprehension, encouragement and sacrifices of my wife Heba Soliman.

Last, but not the least, I praise GOD the Almighty for helping me, supporting me and giving me the strength during the research work.

# TABLE OF CONTENTS

<b>LIST OF FIGURES</b> .....	<b>ix</b>
<b>LIST OF TABLES</b> .....	<b>xiii</b>
<b>LIST OF ABBREVIATIONS</b> .....	<b>xiv</b>
<b>NOMENCLATURE</b> .....	<b>xv</b>
<b>CHAPTER 1 Introduction</b> .....	<b>1</b>
1.1. Introduction.....	1
1.2. Literature Review and Research Background.....	3
<i>1.2.1. Pavement-Vehicle System Dynamics</i> .....	4
<i>1.2.2. Damage Model and Pavement Distress</i> .....	9
1.3. Thesis Objectives and Scope.....	18
1.4. Thesis Structure.....	20
<b>CHAPTER 2 System Modeling and Governing Equations of Motion</b> .....	<b>22</b>
2.1. Introduction.....	22
2.2. Vehicle Model.....	24
2.3. Pavement-Foundation Model.....	28
2.4. Pavement-Vehicle Coupled Model.....	35
2.5. Summary.....	39

<b>CHAPTER 3 Pavement-Vehicle Response under Harmonic Excitation.....</b>	<b>40</b>
3.1. Introduction.....	40
3.2. Linear-Time-Invariant System.....	41
3.3. Direct Time Integration Tequniques Newmark-Beta Formulation.....	51
3.3.1. <i>Model Validation</i> .....	53
3.3.2. <i>Effect of Vehicle Speed on Coupled System Response</i> .....	55
3.3.3. <i>Effect of suspension damping on Coupled system Response</i> .....	58
3.3.4. <i>Pavement Deflection at Different Load Positions</i> .....	61
3.4. Response Comparison of Coupled System with Conventional Uncoupled System.....	67
3.4.1. <i>Effect of Coupling Action on Vehicle-Body Displacement</i> .....	67
3.4.2. <i>Effect of Coupling Action on Vehicle-Wheel Displacement</i> .....	73
3.4.3. <i>Effect of Coupling Action on Dynamic Interaction Force</i> .....	79
3.4.4. <i>Effect of Coupling Action on Pavement Displacement</i> .....	85
3.5. Summary.....	92
<b>CHAPTER 4 Pavement Response due to Random Excitation.....</b>	<b>94</b>
4.1. Introduction.....	94
4.2. Classification of Road Profiles.....	94
4.3. Generation of Road Profiles.....	96
4.4. Effect of Road Roughness on Pavement Response.....	97
4.5. Effect of Vehicle Speed on Pavement Response.....	101
4.6. Effect of Vehicle types on Pavement Response.....	103
4.7. Summary.....	107

<b>CHAPTER 5 Damage Model and Pavement Distress</b> .....	<b>108</b>
5.1. Introduction.....	108
5.2. Pavement Damage and Predicting Fatigue Cracking Formulations .....	109
5.3. Pavement Damage Distribution Models.....	112
5.3.1. <i>Damage Model 1</i> .....	112
5.3.2. <i>Damage Model 2</i> .....	115
5.3.3. <i>Damage Model 3</i> .....	117
5.3.4. <i>Damage Model 4</i> .....	118
5.4. Numerical Results and Discussion.....	119
5.5. Summary.....	122
<b>CHAPTER 6 Conclusions, Contributions, and Recommendations for Future Work</b>	<b>123</b>
6.1. Dissertation Summary and Conclusions.....	123
6.2. Contributions.....	126
6.3. Recommendations for Future Work.....	127
<b>BIBLIOGRAPHY</b> .....	<b>129</b>
<b>APPENDIX I</b> The Non-dimensional Form of The Dynamic Interaction Force.....	<b>140</b>
<b>APPENDIX II</b> CDF of A Random Variable of Normal/Lognormal Distribution.....	<b>141</b>
<b>APPENDIX III</b> CDF and PDF of A Ratio of Two Random Variables.....	<b>143</b>

## LIST OF FIGURES

Figure 1.1 The research scheme .....	3
Figure 2.1 Schematic of two-DOF quarter-vehicle ride model.....	22
Figure 2.2 Schematic of two-DOF pitch plane ride model.....	23
Figure 2.3 Schematic four-DOF pitch plane ride model.....	23
Figure 2.4 Schematic of seven-DOF ride model.....	24
Figure 2.5 Two-DOF quarter vehicle model.....	26
Figure 2.6 Transverse deflection of beam on elastic foundation.....	28
Figure 2.7 Pavement-foundation model.....	30
Figure 2.8 Schematic of Pavement-Vehicle Coupled Model.....	35
Figure 3.1 Vehicle-body displacement against excitation frequency at $k = 40.78 \times 10^4 \text{ N/m/m}$ .....	44
Figure 3.2 Vehicle-body displacement against excitation frequency at $k = 40.78 \times 10^5 \text{ N/m/m}$ .....	44
Figure 3.3 Vehicle-body displacement against excitation frequency at $k = 40.78 \times 10^6 \text{ N/m/m}$ .....	45
Figure 3.4 Vehicle-wheel displacement against excitation frequency at $k = 40.78 \times 10^4 \text{ N/m/m}$ .....	46
Figure 3.5 Vehicle-wheel displacement against excitation frequency at $k = 40.78 \times 10^5 \text{ N/m/m}$ .....	47
Figure 3.6 Vehicle-wheel displacement against excitation frequency at $k = 40.78 \times 10^6 \text{ N/m/m}$ .....	47
Figure 3.7 Dynamic interaction force against excitation frequency at $k = 40.78 \times 10^4 \text{ N/m/m}$ .....	49
Figure 3.8 Dynamic interaction force against excitation frequency at $k = 40.78 \times 10^5 \text{ N/m/m}$ .....	49
Figure 3.9 Dynamic interaction force against excitation frequency at $k = 40.78 \times 10^6 \text{ N/m/m}$ .....	50
Figure 3.10 Comparison of beam deflection of the present model with Senalp et al.....	54
Figure 3.11 Vehicle-body displacement versus vehicle speed at different soil stiffness.....	55
Figure 3.12 Vehicle-wheel displacement versus vehicle speed at different soil stiffness.....	56
Figure 3.13 Dynamic interaction load versus vehicle speed at different soil stiffness.....	56

Figure 3.14 Pavement displacement versus vehicle speed at different soil stiffness.....	57
Figure 3.15 Vehicle-body response for different suspension damping.....	59
Figure 3.16 Vehicle-wheel response for different suspension damping.....	59
Figure 3.17 Force response for different suspension damping.....	60
Figure 3.18 Pavement mid-span response for different suspension damping.....	60
Figure 3.19 Beam discretized to 8 elements with 9 nodal locations.....	61
Figure 3.20 Pavement deflection at different nodal points.....	66
Figure 3.21 Vehicle-body response with $Y_R = 0.002$ m and $k = 40.78 \times 10^4$ N/m/m.....	68
Figure 3.22 Vehicle-body response with $Y_R = 0.002$ m and $k = 40.78 \times 10^5$ N/m/m.....	68
Figure 3.23 Vehicle-body response with $Y_R = 0.002$ m and $k = 40.78 \times 10^6$ N/m/m.....	69
Figure 3.24 Vehicle-body response with $Y_R = 0.025$ m and $k = 40.78 \times 10^4$ N/m/m.....	70
Figure 3.25 Vehicle-body response with $Y_R = 0.025$ m and $k = 40.78 \times 10^5$ N/m/m.....	70
Figure 3.26 Vehicle-body response with $Y_R = 0.025$ m and $k = 40.78 \times 10^6$ N/m/m.....	71
Figure 3.27 Vehicle-body response with $Y_R = 0.054$ m and $k = 40.78 \times 10^4$ N/m/m.....	72
Figure 3.28 Vehicle-body response with $Y_R = 0.054$ m and $k = 40.78 \times 10^5$ N/m/m.....	72
Figure 3.29 Vehicle-body response with $Y_R = 0.054$ m and $k = 40.78 \times 10^6$ N/m/m.....	73
Figure 3.30 Vehicle-wheel response with $Y_R = 0.002$ m and $k = 40.78 \times 10^4$ N/m/m.....	74
Figure 3.31 Vehicle-wheel response with $Y_R = 0.002$ m and $k = 40.78 \times 10^5$ N/m/m.....	74
Figure 3.32 Vehicle-wheel response with $Y_R = 0.002$ m and $k = 40.78 \times 10^6$ N/m/m.....	75
Figure 3.33 Vehicle-wheel response with $Y_R = 0.025$ m and $k = 40.78 \times 10^4$ N/m/m.....	76
Figure 3.34 Vehicle-wheel response with $Y_R = 0.025$ m and $k = 40.78 \times 10^5$ N/m/m.....	76
Figure 3.35 Vehicle-wheel response with $Y_R = 0.025$ m and $k = 40.78 \times 10^6$ N/m/m.....	77
Figure 3.36 Vehicle-wheel response with $Y_R = 0.054$ m and $k = 40.78 \times 10^4$ N/m/m.....	78
Figure 3.37 Vehicle-wheel response with $Y_R = 0.054$ m and $k = 40.78 \times 10^5$ N/m/m.....	78
Figure 3.38 Vehicle-wheel response with $Y_R = 0.054$ m and $k = 40.78 \times 10^6$ N/m/m.....	79

Figure 3.39 Dynamic response of interaction load $Y_R = 0.002$ m and $k = 40.78 \times 10^4$ N/m <sup>2</sup> .....	80
Figure 3.40 Dynamic response of interaction load $Y_R = 0.002$ m and $k = 40.78 \times 10^5$ N/m <sup>2</sup> .....	80
Figure 3.41 Dynamic response of interaction load $Y_R = 0.002$ m and $k = 40.78 \times 10^6$ N/m <sup>2</sup> .....	81
Figure 3.42 Dynamic response of interaction load $Y_R = 0.025$ m and $k = 40.78 \times 10^4$ N/m <sup>2</sup> .....	82
Figure 3.43 Dynamic response of interaction load $Y_R = 0.025$ m and $k = 40.78 \times 10^5$ N/m <sup>2</sup> .....	82
Figure 3.44 Dynamic response of interaction load $Y_R = 0.025$ m and $k = 40.78 \times 10^6$ N/m <sup>2</sup> .....	83
Figure 3.45 Dynamic response of interaction load $Y_R = 0.054$ m and $k = 40.78 \times 10^4$ N/m <sup>2</sup> .....	84
Figure 3.46 Dynamic response of interaction load $Y_R = 0.054$ m and $k = 40.78 \times 10^5$ N/m <sup>2</sup> .....	84
Figure 3.47 Dynamic response of interaction load $Y_R = 0.054$ m and $k = 40.78 \times 10^6$ N/m <sup>2</sup> .....	85
Figure 3.48 Pavement response with $Y_R = 0.002$ m and $k = 40.78 \times 10^4$ N/m/m .....	86
Figure 3.49 Pavement response with $Y_R = 0.002$ m and $k = 40.78 \times 10^5$ N/m/m .....	86
Figure 3.50 Pavement response with $Y_R = 0.002$ m and $k = 40.78 \times 10^6$ N/m/m .....	87
Figure 3.51 Pavement response with $Y_R = 0.025$ m and $k = 40.78 \times 10^4$ N/m/m .....	88
Figure 3.52 Pavement response with $Y_R = 0.025$ m and $k = 40.78 \times 10^5$ N/m/m .....	88
Figure 3.53 Pavement response with $Y_R = 0.025$ m and $k = 40.78 \times 10^6$ N/m/m .....	89
Figure 3.54 Pavement response with $Y_R = 0.054$ m and $k = 40.78 \times 10^4$ N/m/m .....	89
Figure 3.55 Pavement response with $Y_R = 0.054$ m and $k = 40.78 \times 10^5$ N/m/m .....	90
Figure 3.56 Pavement response with $Y_R = 0.054$ m and $k = 40.78 \times 10^6$ N/m/m .....	90
Figure 4.1 Random generated road profile for ISO Class A, C and E .....	97
Figure 4.2 Pavement response due to a car at 16 m/s with different ISO road profiles .....	99
Figure 4.3 Pavement response due to a bus at 16 m/s with different ISO road profiles .....	99
Figure 4.4 Pavement response due to a truck at 16 m/s with different ISO road profiles .....	100
Figure 4.5 Pavement response due to a car with different speeds for ISO Road profile class .....	101
Figure 4.6 Pavement response due to a bus with different speeds for ISO Road profile class .....	102

Figure 4.7 Pavement response due to a truck with different speeds for ISO Road profile class..	102
Figure 4.8 Pavement response due to different vehicles at 10m/s for ISO road profile class C..	104
Figure 4.9 Pavement response due to different vehicles at 15m/s for ISO road profile class C..	104
Figure 4.10 Pavement response due to different vehicles at 20m/s for ISO road profile class C	105
Figure 4.11 Pavement response due to different vehicles at 25m/s for ISO road profile class C	105
Figure 4.12 Pavement response due to different vehicles at 30m/s for ISO road profile class C	106
Figure 5.1 PDFs of pavement damage for different models.....	119
Figure 5.2 CDFs of pavement damage for different models.....	120
Figure 5.3 Fatigue cracking versus time for different models.....	121
Figure III.1 The areas corresponding to the Eq. (III.2).....	143
Figure III.2 The areas corresponding to the Eq. (III.3).....	144

## LIST OF TABLES

Table 3.1 Maximum non-dimensional values for sprung mass displacement.....	45
Table 3.2 Maximum non-dimensional values for unsprung mass displacement.....	48
Table 3.3 Maximum non-dimensional values for interaction force.....	50
Table 3.4 Numerical values of truck parameters.....	52
Table 3.5 Numerical values of pavement and foundation parameters.....	52
Table 3.6 Pavement parameters [82].....	53
Table 3.7 Midpoint deflection obtained by two methods.....	54
Table 3.8 Peak responses of coupled system due to vehicle speed for different soil stiffness.....	58
Table 3.9 Maximum response values of coupled system for different suspension damping.....	61
Table 3.10 Pavement deflection values at different node locations.....	66
Table 3.11 Variation in maximum vehicle-body displacement, $V=16\text{m/s}$ .....	91
Table 3.12 Variation in maximum vehicle-wheel displacement, $V=16\text{m/s}$ .....	91
Table 3.13 Variation in maximum interaction force, $V=16\text{m/s}$ .....	91
Table 3.14 Variation in maximum Pavement deflection at mid-span, $V=16\text{m/s}$ .....	92
Table 4.1 Road surface roughness profiles according to ISO 8608.....	95
Table 4.2 Numerical values of vehicle parameters.....	98
Table 4.3 Maximum pavement response with different vehicles and different road profiles.....	100
Table 4.4 Pavement response with different vehicles at different speeds for ISO road class C.....	103
Table 4.5 Peak response with different vehicles for ISO road profile class C.....	106
Table 5.1 Calculated fatigue cracking (FC) for different models.....	121

## LIST OF ABBREVIATIONS

---

<b>Symbol</b>	<b>Description</b>
AASHTO	American Association of State Highway and Transportation Officials
AFC	Alligator Fatigue Cracking
AI	Asphalt Institute
CDF	Cumulative Distribution Function
Cvpd	commercial vehicle per day
DOF	Degree Of Freedom
ESAL	Equivalent Single Axle Load
FC	Fatigue Cracking
FEM	Finite Element Method
ISO	International Organization for Standardization
LFC	Longitudinal Fatigue Cracking
LTI	Linear Time Invariant
LTTP	Long Term Pavement Performance
M-E	Mechanistic-Empirical
NCHRP	National Cooperative Highway Research Program
PDF	Probability Density Functions
PDG	Pavement Design Guide
PMF	Probability Mass Function
Pois	Poisson
PSD	Power Spectral Density
PVI	Pavement-Vehicle Interaction
SPC	Single Point Contact
WLPPM	Whole-Life Pavement Performance Model

---

## NOMENCLATURE

Symbol	Description
$A$	Average annual commercial vehicle per day
$A_i$	Magnitudes of the harmonics excitation
$B$	Sampling interval
$C$	Laboratory to field adjustment factor (correction factor)
$c$	Soil damping coefficient per unit length of the beam
$C_s$	Vehicle suspension damping coefficient
$C_t$	Tire damping coefficient
$D$	Damage index of fatigue cracking
$E$	Young's modulus of elasticity of pavement layer
$F$	Total force exerted on the pavement surface
$F_{c_{n+1}}$	Updated load
$F_{t_{max}}$	Maximum dynamic interaction force
$F_D(d)$	Cumulative distribution function of the fatigue damage
$F_L$	Conversion factor of different vehicular loads into a common axle load
$F_c$	Excitation force vector of the PVI system
$F_f(x, t)$	Force induced by the foundation per unit length of the beam
$F_p$	Load vector applied on the pavement
$F_t$	Dynamic pavement-vehicle interaction force
$F_v$	Load vector induced by the road profile
$f_D(d)$	Probability density function of the fatigue damage
$f_{X,Y}(x, y)$	Joint probability function of $X$ and $Y$
$f_X(x)$	Probability density functions of $X$
$f_Y(y)$	Probability density functions of $Y$
$g$	Gravitational acceleration

$H(j\omega)$	Complex system transfer Function (Receptance Matrix)
$h$	Pavement thickness
$I$	Second moment of area of the beam cross section
$I_n$	Identity matrix of size $n \times n$
$K_s$	Vehicle suspension stiffness coefficient
$K_T$	Thickness correction factor
$K_t$	Tire stiffness coefficient
$k_1, k_2, k_3, k_4$	Laboratory material coefficients
$k_p$	Pasternak foundation parameter
$K$	Soil stiffness coefficient per unit length of the beam
$L$	Pavement span length
$L_f$	lateral distribution factor
$M_c, C_c, K_c$	Mass, damping and stiffness matrices of the PVI system
$M_{c_{n+1}}, C_{c_{n+1}}, K_{c_{n+1}}$	Updated mass, damping and damping matrices
$M_p, C_p, K_p$	Mass, damping and stiffness matrices of the pavement-foundation
$M_v, C_v, K_v$	Mass, damping and stiffness matrices of the vehicle system
$M(x)$	Bending moment
$m$	Mass per unit length of the beam
$m_s$	Vehicle-body mass (Sprung mass)
$m_u$	Vehicle-wheel mass (Unsprung mass)
$N$	Number of sample points in one meter of pavement length
$N_t$	Total number of sample points in pavement length
$n$	Spatial frequency/wave number
$n_0$	Referenced spatial frequency
$P$	Concentrated load acting on the pavement
$p(x)$	Foundation reactions per unit length of the beam
$q(x)$	Loadings per unit length of the beam
$R(x)$	Residual function

$r_t$	Annual traffic growth rate
$u, \dot{u}, \ddot{u}$	Displacement, velocity, acceleration vectors of the pavement-foundation
$u_i(t)$	Time dependent coefficients
$S_g(n)$	PSD of the roughness profile of road surface
$S_g(n_0)$	Degree of road roughness
$T$	Total number of periods
$t$	Time
$V$	Vehicle speed
$V_a$	Air void content
$V_b$	Volumetric asphalt content
$V(x)$	Shear force
$W$	Dead weight of the vehicle
$W_j(x)$	Weighting function
$X$	Equivalent number of actual traffic load repetitions
$X_i$	Actual traffic for period $i$
$x$	$x$ -direction
$x_t$	load position
$Y$	number of load repetitions to cause failure/crack initiation
$Y_R$	Amplitude of road profile
$Y_i$	Traffic repetitions of a given load to cause failure at period $i$
$y$	$y$ -direction
$y_t$	Design period
$y_c, \dot{y}_c, \ddot{y}_c$	Displacement, velocity and acceleration of pavement contact point
$y_{c_n}, \dot{y}_{c_n}, \ddot{y}_{c_n}$	Old displacement, velocity and acceleration
$y_{c_{n+1}}, \dot{y}_{c_{n+1}}, \ddot{y}_{c_{n+1}}$	Updated displacement, velocity and acceleration
$y_p(x, t)$	Transverse deflection of the beam at any point
$y_p(x_t, t)$	Transverse deflection of the beam at pavement vehicle contact point
$y_{p_{max}}$	Maximum pavement displacement

$y_R, \dot{y}_R, \ddot{y}_R$	Displacement, velocity and acceleration of road profile/road elevation
$y_s, \dot{y}_s, \ddot{y}_s$	Displacement, velocity and acceleration of sprung mass
$y_{s_{max}}$	Maximum vehicle-body displacement
$y_u, \dot{y}_u, \ddot{y}_u$	Displacement, velocity and acceleration of unsprung mass
$y_{u_{max}}$	Maximum vehicle-wheel displacement
$y_v, \dot{y}_v, \ddot{y}_v$	Displacement, velocity and acceleration vectors of the vehicle system
$\bar{Y}_c$	Complex displacement vector
$\Delta n$	Spatial frequency increase step
$\Delta t$	Time step
$\beta, \gamma$	Newmark Beta parameters
$\beta_1, \beta_2, \beta_3$	Field calibration coefficients
$\varepsilon_t$	Magnitude of horizontal tensile strain at the bottom of the asphalt layer
$\zeta_n$	Damping ratio of $n$ -th pavement mode
$\delta$	Dirac-delta function
$\lambda$	Pavement wavelength
$\lambda_X$	Expected number of occurrences
$\mu_D$	Mean value of $D$
$\mu_{\ln D}$	Mean value of $\ln D$
$\mu_{\ln Y}$	Mean value of $\ln Y$
$\mu_x$	Mean value of $X$
$\mu_Y$	Mean value of $Y$
$P$	Pavement density
$\sigma_D$	Standard deviation of $D$
$\sigma_{\ln D}$	Standard deviation of $\ln D$
$\sigma_{\ln Y}$	Standard deviation of $\ln Y$
$\sigma_Y$	Standard deviation of $Y$
$\sigma_D^2 = \text{Var}(D)$	Variance of $D$
$\sigma_{\ln D}^2$	Variance of $\ln D$

$\sigma_{\ln Y}^2$	Variance of $\ln Y$
$\sigma_X^2 = \text{Var}(X)$	Variance of $X$
$\sigma_Y^2 = \text{Var}(Y)$	Variance of $Y$
$\Phi$	Cumulative distribution function of the standard normal distribution
$\Phi_i(x)$	Trial/basis functions
$\varphi_i$	Phases for random road profile
$\omega$	Excitation frequency
$\omega_n$	Natural frequency of $n$ -th pavement mode

---

# CHAPTER 1

## Introduction

### 1.1 Introduction

The increase in road traffic and vehicle loads lead to deterioration of the pavement and reduce the lifetime of the paved roads [1]. Furthermore, traffic with road surface roughness can lead to vibrations that cause environmental nuisance, reduced ride comfort to passengers, malfunctioning of sensitive equipment, and damage to nearby buildings and road substructures such as pavement and sub-grade [2]. As a result, governments around the world spend large amounts of money each year in improving and maintaining their road infrastructure [3]. Traditionally, vehicle dynamics and pavement dynamics are treated as two separate areas of research. However, they are strongly coupled together through their contact points. In vehicle dynamics, the dynamical behavior, ride comfort, stability, safety and the parameters of vehicles are investigated, while the pavement surface unevenness is generally considered as excitation to vehicles. In pavement dynamics, pavement damage and response are examined, while the vehicle is generally considered as moving load/mass acting on the pavement [4]. One of the major concerns is the ability to evaluate the dynamic interaction between a moving vehicle and a rough road and predict effectively the pavement distress in the form of fatigue cracking due to the repetition of traffic loads. Therefore, there is an urgency to study and understand the relationship between pavements and their interaction with moving vehicles, and create a more reliable dynamic pavement-vehicle interaction (PVI) model to investigate and evaluate accurately both

vehicle and pavement responses, and provide a pavement damage model and fatigue cracking prediction due to repeated traffic loads.

The present dissertation focuses on the dynamic analysis of pavement-vehicle coupled system and the effect of coupling action on system responses, as well as on the fatigue study of the pavement due to repeated traffic loads. For the pavement-vehicle interaction model, the system response due to the moving vehicular load on rough road supported by a linear visco-elastic foundation has been investigated. The vehicle is modeled as a two-degree-of-freedom quarter-vehicle model, and the pavement-foundation system is described by a simply supported Euler-Bernoulli beam resting on Pasternak foundation, while the tire is coupled to the flexible pavement with a single point contact. Galerkin method has been applied to the pavement-foundation system to discretize the problem and to obtain a set of ordinary differential equations in the time domain. Direct integration Newmark-Beta approach based on linear average acceleration method has been used to determine the response of the vibrating system numerically. A computer program in the Matlab environment is developed to acquire the response. Results are then validated with previous research work and also compared with those of conventional uncoupled system. Moreover, the effects of parameters such as vehicle speed, road roughness, soil stiffness and suspension damping on the system responses are investigated. For the fatigue study of flexible pavements, a methodology for modeling pavement damage and predicting fatigue cracking based on a combination of deterministic method and stochastic approach using Palmgren-Miner's hypothesis, has been formulated based on Poisson process to characterize the actual load of traffic repetitions. Four damage models are presented to estimate the fatigue life of the pavement surface layer.

## 1.2 Literature Review and Research Background

Over the past few decades, vehicle and pavement dynamics were investigated in which vehicle dynamics and pavement dynamics were studied separately. Previous research mainly focused either on the influence of uneven pavements on moving vehicles or the influence of vehicle loads on the pavement surface. In the mid-nineties, pavement-vehicle-interaction (PVI) received some attention in which the coupling action and the impact of the pavement-vehicle interaction on each of the vehicle dynamics (to improve ride quality) and the pavement dynamics (to investigate pavement damage) were studied. Thus in this section the literature review has been systematically categorized into two main parts: 1- PVI system dynamics including vehicle dynamics, road dynamics and road roughness, and 2- pavement distress and damage model. This has been schematically shown in Figure 1.1.

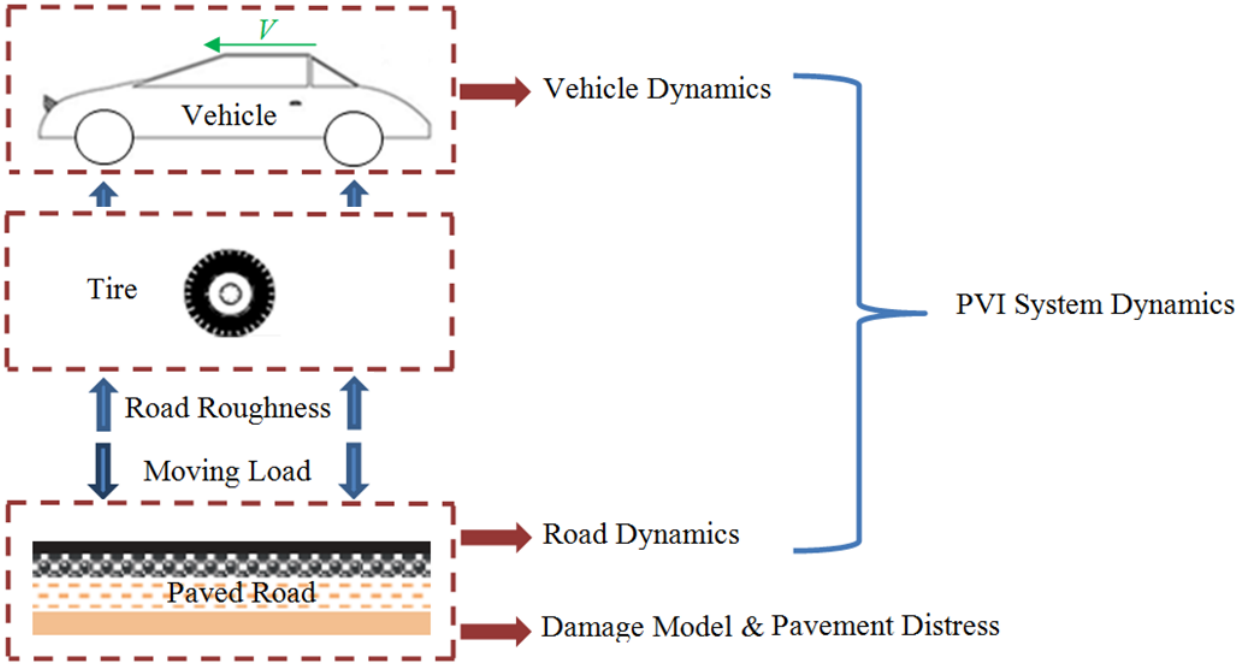


Figure 1.1 Research scheme

### ***1.2.1 Pavement-Vehicle System Dynamics***

In vehicle dynamics, the dynamical behavior of vehicles for different parameters is investigated, while the pavement surface unevenness is generally considered as excitation to vehicles [4]. Yi and Hedrick [5] evaluated dynamic response of heavy trucks with both active and semi-active suspensions by using a non-linear time domain simulation model in order to reduce pavement damage resulting from the moving vehicular loads. Potter et al. [6] assessed the road damage caused by individual axles and whole heavy vehicles. Sun [7] put forward an optimum concept to design road-friendly vehicles based on pavement loads and vehicle suspensions. The results indicated that high air pressure tires with small suspension damping lead to large tire loads. Salama et al. [8] investigated the effects of different truck configurations on flexible pavements. The results showed that rutting damage is caused more by trucks with tridem or more axles, while fatigue cracking is produced more by trucks with single and tandem axles. On the other hand, the results did not indicate sufficient evidence about pavement roughness. Sun and Luo [9] developed numerical method and computer simulation model in order to investigate the effects of acceleration and deceleration on dynamic response of pavements based on state space models by using a quarter-car and a half-car models. They concluded that this study can be applied in dynamic response of pavement structures. Sun et al. [10] applied a genetic algorithm to optimize the design parameters of the suspension systems based on a quarter-car model. Ihsan et al. [11] analysed different control strategies of semi-active system using 2-DOF quarter-car model, and compared the results with that of the passive system. Bogsjö and Rychlik [12] proposed a statistical and analytical study of vehicle damage caused by a high degree of road roughness. Patel et al. [13] developed an algorithm with a half-car model in order to measure road profiles accurately using Matlab software. Cao et al. [14] provided a critical overview of recent

developments of vehicle suspension design, dynamics, and control, and proposed some potential future research directions. Suzuki and Takahashi [15] proposed a new semi-active suspension control method to reduce the vehicle vibration and vehicle lateral motion due to the road input. However, the majority of these studies on vehicle dynamics ignored the flexible nature of pavement, and considered that the pavement is rigid and static.

In the pavement dynamics, the pavement is modeled as a beam, plate, and multi-layer system placed on elastic and visco-elastic foundation, while the vehicle is generally considered as moving load/mass acting on the pavement. Collop and Cebon [16] developed a new whole-life pavement performance model (WLPPM), which has the ability to predict the pavement damage numerically due to realistic traffic environmental loading. This model consists of a linear quarter-car model moving on a layered elastic pavement resting on a semi-infinite sub-grade. Kim and Roesset [17] investigated the dynamic response of an infinite plate on an elastic foundation generated by moving loads based on Fourier transform method. Lin and Weng [18] presented a new closed-form solution to evaluate the peak vehicle load on a rough road surface of rigid pavement subjected to moving vehicular loads. Huang and Thambiratnam [19] presented a numerical analysis to investigate the dynamic response of rectangular plates resting on an elastic Winkler foundation caused by single, multiple, and harmonic moving concentrated loads. Kim and McCullough [20] analysed the dynamic displacement and stress responses of a plate on viscous Winkler foundation under moving tandem-axle loads of varying amplitude, and justified the mathematical form of solution by using Fourier transform method. Kargarnovin and Younesian [21] studied the dynamic response of a Timoshenko beam resting on Pasternak-type visco-elastic foundation under harmonic moving load based on Fourier transformation in conjunction with the residue and convolution integral theorems. Sun [22] investigated the

dynamic displacement of a plate generated by a moving harmonic line and point load. The steady-state response of a uniform elastically supported beam subjected to a concentrated load moving with a constant speed based on Fourier transform has been investigated by Mallik et al. [23]. Kettil et al. [24] presented modeling and simulation of inelastic deformation in road structures leading to rutting due to cyclic mechanical and thermal loads. It is noted that in the majority of the previous research, the pavement dynamics has been investigated considering the tire force as a moving load/mass in which the effect of vehicle vibration on pavement dynamical behaviour has been ignored.

Recent studies have concluded that it is necessary to propose a more realistic and reliable dynamic PVI model to investigate the vehicle and pavement responses simultaneously and accurately. Papagiannakis and Gujarathi [25] were pioneers in incorporating the coupling between vehicle and pavement in their research. They analyzed the dynamic response of heavy vehicles moving along a rough pavement by using a quarter-car model. The results showed that the sprung mass vertical acceleration is very sensitive to a pavement roughness excitation frequency of 3.5 Hz. Wu and Shen [26] analyzed the effects of pavement-vehicle-foundation interaction on the dynamic response of concrete pavements subjected to moving loads based on three-dimensional finite element method in conjunction with Newmark integration scheme. The parametric study showed that the increase in dynamic response of pavements is associated with the decrease in pavement thickness and the increase in the softness of the soil. Mamlouk [27] provided a general overview of pavement and vehicle dynamics and their interaction, and advanced the concept of pavement-vehicle interaction to weigh-in-motion, pavement design and performance, and vehicle regulation. Sun and Deng [28] studied the motion of dynamic loads caused by pavement-vehicle interaction using quarter-truck vehicle model, and presented a series

of statistical characteristics of wheel loads in frequency domain and time domain. Rutka and Sapragnas [29] studied the effect of vehicle tire smoothing function for the investigation of car and road interaction. Lombaert and Degrande [30] presented an experimental validation of a numerical model for the prediction of the vibrations produced by road traffic in the free field. Nassif and Liu [31] built a three-dimensional dynamic model for the bridge-road-vehicle interaction system, and solved the mathematical governing equations by using numerical algorithm based on the Newmark Beta integration method. The results showed that the dynamic load factor (bridge dynamic response) is highly dependent on road roughness, vehicle suspension and bridge geometry. Papagiannakis et al. [32] proposed an experimental study to interpret the interaction between truck dynamic axle loads and pavement roughness profile based on a wavelet approach. Sawant [33] improved an algorithm solution based on the finite-element method to analyse rigid pavements under moving vehicular or aircraft loads. He found that pavement thickness, soil modulus and velocity of aircraft had a significant effect on the pavement response. Shi and Cai [34] built a three-dimensional pavement-vehicle interaction model to simulate the pavement dynamics induced by PVI effects. Xia [35] provided a finite element dynamic model for tire-pavement interaction to predict pavement response and pavement damage due to fatigue cracking and rutting. Yang et al. [4] presented the importance of investigating the dynamics of vehicle and pavement simultaneously based on the vehicle-pavement-foundation coupled system. Sawant et al. [1] presented the effect of soil parameters and coupling action on the pavement response subjected to moving load, and brought out the range of critical velocity. Taheri et al. [36] proposed an empirical pavement damage model incorporating vehicle dynamics in order to predict pavement vibrations induced by dynamic axle loads. Wang et al. [37] developed a two-dimensional axle-tire-pavement interaction finite-

element model to investigate the effects of a rutted surface on near-surface pavement responses. Cao et al. [38] presented analytical, numerical and experimental studies based on a three-dimensional direct vehicle-pavement coupling dynamic model to analyze the dynamic response of asphalt pavement using finite element software package ABAQUS. Patil et al. [39] analyzed the dynamic response of concrete pavements subjected to moving loads considering dynamic pavement-vehicle interaction effects using an improved solution algorithm based on two-dimensional finite element method. Lu et al. [2] developed a new model to predict the pavement vibration due to the dynamic vehicle-road interaction. Patil et al. [40] also analyzed the dynamic response of concrete pavements subjected to moving loads considering dynamic pavement-vehicle interaction effects using an improved solution algorithm based on three-dimensional finite element method. Liu and You [41] presented a fundamental study on pavement-wheel interaction forces through discrete element simulation. Ding et al. [42] built a new model to predict vibration of pavement-vehicle coupled system based on a Timoshenko beam resting on a nonlinear foundation.

Road roughness has been of special interest for many researchers. Rouillard et al. [43] proposed a methodology to classify road profile data for the study of shock and vibrations related to the road transportation process. Waechter et al. [44] presented a new stochastic approach, and achieved a characterization of the complexity of the surface roughness. Fujikawa et al. [45] defined the essential road roughness parameters that control the tire vibration noise. González et al. [46] used the vehicle acceleration measurements to estimate road roughness. Ngwangwa et al. [47] used vehicle responses based on neural networks simulation in order to reconstruct road defects and road roughness classification. Bogsjö et al. [48] studied the accuracy and efficiency of three new road profile models namely homogenous Laplace moving average process, non-homogenous

Laplace process and hybrid model that combines Gaussian and Laplace modeling. Agostinacchio et al. [49] generated a random road surface profile based on ISO 8608 standard to determine the dynamic load induced due to the passage of vehicles. Liu et al. [50] proposed a new method considering Power Spectral Density (PSD) and coherence function to construct road roughness in left and right wheel paths.

### ***1.2.2 Damage Model and Pavement Distress***

Pavement distress or failure is defined as any signs of break or fracture in pavement layer, or any indication of poor or undesirable pavement performance [51]. Guo and Prozzi [52] investigated fatigue life of flexible pavements due to repeated loading. There are many types of pavement distress such as fatigue cracking, rutting, potholes, patches, raveling, bleeding, etc [53]. The previous research revealed that fatigue cracking, caused by repeated and excessive traffic loading, is the most common distress observed in flexible pavements [54, 55].

Fatigue cracking first appears as a set of micro-cracks in the wheel paths, and progresses into a network of interconnecting cracks, and eventually leading to potholes [53]. Fatigue cracking, in flexible pavements, consists of two phases: crack initiation and crack propagation which is caused by tensile strains generated in the pavement due to traffic loading and temperature variations [56]. Crack initiation can be measured using different experiments, while there is no reliable test yet to measure crack propagation [56]. Further, there are different severity levels to further define the fatigue cracking. According to the pavement distress survey manual [53] low severity fatigue cracking consists of some connecting cracks, and the cracks are not spalled or sealed with no signs of pumping. Moderate severity is reached when the cracks become interconnected, and the cracks may be slightly spalled and may be sealed, and pumping is not

evident. A high severity fatigue cracking occurs when pieces may move when subjected to traffic, cracks may be sealed, and pumping is evident. Fatigue cracking can be classified into two main groups: alligator or bottom up fatigue cracking and longitudinal or top down fatigue cracking, and both may look identical on the pavement surface [56]. Alligator fatigue cracking initiates at the bottom of asphalt layer due to mechanical failure caused by the highest tensile stress and strain then propagates randomly upwards to the surface of pavement [57]. Thin pavement layers are most likely to exhibit bottom up fatigue cracking problems, which makes it a problem often aggravated by the cold weather [58]. Longitudinal cracking, conceptually similar to alligator cracking, develops at the surface where high localized tensile stress and strain resulting from tire-pavement interaction exist and propagates downwards to the bottom of asphalt layer. Thick pavement layers are most likely exposed to top bottom fatigue cracking [59].

Reliable models for prediction of pavement performance or damage are one of the major challenges facing researchers and design engineers. In the sixties and seventies several studies of pavement response due to fatigue were carried out based on many laboratory fatigue tests on asphalt (flexible) pavement. As a result, the fatigue life of asphalt pavement was based on a relationship between material coefficients and stress or strain levels induced by repeatedly applied loading [52]. Extensive research has been conducted to model and predict fatigue cracking in the last few years. Based on the prediction results of performance models, these models may be classified as either deterministic or probabilistic. Deterministic models can be divided into mechanistic, empirical and mechanistic-empirical (M-E) models [60, 61]. Mechanistic models are based on the theories of mechanics, in which stresses and strains of pavement layer can be obtained using simple assumptions and simplifications, such as isotropic, linear-elastic and homogeneous material, small strain and static loading. While these models are

simple and can provide the general response behavior of the pavement, they are not practically effective to describe pavement deterioration due to high nonlinearity in the behavior of pavement materials which are anisotropic and depend on time, temperature and other parameters [62]. Empirical models are based on the results of experiments and statistical techniques. They are employed to overcome the limitations of simplified theoretical models used in the mechanistic approach. The empirical models link the pavement distress with the traffic loadings and pavement deflection and provide the number of load repetitions to cause pavement failure [63]. One of the major disadvantages of the empirical models is that they cannot be directly applied for different pavement sections. In other words, they can be used only to a particular section area. M-E models combine mechanistic and empirical approaches into one general model to take advantage of the merits of each model and also to overcome some of the shortcomings when the models are applied individually [63]. In M-E models, the strains generated at the critical locations due to single wheel load of the vehicle are, first, identified, and then the empirical fatigue model can be used to determine the pavement life. Probabilistic models, which predict distribution of events and occurrences, are represented by transition probability process models (e.g., Markov process) and reliability analysis to estimate deterioration with age for different combination of variables [60, 61 and 63].

One of the first empirical models was reported in 1929 [62]. In the fifties, pavement performance received some attention from several researchers utilizing empirical models. Since then, several empirical models were developed to link pavement performance data to design input parameters. The most common empirical model used worldwide is American Association of State Highway and Transportation Officials (AASHTO) which has been improved many times over the years to meet different conditions and for different pavements [62].

In 1953, Kerkhoven and Dormon [62] proposed the first M-E model. They used a failure method to minimize pavement deterioration based on the vertical compressive strain on the bottom of the asphalt layers. Saal and Pell [62], in 1960, suggested another failure criterion to reduce fatigue cracking based on the horizontal tensile strain at the bottom of asphalt layers. The first design concept of pavement appeared in 1965 by Dormon and Metcalf [62]. Fatigue life has been expressed based on the relationship between the number of load repetitions to failure and the tensile strains and material properties obtained from laboratory and experimental design through the following equation [65, 66]:

$$Y = k_1 \left( \frac{1}{\varepsilon_t} \right)^{k_2} \quad (1.1)$$

where:

$Y$  = number of load repetitions to crack initiation (number of cycles to failure)

$\varepsilon_t$  = magnitude of horizontal tensile strain at the bottom of the asphalt layer

$k_1, k_2$  = laboratory material coefficients

Further studies related the fatigue life with structural response (tensile strain at the bottom of the asphalt layer  $\varepsilon_t$ ), material characteristic coefficients  $k_1, k_2, k_3$  and material property  $E$  as given by [55, 56]:

$$Y = k_1 \left( \frac{1}{\varepsilon_t} \right)^{k_2} \left( \frac{1}{E} \right)^{k_3} \quad (1.2)$$

where

$E$  = stiffness modulus of asphalt mixture

$k_3$  = laboratory material coefficient

Later, Pell and Cooper [52] studied the effects of the air void  $V_a$  content and the volumetric asphalt content  $V_b$  on the fatigue performance of asphalt mixture and added new terms to Eq. (1.2) as:

$$Y = k_1 \left( \frac{1}{\varepsilon_t} \right)^{k_2} \left( \frac{1}{E} \right)^{k_3} \left( \frac{V_b}{V_b + V_a} \right)^{k_4} \quad (1.3)$$

where

$V_a$  = air void content

$V_b$  = volumetric asphalt content

$k_4$  = laboratory material coefficient

It has been reported that minimizing the air voids and maximizing the amount of asphalt was beneficial to fatigue life [65]. Further developments were also conducted by Asphalt Institute institution in 1981 and Shell International Petroleum in 1982 to incorporate strain-based criteria in their M-E methods. Several studies over the past three decades have advanced M-E techniques. Most of the work, however, was based on Shell and the Asphalt Institute methods. The Asphalt Institute (AI 1982) incorporated a correction term  $C$  to express the number of load applications to failure as follows [52, 55, 66, and 67]:

$$Y = 18.4 C \left[ 0.00432 \left( \frac{1}{\varepsilon_t} \right)^{3.291} \left( \frac{1}{E} \right)^{0.854} \right] \quad (1.4)$$

where  $C$  represents the laboratory to field adjustment factor (correction factor) defined as:

$$C = 10^M \quad (1.5)$$

where

$$M = 4.84 \left( \frac{V_b}{V_b + V_a} - 0.69 \right) \quad (1.6)$$

In the nineties a large laboratory effort was conducted to predict pavement damage model by researchers at the University of California, Minnesota department of transportation, Illinois department of transportation, etc. As a result, different models were developed in which the effects of other factors on fatigue life have been considered. In 1990, the National Cooperative Highway Research Program (NCHRP) 1-26 project report integrated most of the studies proposed by previous research work and augmented some environmental parameters, such as asphalt layer temperature, and used Miner's criterion to determine damage model and predict fatigue cracking. Uzan et al. [68] in the Federal Highway Administration report of the Texas Flexible Pavement System, proposed a modified equation considering the cracking propagation phase as:

$$\text{Log}(Y) = -3.13 + \frac{h}{380} - 3.291 \log(\epsilon_t) - 0.854 \log(E) \quad (1.7)$$

where  $h$  represents the thickness of the asphalt layer (mm).

In 2007, Schwartz et al. [62] published a design guide for the NCHRP 1-37A project including most of the M-E method to predict pavement distresses due to traffic load incorporating the environmental conditions. Moreover, the NCHRP 1-37A project replaced the Equivalent Single Axle Load (ESAL) by distribution of vehicular loads. The M-E PDG model used to predict fatigue cracking using the Asphalt Institute method in 1991 was calibrated using 82 LTPP (Long Term Pavement Performance) section data in 24 states across the USA. First, the pavement damage is determined and then the damage is converted into cracked area. Several revised M-E

fatigue models have been suggested by other researchers such as El-Basyouny and Witezack, in 2005 [64]. The number of repetitions to cause failure for a given load magnitude can be expressed as follows [62]:

$$Y = k_T \left[ \beta_1 k_1 C \left( \frac{1}{\varepsilon_t} \right)^{\beta_2 k_2} \left( \frac{1}{E} \right)^{\beta_3 k_3} \right] \quad (1.8)$$

in which  $k_T$  represents the thickness correction factor, and given by:

$$k_T = \frac{1}{0.000398 + \frac{0.003602}{1 + e^{(11.02 - 3.49 h)}}} \quad (1.9)$$

where

$\beta_1, \beta_2, \beta_3$  = field calibration coefficients ( $\beta_1 = \beta_2 = \beta_3 = 1$ )

$k_1, k_2, k_3$  = laboratory material coefficient ( $k_1 = 0.00432, k_2 = 3.9492$  and  $k_3 = 1.281$ ).

Based on Miner's law the damage due to a given load magnitude can be expressed as follows:

$$D = \sum_{i=1}^T \frac{X_i}{Y_i} \quad (1.10)$$

where

$D$  = Damage index (overall cumulated damage up to  $T$  in pavement).

$T$  = total number of periods.

$X_i$  = actual traffic for period  $i$ .

$Y_i$  = traffic repetitions of a given load to cause failure at period  $i$ .

To convert damage into cracked area, the following expressions are used:

**a) For alligator fatigue cracking (bottom-up fatigue cracking)**

$$AFC = \left( \frac{6000}{1 + e^{[C_1 + C_2 \log(100 D)]}} \right) \left( \frac{1}{60} \right) \quad (1.11)$$

where

$AFC$  = alligator fatigue cracking (% of lane area)

$$C_1 = -2C_2$$

$$C_2 = -2.40874 - 39.748(1 + h)^{-2.856}$$

**b) For longitudinal fatigue cracking (top-down fatigue cracking)**

$$LFC = 10.56 \left( \frac{1000}{1 + e^{[7 - 3.5 \log(100D)]}} \right) \quad (1.12)$$

where  $LFC$  represents the longitudinal fatigue cracking

While deterministic models have received appropriate attention in improving methods to determine pavement failure, they may not be accurate enough to predict the pavement distress due to the uncertainty and variability of some pavement parameters. Thus, many probabilistic models have been proposed to cover the stochastic nature of the pavement performance. Golabi et al. [69] in 1982 developed a pavement management system to capture the dynamic and probabilistic aspects of pavement maintenance using the Markov Chain method. Madanat et al. [70] in 1995 used a structured econometric approach using a joint discrete-continuous model to predict pavement cracking initiation and progression. Further studies have been suggested by several researchers to investigate the pavement deterioration based on Markov chain processes such as that of Li et al. [71] who in 1996 developed a Markov probabilistic method to determine

pavement deterioration rates in which the transition probability matrices are determined based on a reliability analysis using Monte Carlo simulation technique. An improved Markov Chain model based on the probability distributions using time-based models was proposed by Mishalani and Madanat [72] in 2002. In 2010, Retherford et al. [73] discussed the advantages and disadvantages of reliability methods used in M-E approach for the pavement design.

Other efforts are made for the pavement performance prediction considering the uncertainties and random factors in the pavement deterioration process using techniques such as neural networks, fuzzy logic and hybrid systems [74]. However, these attempts are still in the research and development stage. Despite the various efforts in improving the pavement performance prediction effectively based on either deterministic or probabilistic methods, these attempts suffer from the restrictions associated with the difficulty of considering accurately the dynamic and stochastic nature of pavement distress modes.

### **1.3 Thesis Objectives and Scope**

In the previous sections, various methods to model, analyze and improve vehicle dynamics, pavement dynamics and pavement distress predictions were systematically reviewed. Most studies unanimously agree that the analysis considering the coupling action between vehicles and pavements will give more accurate results in investigating the vibrations of vehicle moving along paved roads in comparison with the conventional uncoupled system analysis. Moreover, researchers recommend that providing highly accurate results in pavement distress prediction necessitates more studies in order to examine the pavement damage caused by traffic loads. While significant effort has been applied to investigate the dynamics of the vehicle-pavement interaction and its effect on the pavement distress, there is still a significant research gap to fully understand the effect of coupling and also predicting the fatigue life of the pavement duly considering combined deterministic and probabilistic approaches. Therefore, more detailed studies are required in some aspects that are not fully covered, such as investigations on the pavement deterioration due to traffic loads and to formulate a damage model considering the stochastic nature associated with traffic arrival times and pavement performance, and effects of coupling action on system response due to the variations in some parameters. Considering the above, the overall objective of this research is twofold: 1- To develop a model for the moving vehicular load on a flexible pavement considering the coupling action, and also to develop an efficient numerical approach to study the dynamic response of vehicle road interaction and to evaluate the effect of coupling action under different system configurations, 2- To develop a methodology to predict traffic arrival rates and fatigue cracking due to traffic loads by combining deterministic and probabilistic approaches.

The specific objectives of this research study have been specified below:

- I. The passage of vehicular loads on rough roads depends on spatial and temporal variables which makes the analysis very complicated. In order to separate these variables, utilize Galerkin method to discretize the problem and to obtain a set of ordinary differential equations in the time domain.
- II. The governing differential equations of the proposed pavement-vehicle coupled model form a time varying system that has no closed form solution. Therefore, use a numerical approach based on direct integration Newmark-Beta method to solve the problem and validate the method comparing the results with previous research work in the literature.
- III. Examine the effects of variation in suspension damping, vehicle speed and soil stiffness as well as amplitude of harmonic road surface roughness on the coupling action and compare the results with those of conventional uncoupled systems.
- IV. Develop a more realistic analysis of pavement response due to different types of vehicles considering different random road surface profiles.
- V. Determine the pavement distress in the form of fatigue cracking and predict a damage model based on Poisson process to characterize the traffic load arrivals, using a deterministic-stochastic approach along with Miner's hypothesis.

## 1.4 Thesis Structure

The dissertation is organized into six chapters. Each chapter begins with an introduction that describes the aim of the work, followed by a detailed study and ends with a brief summary.

*Chapter 1* presents a systematic literature review on pertinent research works in the area, background and development history of moving vehicles on flexible pavements and the relationship between traffic loads and pavement distress.

*Chapter 2* covers the mathematical modeling of vehicle, pavement-foundation and pavement-vehicle coupled systems. Galerkin method is used to discretize the pavement-foundation system in order to obtain a set of ordinary differential equations in the time domain.

*Chapter 3* provides an investigation about the effects of coupling action on system response due to the variations in parameters such as road roughness amplitude, soil stiffness, vehicle speed and suspension damping, and the results are validated with previous research work and compared with conventional uncoupled system. The responses are obtained based on Newmark-Beta approach using linear average acceleration method considering sinusoidal road surface profile as internal excitation.

*Chapter 4* presents the influence of different random road surface roughness and vehicle speed on the pavement response due to the passage of different types of vehicles (car, bus and truck) considering the coupling action between the pavement and the vehicles. The road roughness profiles are generated based on ISO 8608 criterion considering three different ISO classes of road roughness.

*Chapter 5* gives a methodology for modeling pavement damage and predicting fatigue cracking of flexible pavements based on a combination of deterministic method and stochastic approach using Palmgren-Miner's hypothesis, and Poisson process to characterize the traffic load arrivals. Four pavement damage models are used for a case study to estimate the fatigue life of the pavement surface layer.

*Chapter 6* integrates the findings derived from the previous chapters and provides the main conclusions that can be drawn from the research and proposes a number of recommendations for future works.

# CHAPTER 2

## System Modeling and Governing Equations of Motion

### 2.1 Introduction

Dynamic models of any type of vehicles can be represented in many ways from a single degree-of-freedom (DOF) quarter vehicle model to more complicated multi-DOF three-dimensional models. The more popular models are two-DOF quarter vehicle, two-DOF pitch plane, four-DOF pitch plane (half car) and seven-DOF ride models (full car) [75]. Two-DOF quarter vehicle model, in which one-quarter of the sprung mass (vehicle-body mass) with only one set of suspension and wheels are considered, is used mainly to determine the bounce natural frequencies and dynamics of both sprung and unsprung masses as shown in Figure 2.1.

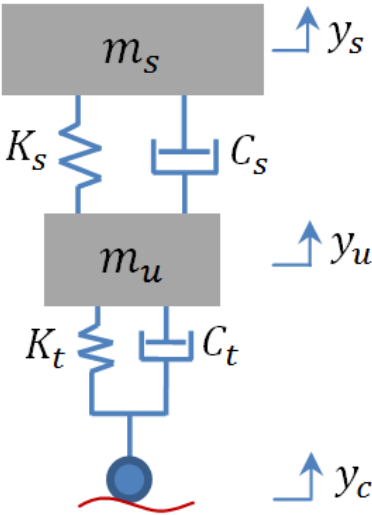


Figure 2.1 Schematic of two-DOF quarter-vehicle ride model

Two-DOF pitch plane ride model, in Figure 2.2, is used to study only the bounce and pitch motions of the sprung mass without taking into consideration the effects of the unsprung mass motions.

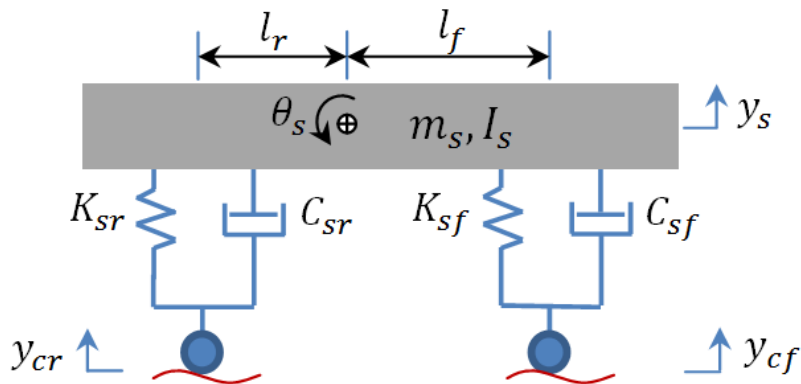


Figure 2.2 Schematic of two-DOF pitch plane ride model

Four-DOF pitch plane ride model, which is shown in Figure 2.3, can be effectively used to study the bounce and pitch motions of the sprung mass and the bounce motions of the unsprung mass.

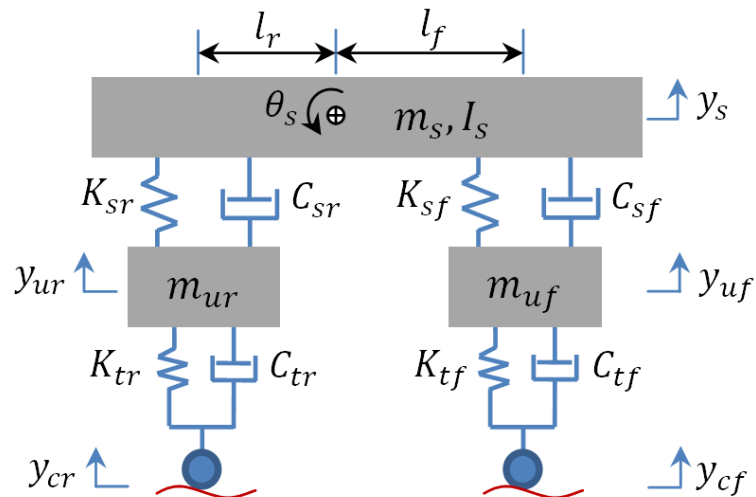


Figure 2.3 Schematic of four-DOF pitch plane ride model

If the roll motion is included, and assuming that the vehicle has a constant speed with no steering angle, and independent wheel suspensions, the full car model may be considered as the best representation to simulate the dynamics of the suspension system [76]. The full car model can be represented by seven-DOF, namely sprung mass bounce, pitch and roll motions, and the bounce motion of the four wheels as shown in Figure 2.4.

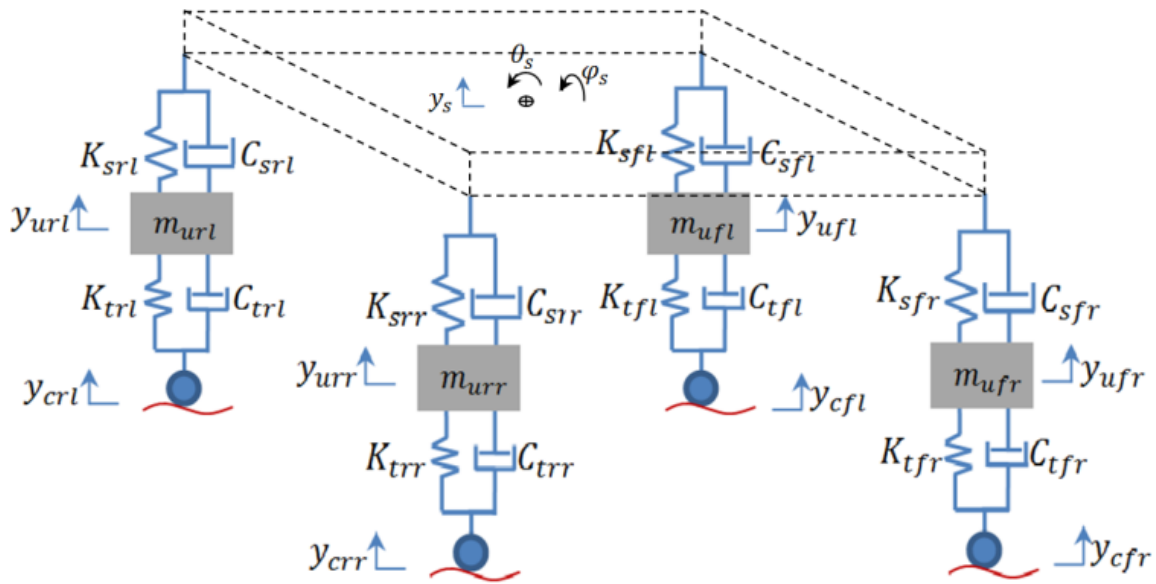


Figure 2.4 Schematic of seven-DOF ride model

## 2.2 Vehicle Model

Pavement vehicle interaction is generated via tire force, especially vertical force that can lead to fatigue cracking. So the vehicle model used to study pavement failure problems should at least reflect its vertical dynamics. Other properties, like horizontal motion and wheel slip, are neglected. Two-DOF quarter-vehicle model, subjected to road excitation, is widely used for vertical dynamic analysis of vehicle due to its simplicity and the qualitatively correct information it provides, at least in the preliminary studies. The half vehicle model adds pitch characteristics

compared to the quarter vehicle model, and the full vehicle model adds the roll motion compared to the half vehicle model. Moreover, linear model (fixed suspension damping and stiffness coefficients) is adopted in this study to avoid the complicated analysis due to the strong nonlinearities in cases where the damping or the stiffness coefficient is variable. In order to achieve the conflicting requirements and the fact that the vehicle has to operate over a wide range of running conditions, the vehicle is assumed to move with a constant velocity in a straight line (no turn or lane changing) and the choice of fixed stiffness and damping parameters must be a compromise. However, as the complexity increases, so do the computation time and the complexity to analyse the results. Furthermore, In view of the high inflation pressure used in the commercial vehicle tires, a point-contact model is considered appropriate for the analysis in this research. Therefore, in this research study a linear two-DOF quarter vehicle ride model (Figure 2.5) is adopted to characterize vehicle dynamics since this model is believed to provide sufficiently accurate results. Such a quarter vehicle ride model is based on the following assumptions: constant vehicle velocity, vehicle system vibrates only in the vertical direction, no vehicle body or axle roll and pitch, linear suspension and tire characteristics, single point contact tire model, and the tire is always in contact with the road surface.

The governing equations describing the vehicle motion are obtained using d'Alembert's principle. As shown in Figure 2.5, the sprung body mass of the vehicle,  $m_s$ , is supported by a passive suspension system, and has vertical displacement  $y_s(t)$ . The unsprung wheel mass,  $m_u$ , has vertical displacement  $y_u(t)$ , while the tire stiffness and damping are represented, respectively, by coefficients  $K_t$  and  $C_t$ . Two road surface roughness profiles are considered: (i) simple harmonic function of the form  $y_R(t) = Y_R \sin(\omega t)$ , where  $Y_R$  and  $\omega$  are, respectively,

amplitude and excitation frequency, in which  $\omega = \frac{2\pi V}{\lambda}$ , and  $\lambda$  is the pavement wavelength; (ii) random function described by a number of simple harmonic functions with different amplitudes.

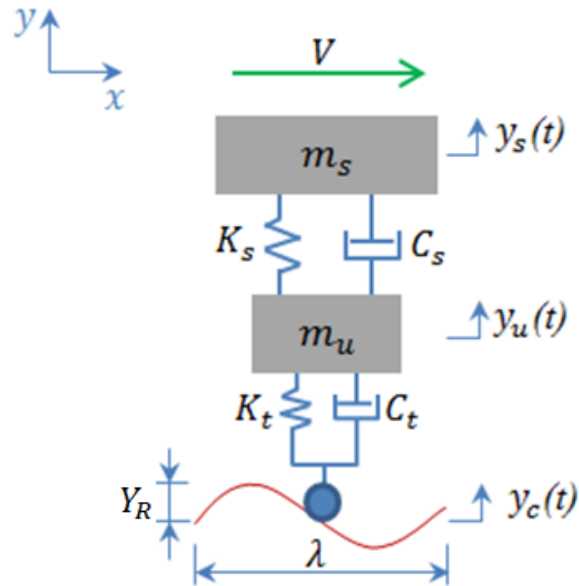


Figure 2.5 Two-DOF quarter vehicle model

In fact, tire dynamics refers to the relationship between forces (vertical and lateral), aligning torque, deformation and response of a tire subjected to different driving conditions. Tires are important components of vehicles because they are the only means to transfer forces between the vehicle and the road. There are several tire mechanical models the simplest and also widely used model is the single point contact (SPC) tire model, which has been adopted in this study. SPC model is described by parallel spring and damper that transfer vertical forces between the road and the vehicle. The spring stiffness coefficient  $K_t$  represents the tire elasticity and inflation pressure, while the damping coefficient  $C_t$  stands for the dissipation energy in the tire.

The system differential equations of motion of the vehicle in Figure 2.5 can be expressed as:

$$m_s \ddot{y}_s + C_s \dot{y}_s + K_s y_s - C_s \dot{y}_u - K_s y_u = 0 \quad (2.1)$$

$$m_u \ddot{y}_u + (C_s + C_t) \dot{y}_u + (K_s + K_t) y_u - C_s \dot{y}_s - K_s y_s = C_t \dot{y}_c + K_t y_c \quad (2.2)$$

let

$$F_t = C_t(\dot{y}_u - \dot{y}_c) + K_t(y_u - y_c) \quad (2.3)$$

where  $F_t$  represents the dynamic interaction force between the vehicle and the pavement. So Eq. (2.2) becomes:

$$m_u \ddot{y}_u + C_s \dot{y}_u + K_s y_u - C_s \dot{y}_s - K_s y_s = -F_t(t) \quad (2.4)$$

The system differential equations of motion of the vehicle in matrix form, using Eqs. (2.1) and (2.4), can be expressed as

$$M_v \ddot{y}_v + C_v \dot{y}_v + K_v y_v = F_v \quad (2.5)$$

where  $\{y_v\} = \{y_s, y_u\}^T$ ,  $\{\dot{y}_v\} = \{\dot{y}_s, \dot{y}_u\}^T$  and  $\{\ddot{y}_v\} = \{\ddot{y}_s, \ddot{y}_u\}^T$  are, respectively, displacement, velocity and acceleration vectors of the vehicle system including sprung and unsprung masses, and  $\{F_v\} = \{0, -F_t\}^T$  denotes the load vector induced by the road surface roughness profile,  $y_c$  and  $\dot{y}_c$  represent the displacement and velocity of the contact point, respectively.  $M_v$ ,  $C_v$  and  $K_v$  are the mass, damping and stiffness matrices of the vehicle, respectively, and are given as

$$M_v = \begin{bmatrix} m_s & 0 \\ 0 & m_u \end{bmatrix}; \quad C_v = \begin{bmatrix} C_s & -C_s \\ -C_s & C_s \end{bmatrix}; \quad K_v = \begin{bmatrix} K_s & -K_s \\ -K_s & K_s \end{bmatrix}$$

It should be remarked that in the conventional uncoupled system, in which vehicle dynamics considers the pavement as stationary and rigid (pavement vibration is not taken into account),  $y_c = y_R$  and  $\dot{y}_c = \dot{y}_R$ .

### 2.3 Pavement-Foundation Model

Pavement layer is one of the most important elements in the design of roads. It is generally a processed material which is placed on roads to provide a safe passage of vehicles and ride comfort to the passengers. Pavements are classified into two main categories namely: (i) Flexible pavements, and (ii) Rigid pavements. Flexible pavements consist of asphalt materials which deflect due to traffic loads, while rigid pavements are composed of cement concrete materials and are substantially stiffer than flexible pavements due to their high stiffness [77]. The remainder of this thesis will concentrate solely on flexible pavement.

The use of beams on elastic foundations is common in modeling flexible roads. Figure 2.6 shows the transverse deflection of beam on elastic foundation. Here,  $q(x)$  represents the loadings per unit length of the beam,  $V(x)$  and  $M(x)$  are shear and bending moments, respectively, while  $p(x)$  stands for the foundation reactions per unit length of the beam.

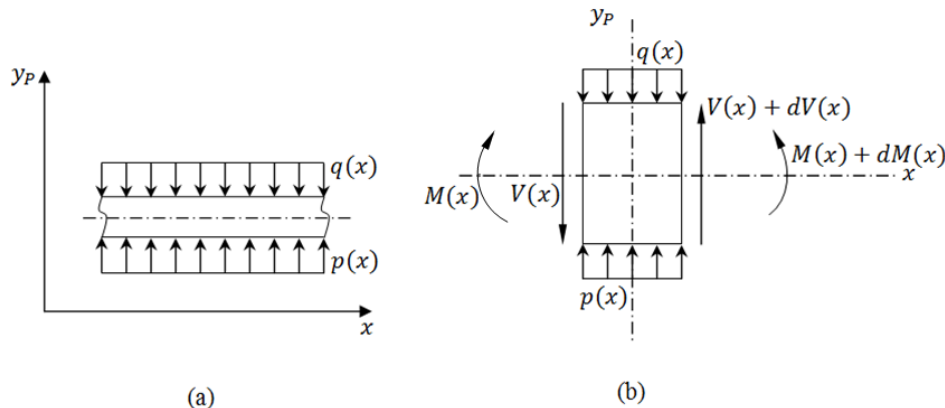


Figure 2.6 Transverse deflection of beam on elastic foundation (a) beam, and (b) Loads, moments and foundation reaction acting on a beam element

The foundation reaction  $p(x)$  can be defined depending on the foundation models as follows [78]:

**Winkler Foundation:** This foundation model considers only one parameter,  $k$ , which represents the proportionality constant between  $p(x)$  and the beam deflection  $y_p(x)$ . The Winkler foundation reaction can be expressed as:

$$p(x) = k y_p(x) \quad (2.6)$$

An improved Winkler foundation model has been proposed by some researchers assuming interactions between the springs and adding a second parameter to Eq. (2.6) such as Pasternak foundation, Filonenko-Borodich foundation, generalized foundation, and Vlasov foundation.

**Pasternak Foundation:** This is the most commonly used two-parameter foundation model. Pasternak assumes that the top ends of the springs are connected to an incompressible layer that resists only transverse shear deformation, and introduces shear interactions between the springs, that is:

$$p(x) = k y_p(x) - k_p \frac{\partial^2 y_p(x)}{\partial x^2} \quad (2.7)$$

in which  $k_p$  represents the Pasternak foundation parameter of the shear layer.

In this study, the pavement-foundation system is modeled as a simply supported Euler-Bernoulli beam resting on a linear visco-elastic foundation represented by Pasternak foundation model as shown in Figure 2.7 subjected to vertically moving concentrated load. It is assumed that the beam is initially straight, the beam and soil materials are linearly elastic with same moduli in tension and compression, and structural deformations are small.

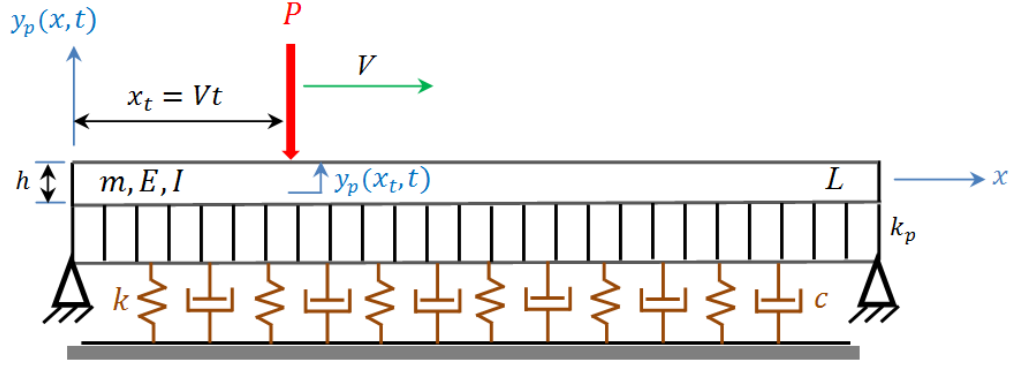


Figure 2.7 Pavement-foundation model

The governing differential equation for a finite beam resting on a linear visco-elastic two-parameter foundation (Pasternak foundation) in fixed Cartesian coordinates  $(x, y)$  at time  $t$  can be described as [79]:

$$EI \frac{\partial^4 y_p}{\partial x^4} - k_p \frac{\partial^2 y_p}{\partial x^2} + m \frac{\partial^2 y_p}{\partial t^2} = P - F_f \quad (2.8)$$

where  $y_p = y_p(x, t)$  is the transverse deflection of the beam at any point.  $EI$  is the flexural rigidity of the beam,  $E$  is the Young's modulus of elasticity of beam material and  $I$  is the second moment of area of the beam cross section about its neutral axis,  $m$  is the mass per unit length of the beam, and  $k_p$  is the shear layer parameter. The concentrated load  $P$  which moves with a constant velocity  $V$  along the  $x$  direction, can be expressed as

$$P = F \delta(x - x_t) \quad (2.9)$$

in which  $x_t$  represents the load position ( $0 \leq x_t \leq L$ ), here  $x_t = Vt$ ,  $L$  is the pavement span length,  $F$  is the total force exerted on the pavement surface, and  $\delta(x - x_t)$  is the Dirac-delta function used to deal with the moving concentrated load. Further,  $t$  represents the time and

$F_f = F_f(x, t)$  represents the force induced by the foundation per unit length of the beam.

Assuming a linear pressure response and damping,  $F_f$  can be expressed as [79]:

$$F_f = c \frac{\partial y_p}{\partial t} + k y_p \quad (2.10)$$

where  $k$  represents the soil stiffness coefficient, and  $c$  stands for the soil damping coefficient.

Substituting Eqs. (2.9) and (2.10) into Eq. (2.8) yields:

$$EI \frac{\partial^4 y_p}{\partial x^4} - k_p \frac{\partial^2 y_p}{\partial x^2} + m \frac{\partial^2 y_p}{\partial t^2} + c \frac{\partial y_p}{\partial t} + k y_p = F \delta(x - x_t) \quad (2.11)$$

The initial and boundary conditions of simply-supported beam can be described as:

$$y_p(x, t) \Big|_{t=0} = \frac{\partial y_p(x, t)}{\partial t} \Big|_{t=0} = 0 \quad (2.12)$$

$$y_p(x, t) \Big|_{x=0} = y_p(x, t) \Big|_{x=L} = \frac{\partial^2 y_p(x, t)}{\partial x^2} \Big|_{x=0} = \frac{\partial^2 y_p(x, t)}{\partial x^2} \Big|_{x=L} = 0 \quad (2.13)$$

In this research study, the Galerkin method is applied to Eq. (2.11) to discretize the problem and to obtain a set of ordinary differential equations in the time domain. Using Galerkin method, the approximate solution of the transverse deflection of a simply-supported Euler-Bernoulli beam of length  $L$  with a uniform cross-section, and resting on a linear visco-elastic foundation can be expressed as a linear combination of trial functions:

$$\tilde{y}_p(x, t) = \sum_{i=1}^n u_i(t) \Phi_i(x) \quad , \quad (i = 1, 2, \dots, n) \quad (2.14)$$

where  $u_i(t)$  is a set of time dependent coefficients to be found and  $\Phi_i(x)$  represent trial/basis functions which should satisfy all the boundary conditions and are assumed to be of the following form:

$$\Phi_i(x) = \sin\left(\frac{i\pi}{L}x\right) \quad (2.15)$$

Galerkin weighted residual method can be mathematically expressed as:

$$\int_0^L R(x)W_j(x) dx = 0 \quad (2.16)$$

where  $R(x)$  and  $W_j(x)$  are residual and weighting functions, respectively, and can be defined as:

$$R(x) = EI \frac{\partial^4 \tilde{y}_p}{\partial x^4} - k_p \frac{\partial^2 \tilde{y}_p}{\partial x^2} + m \frac{\partial^2 \tilde{y}_p}{\partial t^2} + c \frac{\partial \tilde{y}_p}{\partial t} + k \tilde{y}_p - F \delta(x - x_t) \quad (2.17)$$

$$W_j(x) = \Phi_j(x) = \sin\left(\frac{j\pi}{L}x\right) \quad , \quad (j = 1, 2, \dots, n) \quad (2.18)$$

Substituting Eq. (2.14) into Eq. (2.17), Eq. (2.17) and Eq. (2.18) into Eq. (2.16) and then using integration by parts with appropriate boundary conditions yields:

$$\int_0^L \left[ EI \frac{\partial^2 \Phi_j}{\partial x^2} \sum_{i=1}^n \frac{\partial^2 \Phi_i}{\partial x^2} u_i + k_p \frac{\partial \Phi_j}{\partial x} \sum_{i=1}^n \frac{\partial \Phi_i}{\partial x} u_i + m \Phi_j \sum_{i=1}^n \Phi_i \ddot{u}_i + c \Phi_j \sum_{i=1}^n \Phi_i \dot{u}_i + k \Phi_j \sum_{i=1}^n \Phi_i u_i - F \delta(x - x_t) \Phi_j \right] dx = 0 \quad (2.19)$$

Considering orthogonality of the chosen trial functions and by integrating equation (2.19) the following system of ordinary differential equations can be obtained:

$$\frac{mL}{2}\ddot{u}_i + \frac{cL}{2}\dot{u}_i + \left[ k + EI \left( \frac{i\pi}{L} \right)^4 + k_p \left( \frac{i\pi}{L} \right)^2 \right] \frac{L}{2} u_i = F \sin \frac{i\pi}{L} x_t \quad (2.20)$$

Multiplying both sides by  $\frac{2}{mL}$  yields:

$$\ddot{u}_i + 2\zeta_i\omega_i\dot{u}_i + \omega_i^2 u_i = F\varphi_i(x_t) \quad (2.21)$$

where

$$2\zeta_i\omega_i = \frac{c}{m} \quad (2.22)$$

$$\omega_i^2 = \left[ EI \left( \frac{i\pi}{L} \right)^4 + k_p \left( \frac{i\pi}{L} \right)^2 + k \right] \frac{1}{m} \quad (2.23)$$

$$\varphi_i(x_t) = \frac{2}{mL} \sin \frac{i\pi}{L} x_t \quad (2.24)$$

Considering  $n$ -th mode, the differential equation of motion of the pavement-foundation system in matrix form can be expressed as

$$M_p \ddot{u} + C_p \dot{u} + K_p u = F_p \quad (2.25)$$

where  $\{u\} = \{u_1, u_2, \dots, u_n\}^T$ ,  $\{\dot{u}\} = \{\dot{u}_1, \dot{u}_2, \dots, \dot{u}_n\}^T$  and  $\{\ddot{u}\} = \{\ddot{u}_1, \ddot{u}_2, \dots, \ddot{u}_n\}^T$  are, respectively, displacement, velocity and acceleration vectors of the pavement-foundation system, and  $\{F_p\} = \{F\varphi_1, F\varphi_2, \dots, F\varphi_n\}^T$  denotes the generalized load vector applied on the pavement. The matrices  $M_p$ ,  $C_p$  and  $K_p$  can be expressed as follows:

$$M_p = \begin{bmatrix} 1 & 0 & \dots & 0 \\ 0 & 1 & \dots & 0 \\ \vdots & \vdots & \ddots & \vdots \\ 0 & 0 & \dots & 1 \end{bmatrix}$$

$$C_p = \begin{bmatrix} 2\zeta_1\omega_1 & 0 & \dots & 0 \\ 0 & 2\zeta_2\omega_2 & \dots & 0 \\ \vdots & \vdots & \ddots & \vdots \\ 0 & 0 & \dots & 2\zeta_n\omega_n \end{bmatrix}$$

$$K_p = \begin{bmatrix} \omega_1^2 & 0 & \dots & 0 \\ 0 & \omega_2^2 & \dots & 0 \\ \vdots & \vdots & \ddots & \vdots \\ 0 & 0 & \dots & \omega_n^2 \end{bmatrix}$$

It should be noted that in conventional uncoupled system, in which pavement dynamics considers the vehicle as moving mass/load, the vehicle vibrations are not taken into account.

## 2.4 Pavement-Vehicle Coupled Model

The pavement-vehicle coupled system has both vehicle and pavement integrated together considering the road surface roughness as internal excitation as shown in Figure 2.8.

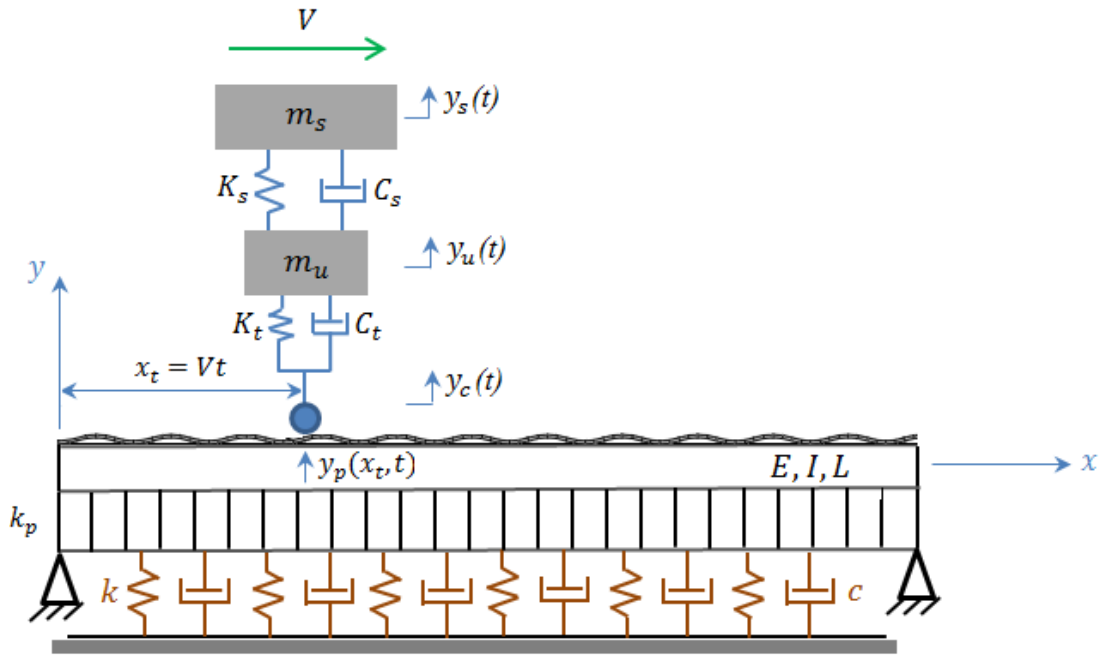


Figure 2.8 Schematic of Pavement-Vehicle Coupled Model

Considering the coupling action between the vehicle and the pavement, the displacement of the contact point between the tire and the pavement,  $y_c$ , depends not only on road surface roughness,  $y_R$ , but also on pavement deflection at contact point,  $\tilde{y}_p(x_t, t)$ . Therefore, the displacement and velocity of this contact point can be expressed as:

$$y_c = y_R + \tilde{y}_p(x_t, t) \quad (2.26)$$

$$\dot{y}_c = \dot{y}_R + \dot{\tilde{y}}_p(x_t, t) \quad (2.27)$$

where, as mentioned in Section 2.3:

$$\tilde{y}_p(x_t, t) = \sum_{i=1}^n u_i(t) \Phi_i(x_t) \quad (2.28)$$

$$\Phi_i(x_t) = \sin\left(\frac{i\pi}{L} x_t\right) \quad (2.29)$$

and

$$\dot{\tilde{y}}_p(x_t, t) = \sum_{i=1}^n \dot{u}_i(t) \Phi_i(x_t) + \sum_{i=1}^n u_i(t) \dot{\Phi}_i(x_t) \quad (2.30)$$

$$\dot{\Phi}_i(x_t) = \frac{i\pi V}{L} \cos\left(\frac{i\pi}{L} x_t\right) \quad (2.31)$$

Therefore, the dynamic interaction force  $F_t$  considering the coupling action becomes:

$$F_t = C_t[\dot{y}_u - \dot{y}_R - \dot{\tilde{y}}_p(x_t, t)] + K_t[y_u - y_R - \tilde{y}_p(x_t, t)] \quad (2.32)$$

Substituting Eq. (2.28) and Eq. (2.30) into Eq. (2.32), yields

$$\begin{aligned} F_t = & C_t(\dot{y}_u - \dot{y}_R) + K_t(y_u - y_R) - C_t \sum_{i=1}^n \dot{u}_i(t) \Phi_i(x_t) - C_t \sum_{i=1}^n u_i(t) \dot{\Phi}_i(x_t) \\ & - K_t \sum_{i=1}^n u_i(t) \Phi_i(x_t) \end{aligned} \quad (2.33)$$

The total load acting on the pavement can be expressed as

$$F = W - m_s \ddot{y}_s - m_u \ddot{y}_u \quad (2.34)$$

where  $W = (m_s + m_u) g$  is the dead weight of the vehicle (static part), and  $g$  is the gravitational acceleration ( $g = 9.81 \text{ m/s}^2$ ).

Substituting Eq. (2.33) into Eq. (2.5) and substituting Eq. (2.34) into Eq. (2.25) will compose a set of ordinary differential equations of the pavement-vehicle coupled system as:

$$M_c(t)\ddot{y}_c + C_c(t)\dot{y}_c + K_c(t) y_c = F_c(t) \quad (2.35)$$

where  $\{y_c\} = \{y_s, y_u, u_1, u_2, \dots, u_n\}^T$ ,  $\{\dot{y}_c\} = \{\dot{y}_s, \dot{y}_u, \dot{u}_1, \dot{u}_2, \dots, \dot{u}_n\}^T$ , and  $\{\ddot{y}_c\} = \{\ddot{y}_s, \ddot{y}_u, \ddot{u}_1, \ddot{u}_2, \dots, \ddot{u}_n\}^T$  are, respectively, displacement, velocity and acceleration vectors of the pavement-vehicle coupled system, and  $\{F_c\}$  denotes the excitation force vector.  $M_c(t)$ ,  $C_c(t)$  and  $K_c(t)$  are, respectively, the generalized mass, damping and stiffness matrices of the system, and are given as

$$M_c(t) = \begin{bmatrix} 1 & 0 & 0 & 0 & \dots & 0 \\ 0 & 1 & 0 & 0 & \dots & 0 \\ m_s \varphi_1 & m_u \varphi_1 & 1 & 0 & \dots & 0 \\ m_s \varphi_2 & m_u \varphi_2 & 0 & 1 & \dots & 0 \\ \vdots & \vdots & \vdots & \vdots & \ddots & \vdots \\ m_s \varphi_n & m_u \varphi_n & 0 & 0 & \dots & 1 \end{bmatrix}$$

$$C_c(t) = \begin{bmatrix} C_s/m_s & -C_s/m_s & 0 & 0 & \dots & 0 \\ -C_s/m_u & (C_s + C_t)/m_u & -C_{tu}\Phi_1 & -C_{tu}\Phi_2 & \dots & -C_{tu}\Phi_N \\ 0 & 0 & 2\zeta_1\omega_{n_1} & 0 & \dots & 0 \\ 0 & 0 & 0 & 2\zeta_2\omega_{n_2} & \dots & 0 \\ \vdots & \vdots & \vdots & \vdots & \ddots & \vdots \\ 0 & 0 & 0 & 0 & \dots & 2\zeta_N\omega_{n_N} \end{bmatrix}$$

$$K_c(t) = \begin{bmatrix} K_{ss} & -K_{ss} & 0 & 0 & \dots & 0 \\ -K_{su} & K_{st} & -C_{tu}\dot{\Phi}_1 - K_{tu}\Phi_1 & -C_{tu}\dot{\Phi}_2 - K_{tu}\Phi_2 & \dots & -C_{tu}\dot{\Phi}_n - K_{tu}\Phi_n \\ 0 & 0 & \omega_1^2 & 0 & \dots & 0 \\ 0 & 0 & 0 & \omega_2^2 & \dots & 0 \\ \vdots & \vdots & \vdots & \vdots & \ddots & \vdots \\ 0 & 0 & 0 & 0 & \dots & \omega_n^2 \end{bmatrix}$$

where

$$\{F_c\} = \begin{Bmatrix} 0 \\ C_{tu}\dot{y}_R + C_{tu}y_R \\ -W\varphi_1 \\ -W\varphi_2 \\ \vdots \\ -W\varphi_n \end{Bmatrix}$$

and

$$K_{ss} = K_s/m_s$$

$$K_{su} = K_s/m_u$$

$$K_{st} = (K_s + K_t)/m_u$$

$$K_{tu} = K_t/m_u$$

$$C_{tu} = C_t/m_u$$

## 2.5 Summary

In this chapter a brief discussion about common vehicle ride models and pavement-foundation models, as well as the formulation of the governing differential equations of motion of the pavement vehicle coupled model have been presented. The system differential equations of motion of the two-DOF quarter-vehicle ride model are obtained based on d'Alembert's principle. The pavement-foundation model is described by an Euler-Bernoulli beam with simply supported boundaries supported by Pasternak foundation and subjected to a moving concentrated load representing the dynamic interaction force. Based on Galerkin method the pavement-foundation system has been discretized to obtain a system of ordinary differential equations in the time domain. The coupled pavement-vehicle governing equations have then been formulated which can then be effectively used to evaluate the vehicle-pavement response considering the coupling action.

# CHAPTER 3

## Pavement-Vehicle Response under Harmonic

### Excitation

#### 3.1 Introduction

In order to study and understand the effect of coupling action between a moving vehicle and a rough road, dynamic response of pavement-vehicle coupled system (considering the interaction) is compared with those of conventional uncoupled vehicle system and pavement system (neglecting the interaction). Road surface roughness is an important factor in studying pavement and vehicle dynamics. For simplicity the road roughness profile can be regarded as a simple harmonic function of the form  $y_R(t) = Y_R \sin(\omega t)$ , where  $Y_R$  and  $\omega$  are, respectively, amplitude and excitation frequency, in which  $\omega = \frac{2\pi V}{\lambda}$ , and  $\lambda$  is the pavement wavelength. In this study, using pavement-vehicle coupled governing equations developed in Chapter 2, the influence of coupling action on vehicle-body displacement, vehicle-wheel displacement, pavement displacement and dynamic interaction force are investigated due to the variations in soil stiffness, road roughness, suspension damping and vehicle speed. Direct integration Newmark-Beta approach based on the linear average acceleration method has been utilized to numerically find the response of the pavement-vehicle vibrating system due to moving vehicular load and the results are validated with those reported in the previous research work.

### 3.2 Linear-Time-Invariant System

To understand the effect of the coupling action between vehicle and flexible pavement, a simple preliminary study (with closed form solution) has been carried out considering a Two-DOF quarter-truck as a fixed system at the mid-span ( $x_t = L/2$ ). As a result the system in Eq. (2.35) becomes a Linear Time Invariant (LTI) under an excitation of the form:

$$y_R = Y_R e^{j\omega t} \quad (3.1)$$

The coupled system equation (2.30) can be expressed as

$$M_c \ddot{y}_c + C_c \dot{y}_c + K_c y_c = \{F_c\} \quad (3.2)$$

Let

$$y_c = Y_c e^{j(\omega t - \phi_c)} = Y_c e^{j\omega t} e^{-j\phi_c} = \bar{Y}_c e^{j\omega t}$$

$$\dot{y}_c = j Y_c \omega e^{j(\omega t - \phi_c)} = j \bar{Y}_c \omega e^{j\omega t} \quad (3.3)$$

$$\ddot{y}_c = -Y_c \omega^2 e^{j(\omega t - \phi_c)} = -\bar{Y}_c \omega^2 e^{j\omega t}$$

Here  $\bar{Y}_c = Y_c e^{-j\phi_c}$  is the complex displacement vector.

Substituting Eq. (3.1) and Eq. (3.3) into Eq. (3.2), yields:

$$H(j\omega) = [[K_c] - [M_c]\omega^2 + j\omega[C_c]]^{-1}[Q] = \begin{bmatrix} H_1(j\omega) \\ H_2(j\omega) \\ H_3(j\omega) \\ H_4(j\omega) \\ \vdots \\ H_n(j\omega) \end{bmatrix} \quad (3.4)$$

where  $H(j\omega)$  represents the complex system transfer Function (Receptance Matrix), in which the non-dimensional forms of vehicle-body, vehicle-wheel and pavement displacements are:

$$\frac{\bar{Y}_s}{Y_R} = H_1(j\omega)$$

$$\frac{\bar{Y}_u}{Y_R} = H_2(j\omega)$$

$$\frac{\bar{U}_1}{Y_R} = H_3(j\omega)$$

$$\frac{\bar{U}_2}{Y_R} = H_4(j\omega)$$

⋮

$$\frac{\bar{U}_n}{Y_R} = H_n(j\omega)$$

Thus

$$\frac{\bar{Y}_p}{Y_R} = H_3(j\omega) \sin \frac{1\pi}{L} x_t + H_4(j\omega) \sin \frac{2\pi}{L} x_t + \dots + H_n(j\omega) \sin \frac{n\pi}{L} x_t$$

The non-dimensional form of the dynamic interaction force considering the coupling action can be expressed as (Appendix I):

$$\frac{F_{t_0}}{k_t Y_R} = \left[ 1 + j \left( \frac{c_t}{k_t} \right) \omega \right] \left( \frac{\bar{Y}_u}{Y_R} - \frac{\bar{Y}_p}{Y_R} - 1 \right) \quad (3.5)$$

Using Eqs. (3.4) and (3.5) the dynamic response of coupled system can be obtained and compared with that of uncoupled system. The results are as shown in Figures 3.1-3.8 in which the influence of coupling action on non-dimensional vehicle-body displacement  $\left| \frac{\bar{Y}_s}{Y_R} \right|$ , vehicle-

wheel displacement  $\left| \frac{\bar{Y}_u}{Y_R} \right|$ , and dynamic interaction force  $\left| \frac{F_{t0}}{k_t Y_R} \right|$  are analysed for different values of soil stiffness. It can be seen that the maximum peaks occur at approximately 10 rad/s (nearly 1.6 Hz) and 60 rad/s (9.5 Hz) that corresponds to vehicle-body and vehicle-wheel bounce modes of vibrations, respectively. The model is an underdamped system with suspension damping ratio of 0.233. To clearly demonstrate the effect of coupling action, the maximum non-dimensional values of vehicle-body, vehicle-wheel and dynamic interaction force corresponding to different soil stiffness coefficients are reported in tables 3.1-3.3 for both coupled system and conventional uncoupled system.

Figures 3.1-3.3 show variations in non-dimensional vehicle-body displacement against excitation frequency for coupled system and conventional uncoupled system at different soil stiffness coefficients. For a soil stiffness of  $k = 40.78 \times 10^4 \text{N/m/m}$ , the maximum relative displacement of coupled system is found to be about 4.4% smaller than that of uncoupled system, as shown in Figure 3.1. With the increase in soil stiffness from  $40.78 \times 10^4 \text{N/m/m}$  to  $40.78 \times 10^5 \text{N/m/m}$ , as shown in Figure 3.2, the maximum relative displacement of coupled system increases towards that of the uncoupled system, but is still about 1% smaller than that of the uncoupled system. In Figure 3.3, in which  $k = 40.78 \times 10^6 \text{N/m/m}$ , the maximum relative displacement of coupled system is found to be 0.1% greater than that of uncoupled system. This clearly demonstrates that the effect of coupling action on the relative vehicle-body displacement is more pronounced for small soil stiffness. In other words, as pavement stiffness increases (becoming more rigid) coupling between the vehicle and pavement would have insignificant effect on the sprung mass response.

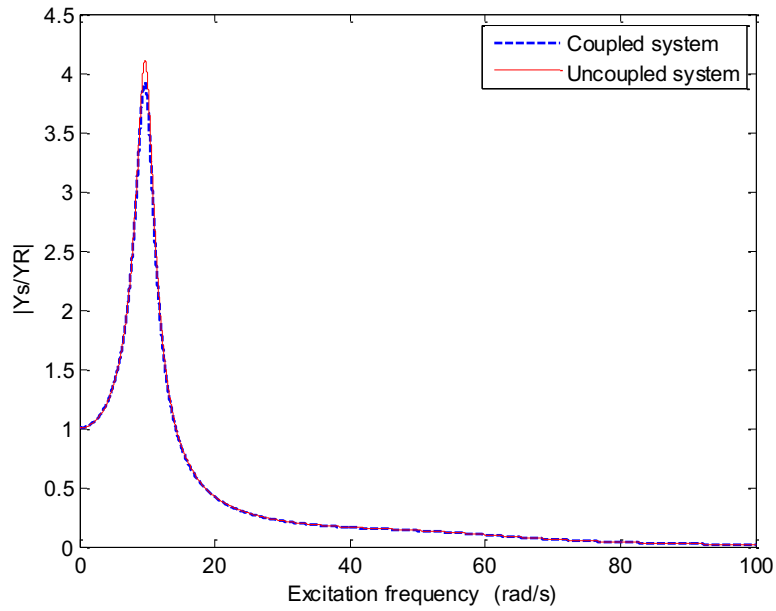


Figure 3.1 Relative vehicle-body displacement against excitation frequency  
 $(k = 40.78 \times 10^4 \text{N/m/m})$

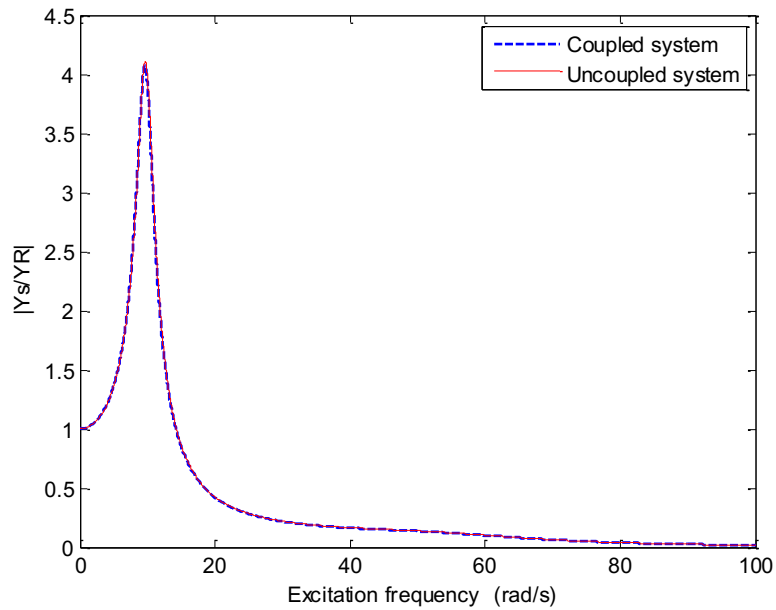


Figure 3.2 Relative vehicle-body displacement against excitation frequency  
 $(k = 40.78 \times 10^5 \text{N/m/m})$

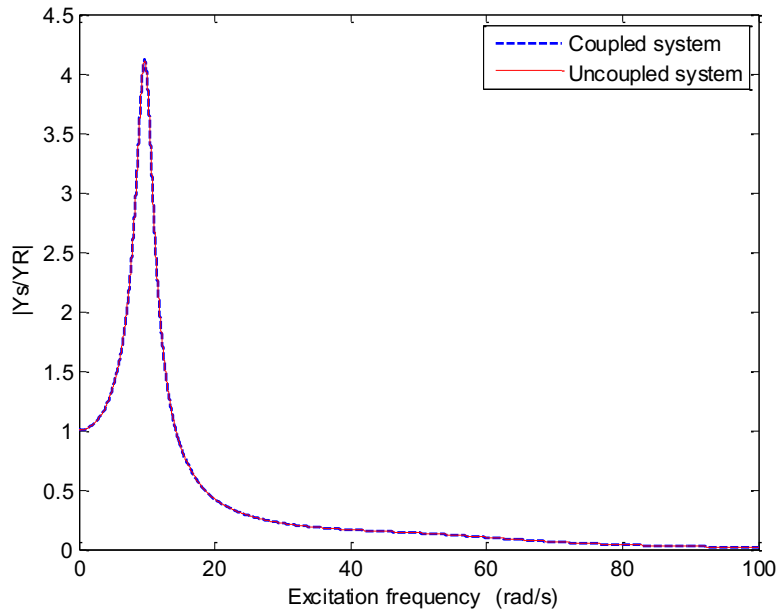


Figure 3.3 Relative vehicle-body displacement against excitation frequency  
 $(k = 40.78 \times 10^6 \text{ N/m/m})$

Table 3.1 Maximum non-dimensional values for sprung mass displacement

$k$ (N/m/m)	$ \bar{Y}_S/Y_R $ at first peak		
	Coupled	Uncoupled	%
$40.78 \times 10^4$	3.927	4.110	4.4
$40.78 \times 10^5$	4.068	4.110	1.0
$40.78 \times 10^6$	4.115	4.110	0.1

The variation in non-dimensional vehicle-wheel displacement against the excitation frequency for coupled system and conventional uncoupled system at different soil stiffness coefficients is also presented in Figures 3.4-3.6. Examination of results show that similar to the sprung mass, unsprung mass relative displacement for the coupled system increases as the soil stiffness

increases and approaches toward that of uncoupled system. For soil stiffness of  $k = 40.78 \times 10^4 \text{N/m/m}$ , the maximum relative displacements of coupled system are about 3.6% and 3.1% smaller than those of the uncoupled system, for the first and the second peaks, respectively, while they reduce to 0.63% and 1.2% for the first and the second peaks, respectively, for the soil stiffness of  $k = 40.78 \times 10^5 \text{N/m/m}$ , and become very close (0.15% and 0.5% for the first and the second peaks, respectively) to those of the uncoupled system for soil stiffness of  $k = 40.78 \times 10^6 \text{N/m/m}$ . Thus, the effect of coupling action on vehicle-wheel relative displacement decreases with the increase in the soil stiffness.

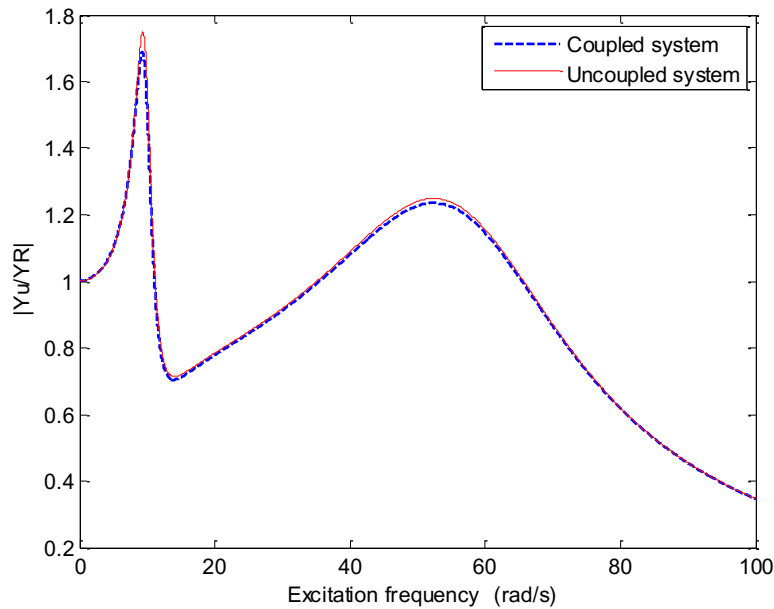


Figure 3.4 Relative vehicle-wheel displacement against excitation frequency  
 $(k = 40.78 \times 10^4 \text{N/m/m})$

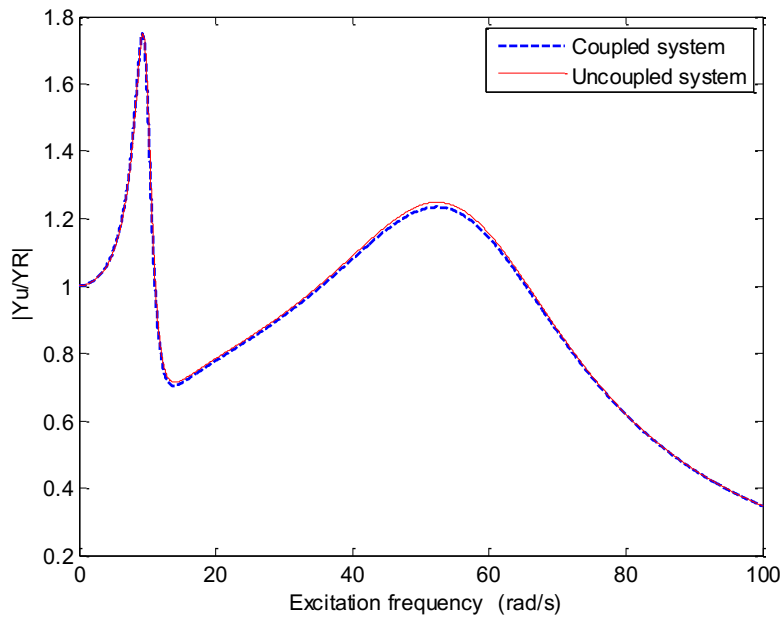


Figure 3.5 Relative vehicle-wheel displacement against excitation frequency  
 $(k = 40.78 \times 10^5 \text{ N/m/m})$

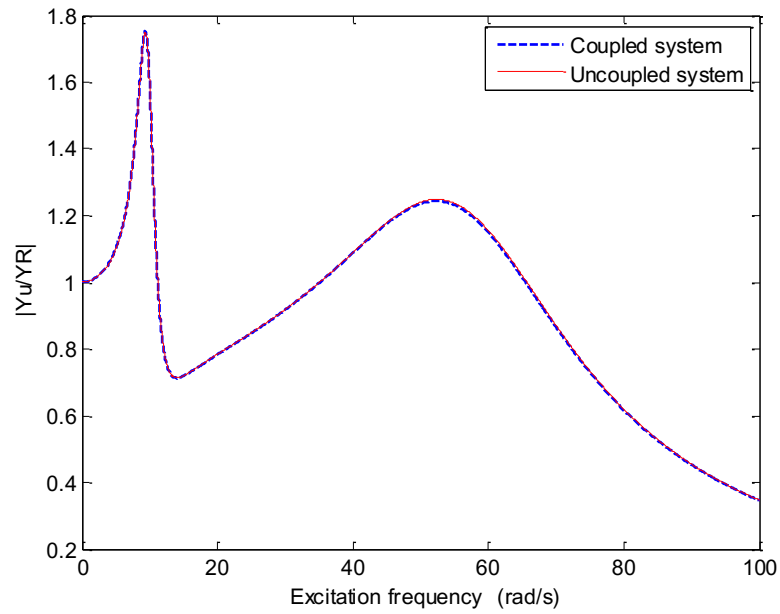


Figure 3.6 Relative vehicle-wheel displacement against excitation frequency  
 $(k = 40.78 \times 10^6 \text{ N/m/m})$

Table 3.2 Maximum non-dimensional values for unsprung mass displacement

$k$ (N/m/m)	$ \bar{Y}_u/Y_R $					
	First peak			Second peak		
	Coupled	Uncoupled	%	Coupled	Uncoupled	%
$40.78 \times 10^4$	1.689	1.751	3.6	1.210	1.249	3.1
$40.78 \times 10^5$	1.740	1.751	0.63	1.234	1.249	1.2
$40.78 \times 10^6$	1.754	1.751	0.15	1.242	1.249	0.5

Figures 3.7-3.9 show the variation of non-dimensional dynamic interaction force with the excitation frequency at different soil stiffness coefficients for both coupled and uncoupled systems. From Figure 3.7, as expected the effect coupling on relative dynamic interaction force is considerable for small soil stiffness and becomes insignificant as the pavement becomes more rigid. The maximum relative force amplitudes of coupled system are approximately 4.5% and 0.9% smaller for the first peak and 0.7% and 0.6% smaller for the second peak compared with those of uncoupled system for soil stiffness of  $k = 40.78 \times 10^4$  and  $40.78 \times 10^5$  N/m/m, respectively as shown in Figures 3.7 and 3.8. While for the soil stiffness of  $k = 40.78 \times 10^6$  N/m/m, the maximum relative forces for the coupled system for the first and second peaks become very close to those of uncoupled system (only 0.5 % and 0.2% differences) as shown in Figure 3.9. This also confirms that the effect of coupling action on the relative dynamic interaction force decreases with the increase in the soil stiffness and its effect can be neglected.

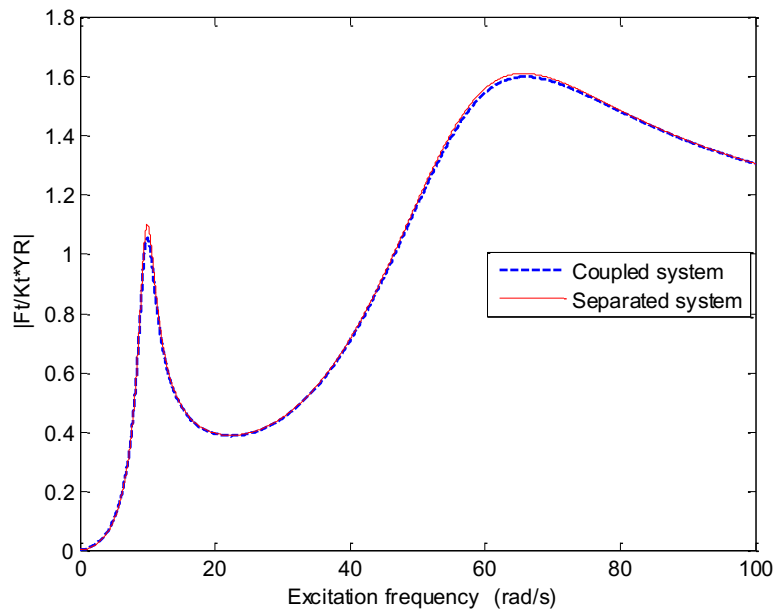


Figure 3.7 Relative dynamic interaction force against excitation frequency  
 $(k = 40.78 \times 10^4 \text{N/m/m})$

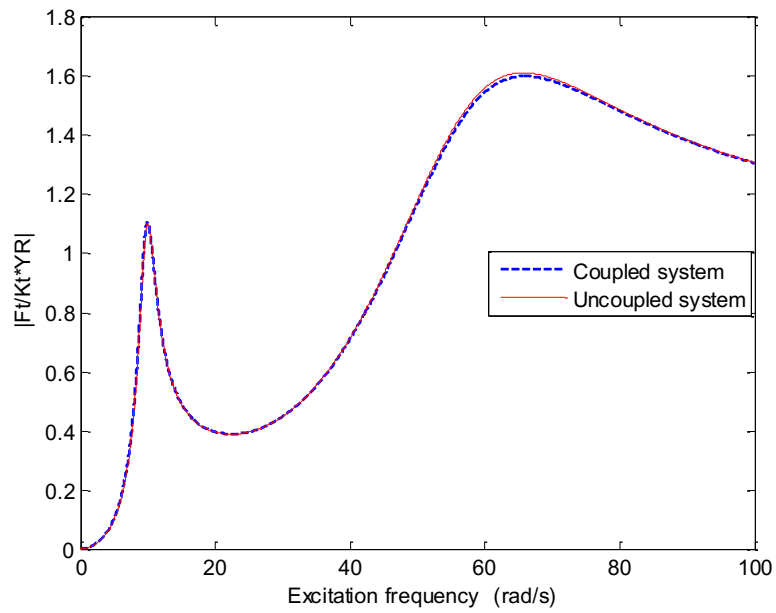


Figure 3.8 Relative dynamic interaction force against excitation frequency  
 $(k = 40.78 \times 10^5 \text{N/m/m})$

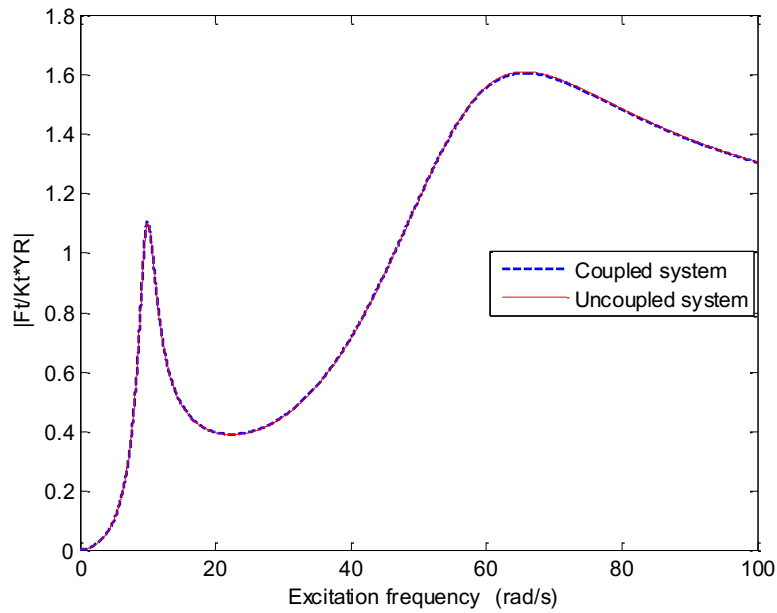


Figure 3.9 Relative dynamic interaction force against excitation frequency  
 $(k = 40.78 \times 10^6 \text{ N/m/m})$

Table 3.3 Maximum non-dimensional values for interaction force

$k$ (N/m/m)	$ F_{t_0}/K_t Y_R $					
	First peak			Second peak		
	Coupled	Uncoupled	%	Coupled	Uncoupled	%
$40.78 \times 10^4$	1.050	1.100	4.5	1.600	1.612	0.7
$40.78 \times 10^5$	1.090	1.100	0.9	1.601	1.612	0.6
$40.78 \times 10^6$	1.106	1.100	0.5	1.608	1.612	0.2

### 3.3 Direct Time Integration Technique Newmark-Beta Formulation

The system of equations (2.35) form a time varying system (has no closed form solution) and has been solved by the direct integration Newmark-Beta method using the average constant acceleration formula, which ensures an unconditional numerical stability.

Updated displacement and velocity in the Newmark average constant acceleration method may be described as [1, 80, and 81]:

$$y_{c_{i+1}} \approx y_{c_i} + \Delta t \dot{y}_{c_i} + \Delta t^2 \left[ \left( \frac{1}{2} - \beta \right) \ddot{y}_{c_i} + \beta \ddot{y}_{c_{i+1}} \right] \quad (3.6)$$

$$\dot{y}_{c_{i+1}} \approx \dot{y}_{c_i} + \Delta t [(1 - \gamma) \ddot{y}_{c_i} + \gamma \ddot{y}_{c_{i+1}}] \quad (3.7)$$

Substituting Eqs. (3.6) and (3.7) into Eq. (2.35), yields:

$$M_{c_{i+1}} \ddot{y}_{c_{i+1}} + C_{c_{i+1}} \left\{ \dot{y}_{c_i} + \Delta t [(1 - \gamma) \ddot{y}_{c_i} + \gamma \ddot{y}_{c_{i+1}}] \right\} + K_{c_{i+1}} \left\{ y_{c_n} + \Delta t \dot{y}_{c_i} + \Delta t^2 \left[ \left( \frac{1}{2} - \beta \right) \ddot{y}_{c_i} + \beta \ddot{y}_{c_{i+1}} \right] \right\} = F_{c_{i+1}} \quad (3.8)$$

Eq. (3.8) can be rearranged to obtain the updated acceleration as:

$$\ddot{y}_{c_{i+1}} = \left\{ M_{c_{i+1}} + C_{c_{i+1}} \Delta t \gamma + K_{c_{i+1}} \Delta t^2 \beta \right\}^{-1} \left[ F_{c_{i+1}} - C_{c_{i+1}} \dot{y}_{c_i} - (1 - \gamma) C_{c_{i+1}} \Delta t \ddot{y}_{c_i} - K_{c_{i+1}} y_{c_i} - K_{c_{i+1}} \Delta t \dot{y}_{c_i} - \left( \frac{1}{2} - \beta \right) K_{c_{i+1}} \Delta t^2 \ddot{y}_{c_i} \right] \quad (3.9)$$

where the Newmark's parameters are selected as  $\beta = 0.25$ ,  $\gamma = 0.5$  which assures unconditional numerical stability. After several trials, for computational efficiency it has been found that the appropriate pavement mode number and step time are  $n = 15$  and  $\Delta t = 1$  ms, respectively.

A programming code in Matlab environment has been developed to numerically solve the governing equations for the coupled system stated in Eqs. (3.8). The pavement and vehicle (truck) parameters are provided in Table 3.4 and 3.5, respectively. The simulation results for different configurations are provided in the following subsections.

Table 3.4 Numerical values of vehicle (truck) parameters [4, 28, 100 and 101]

Symbol	Physical quantity	Value	Unit
$m_s$	Vehicle-body mass (Sprung mass)	4500	kg
$m_u$	Vehicle-wheel mass (Unsprung mass)	650	kg
$K_s$	Suspension stiffness constant	$570 \times 10^3$	N/m
$K_t$	Tire stiffness constant	$1700 \times 10^3$	N/m
$C_s$	Suspension damping constant	$21 \times 10^3$	N.s/m
$C_t$	Tire damping constant	$2 \times 10^3$	N.s/m
$V$	Vehicle speed	16	m/s

Table 3.5 Numerical values of pavement and foundation parameters [4, 28, and 100]

Symbol	Physical quantity	Value	Unit
$E$	Young's modulus of elasticity of pavement	$6.223 \times 10^9$	Pa
$b$	Pavement width	1	m
$h$	Pavement thickness	0.15	m
$\rho$	Pavement density	2500	Kg/m <sup>3</sup>
$k_p$	Pasternak foundation parameter	$66.687 \times 10^4$	N
$k$	Soil stiffness coefficient	$40.78 \times 10^5$	N/m/m
$c$	Soil damping coefficient	$0.35 \times 10^6$	N.s/m/m
$Y_R$	Surface roughness amplitude	0.054	m
$\lambda$	Pavement wavelength	10	m
$L$	Pavement span length	160	m

### 3.3.1 Model Validation

This subsection aims to verify the accuracy of the pavement-foundation model, in which the system is discretized using Galerkin method and solved based on direct integration method using Newmark-Beta scheme. The deflection of the pavement (beam) at the mid-span  $y_p(L/2, t)$  is compared with that of the model proposed by Senalp et al. [82] who carried out the study based on the Finite Element Method (FEM). All the parameters considered in the validation are taken from Senalp et al. [82] and presented in Table 3.6.

Table 3.6 Pavement Parameters [82]

Symbol	Description	Value	Unit
$E$	Young's modulus	$21 \times 10^{10}$	N/m <sup>2</sup>
$I$	Second moment of area	$3.055 \times 10^{-5}$	m <sup>4</sup>
$A$	Cross sectional area	$7.69 \times 10^{-3}$	m <sup>2</sup>
$\rho$	Density of the material	7850	kg/m <sup>3</sup>
$L$	Beam length	50	M
$k$	Linear spring stiffness per length	$1.386 \times 10^8$	N/m/m
$P$	Moving load	65	kN

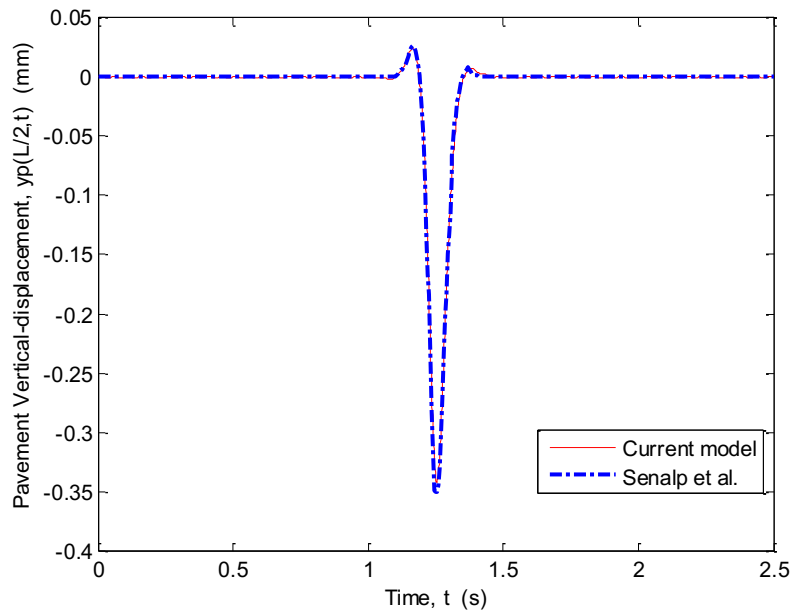


Figure 3.10 Comparison of beam deflection of the present model with that reported by Senalp et al.

The results obtained using the present model and those of Senalp’s model are compared in Figure 3.10, and summarized in Table 3.7. As it can be seen, the results show a good agreement between these two models.

Table 3.7 Midpoint deflection obtained by two methods

	Central Deflection
Senalp et al.	0.351
Present model	0.342
% error	2.5

### 3.3.2 Effect of Vehicle Speed on Coupled System Response at Different Soil Stiffness

Figure 3.11 presents variation of the vehicle-body displacement against vehicle speed at different soil stiffness coefficients. As it can be seen the maximum displacement increases with the increase in soil stiffness.

Figure 3.12 presents variation of the vehicle-wheel displacement against vehicle speed at different soil stiffness coefficients. Similar to the vehicle-body displacement, the maximum vehicle-wheel displacement increases with the increase in soil stiffness (for the two peaks).

Figure 3.13 presents variation of the dynamic interaction force against vehicle speed at different soil stiffness coefficients which also confirms that the maximum force amplitude increases with the increase in soil stiffness (for the two peaks).

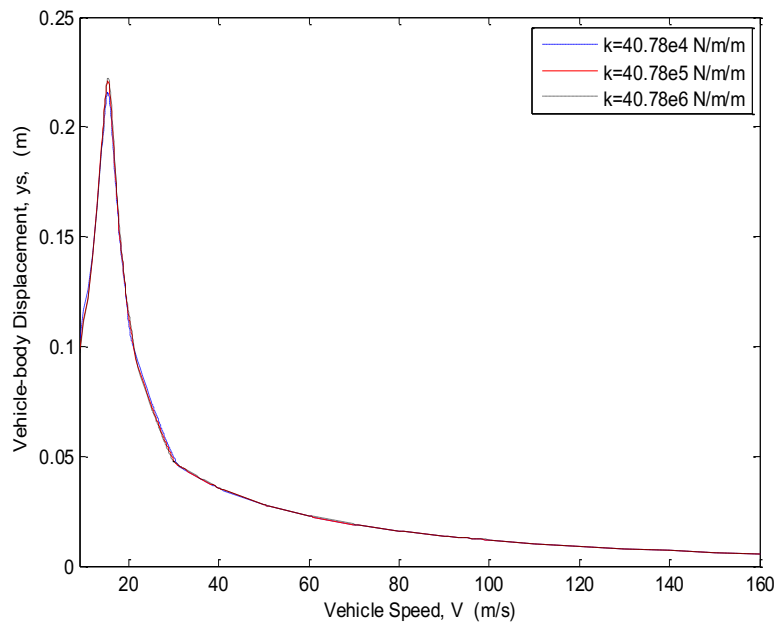


Figure 3.11 Vehicle-body displacement versus vehicle speed at different soil stiffness

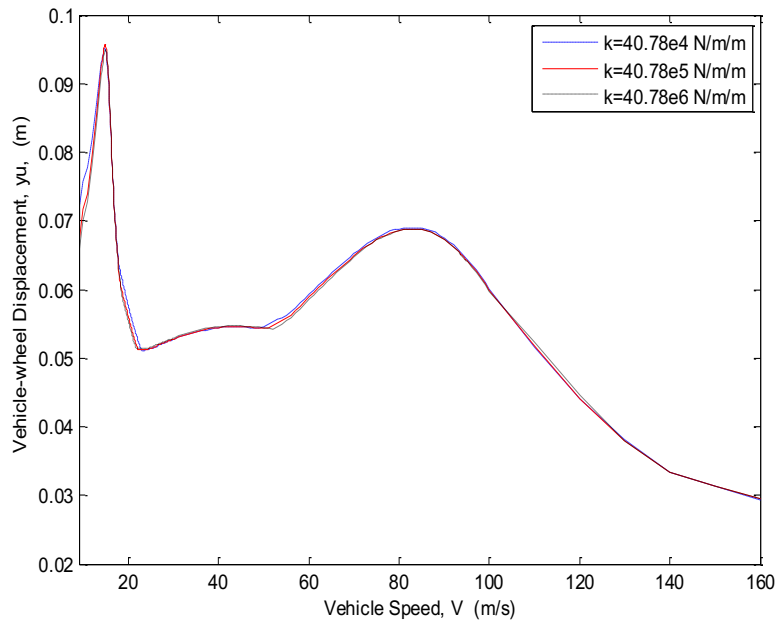


Figure 3.12 Vehicle-wheel displacement versus vehicle speed at different soil stiffness

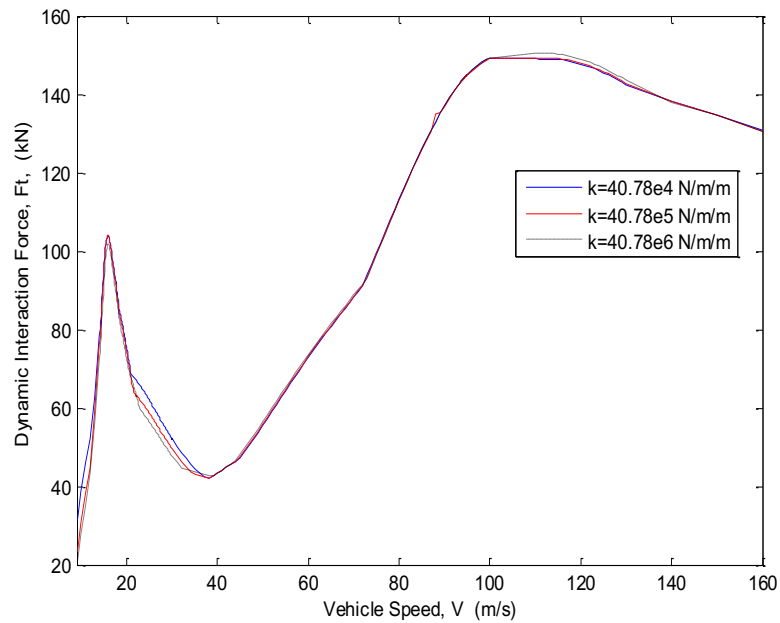


Figure 3.13 Dynamic interaction load versus vehicle speed at different soil stiffness

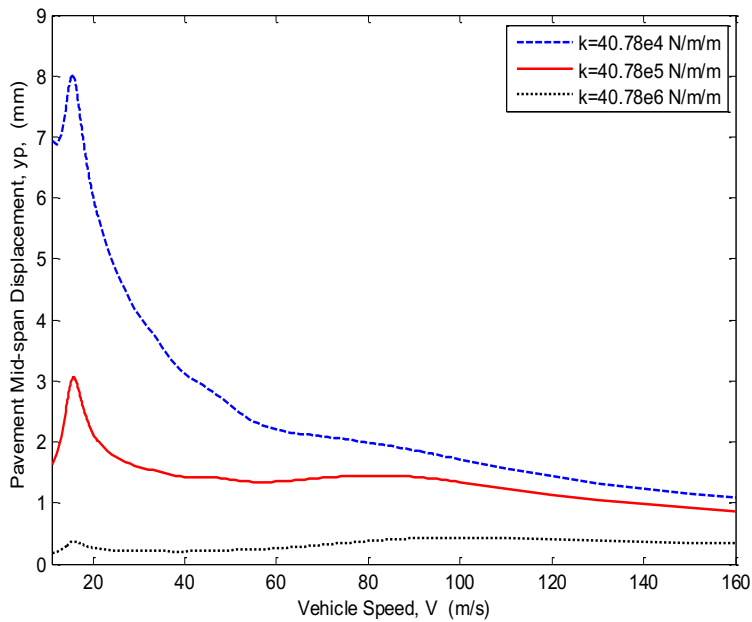


Figure 3.14 Pavement displacement with vehicle speed at different soil stiffness

Figure 3.14 shows variation of the pavement mid-span displacement against vehicle speed at different soil stiffness coefficients. As expected, the maximum pavement displacement (for the two peaks) decreases considerably with the increase in soil stiffness. It can be realized from Figures 3.11-3.14 that the peak occurs at critical velocity around 16 m/s for the first peak, and 82 m/s for the second peak which slightly increases with the increase in soil stiffness.

For the sake of better comparison, the maximum values of vehicle-body, vehicle-wheel, pavement displacements and dynamic interaction force corresponding to vehicle speed for different soil stiffness coefficients are also provided in Table 3.8.

Table 3.8 Peak responses of coupled system due to vehicle speed for different soil stiffness,  $k$

$k$ (N/m/m)	$y_{s_{max}}$ (m)	$y_{u_{max}}$ (m)		$F_{t_{max}}$ (kN)		$y_{p_{max}}$ (mm)	
		1 <sup>st</sup> peak	2 <sup>nd</sup> peak	1 <sup>st</sup> peak	2 <sup>nd</sup> peak	1 <sup>st</sup> peak	2 <sup>nd</sup> peak
$40.78 \times 10^4$	0.2155	0.0952	0.0690	103.9	149.1	8.014	-----
$40.78 \times 10^5$	0.2210	0.0956	0.0697	104.3	149.5	3.057	1.451
$40.78 \times 10^6$	0.2223	0.0960	0.0699	104.7	150.4	0.370	0.432

### 3.3.3 Effect of Suspension Damping on Coupled system Response

A paved road traversed by a truck at a speed of 16 m/s (around 57.6 km/h) is considered. The vehicle suspension damping ( $C_s$ ) was varied (10.5, 21, 42 kN.s/m), and the road surface roughness amplitude and the soil stiffness coefficients were fixed at 0.054 m and  $40.78 \times 10^5$  N/m/m, respectively. The effect of vehicle suspension damping on the coupled system response is shown in Figures 3.15-3.18

It can be observed that all the system responses decrease with the increase in suspension damping. Therefore, tuning the suspension of the vehicle is one possible way to control and mitigate the amplitude responses.

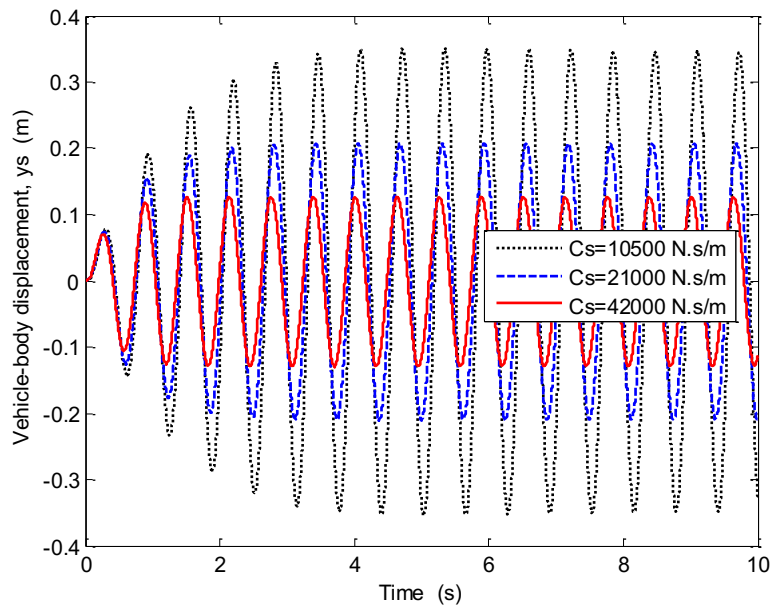


Figure 3.15 Vehicle-body response for different suspension damping

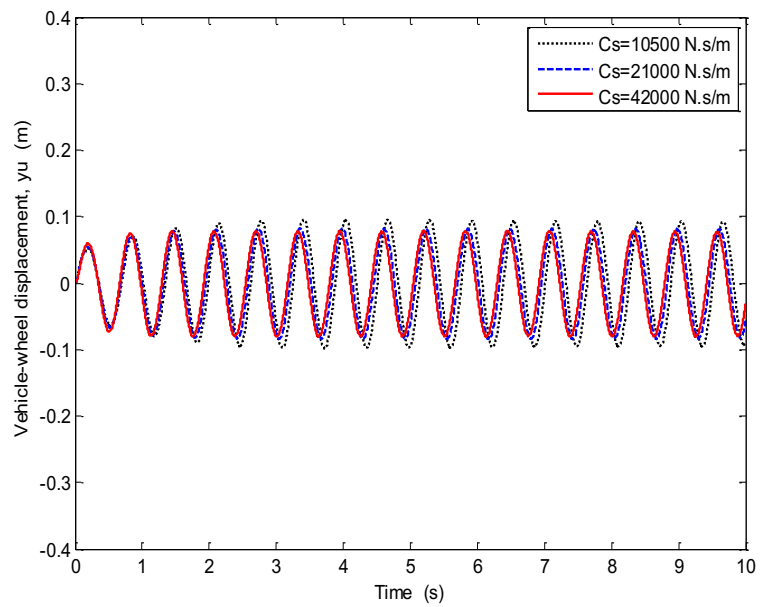


Figure 3.16 Vehicle-wheel response for different suspension damping

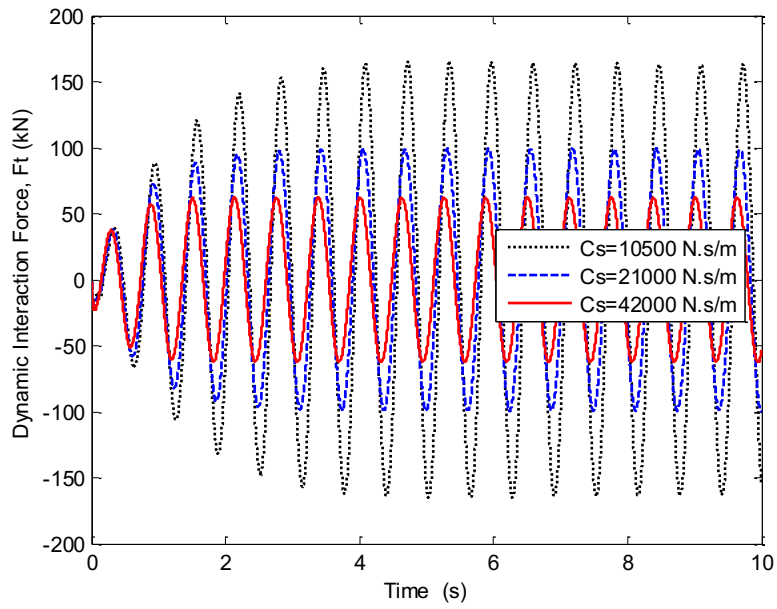


Figure 3.17 Force response for different suspension damping

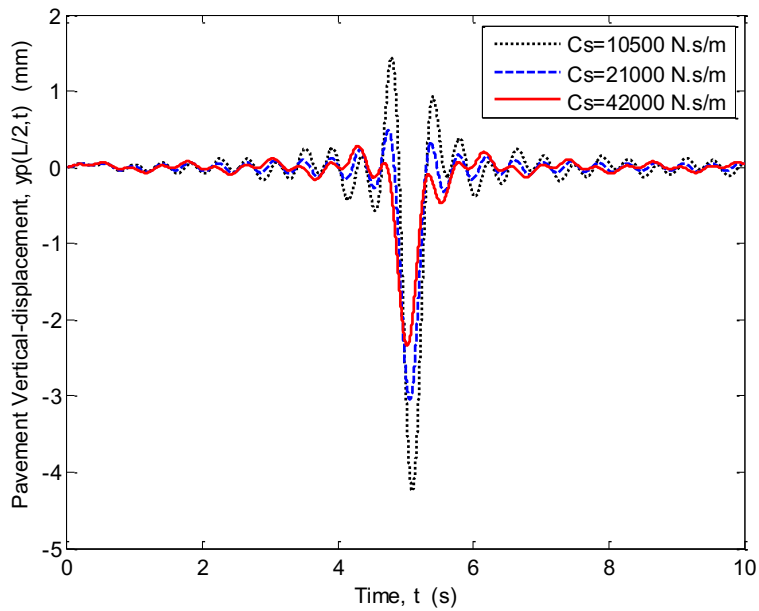


Figure 3.18 Pavement mid-span response for different suspension damping

The maximum response values of vehicle-body, vehicle-wheel, pavement and dynamic interaction force for different suspension damping are also provided in Table 3.9

Table 3.9 Maximum response values of coupled system for different suspension damping

$C_s$ (kN.s/m)	$y_{s_{max}}$ (m)	$y_{u_{max}}$ (m)	$F_{t_{max}}$ (kN)	$y_{p_{max}}$ (mm)
10.5	0.353	0.098	165.08	4.248
21	0.210	0.083	99.560	3.044
42	0.129	0.080	62.751	2.339

### 3.3.4 Pavement Deflection at Different Load Positions

Considering the coupling action between the flexible pavement and a moving vehicle, the pavement deflection at different load locations is investigated. The pavement is divided into 8 chosen intervals of length 20 m each for the total span of 160 m, as shown in Figure 3.19 and the displacement of the beam has been found at 7 nodal points between end supports while the vehicle is moving on the span from  $x = 0$  to  $x = 160$  m with velocity of 16 m/s.

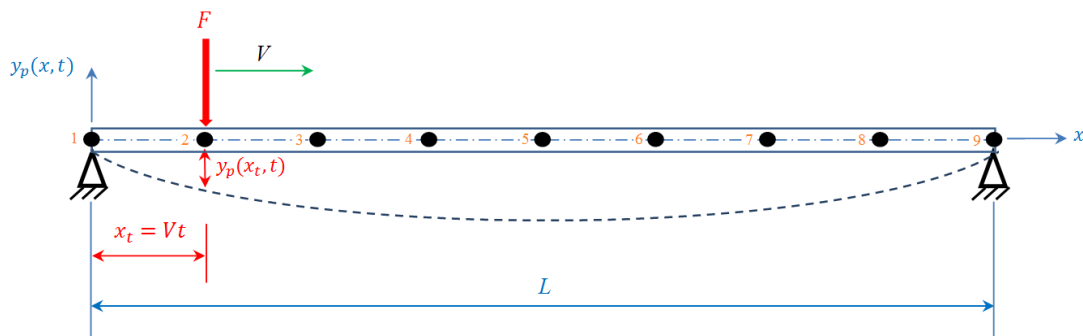


Figure 3.19 Beam discretized to 8 elements with 9 nodal locations

The simulation results for pavement deflection while the vehicle arrives at different nodal points are shown in Figure 3.20. Table 3.10 also summarizes the pavement displacement at the vehicle position and also the maximum deformation of the pavement at each vehicle position. It can be seen that the maximum deflection of the pavement occurs at a point close to the vehicle position. Moreover, as expected the maximum deflection of the pavement when the vehicle is moving from  $x = 0$  to  $x = 160$  m takes place around the mid-span of the pavement.

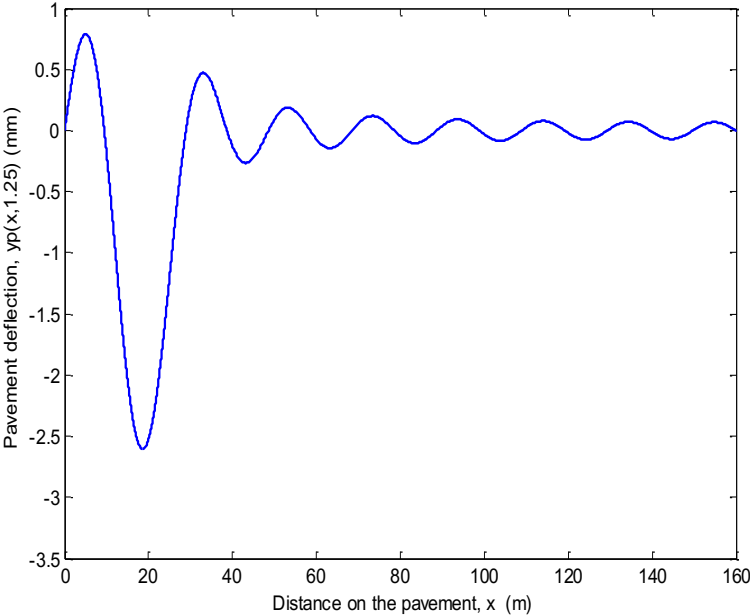


Figure 3.20(a) Pavement deflection at Node 2

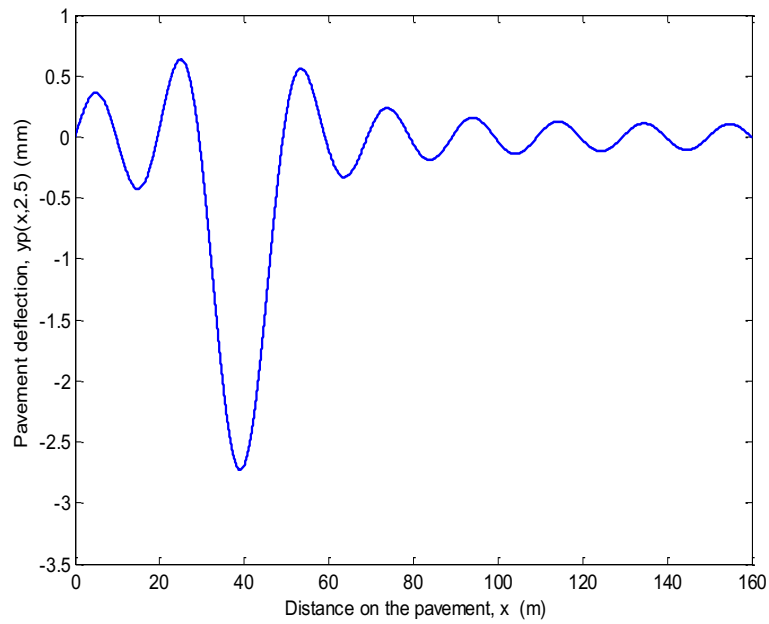


Figure 3.20(b) Pavement deflection at Node 3

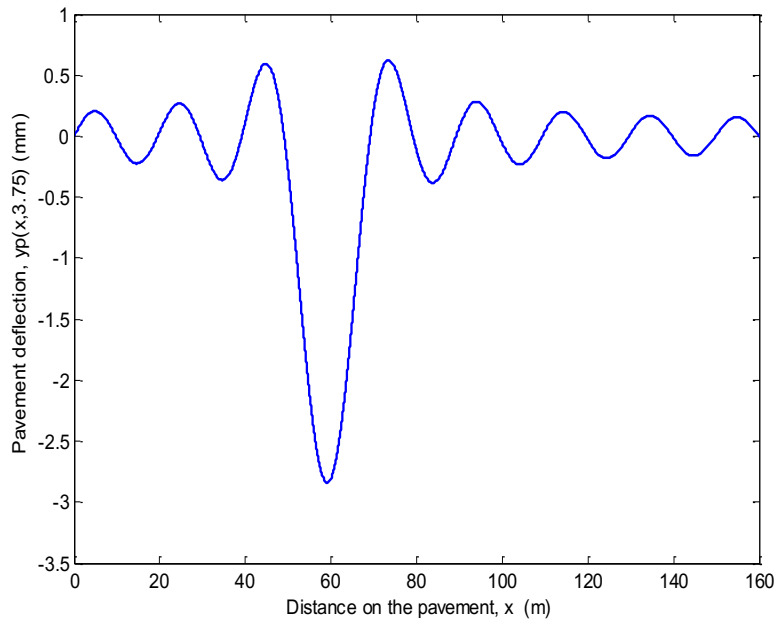


Figure 3.20(c) Pavement deflection at Node 4

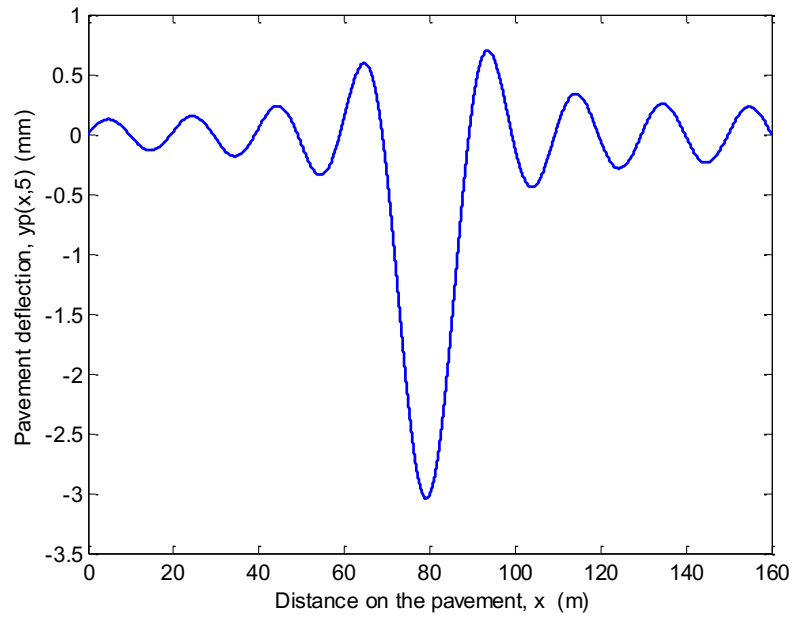


Figure 3.20(d) Pavement deflection at Node 5

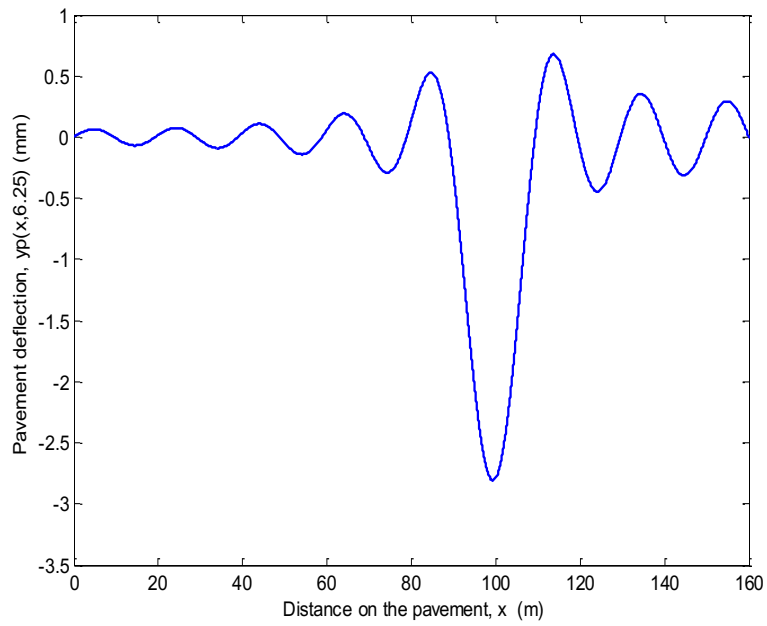


Figure 3.20(e) Pavement deflection at Node 6

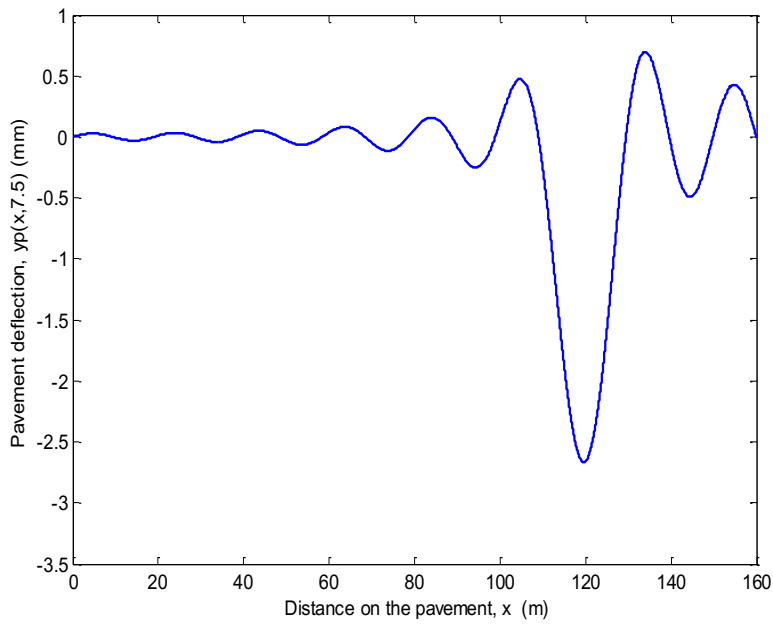


Figure 3.20(f) Pavement deflection at Node 7

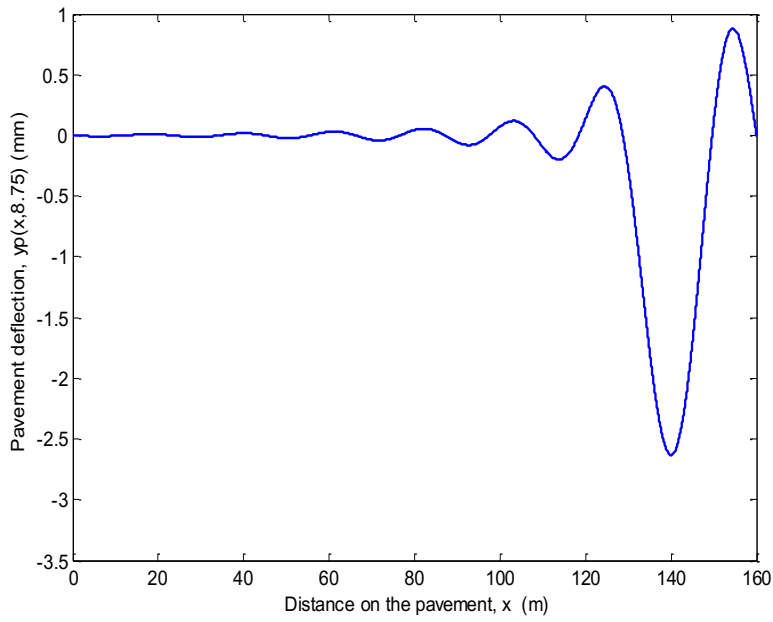


Figure 3.20(g) Pavement deflection at Node 8

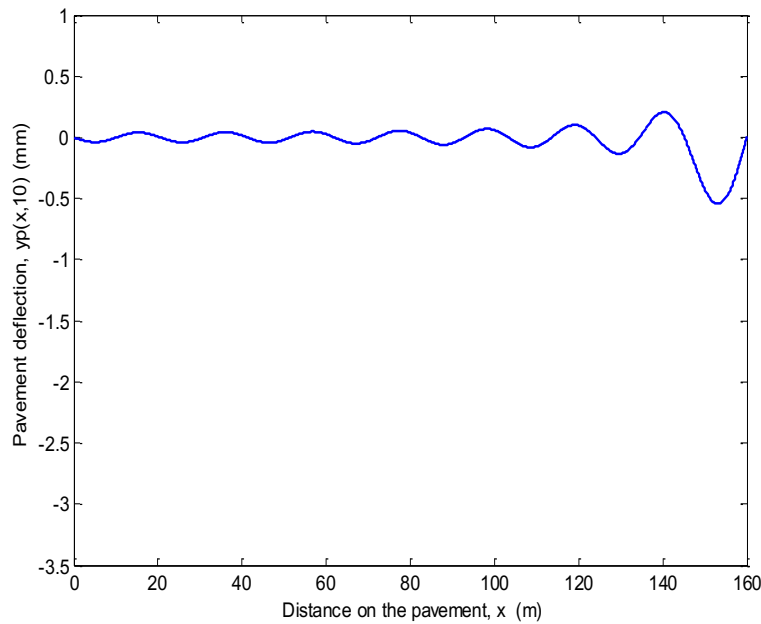


Figure 3.20(h) Pavement deflection at Node 9

Figure 3.20 Pavement deflection at different nodal points; (a) at Node 2, (b) at Node 3, (c) at Node 4, (d) at Node 5, (e) at Node 6, (f) at Node 7, (g) at Node 8, (h) at Node 9.

Table 3.10 Pavement deflection values at different node locations

Node	$t$ (s)	$x_t$ (m)	$y_p(x_t, t)$ , (mm)	$y_{pmax}(x, t)$ (mm)	$x$ (m)
1	0	0	0	0	0
2	1.25	20	2.529	2.608	18.70
3	2.5	40	2.691	2.730	39.09
4	3.75	60	2.790	2.839	59.2
5	5	80	3.009	3.041	79.28
6	6.25	100	2.789	2.808	99.34
7	7.5	120	2.659	2.664	119.7
8	8.75	140	2.631	2.631	140
9	10	160	0	0.543	153.2

### **3.4 Response Comparison of Coupled System with Conventional Uncoupled System**

The effect of coupling action on vehicle-body displacement, vehicle-wheel displacement, dynamic interaction force, and pavement mid-span displacement can be found by comparing the dynamics of the pavement-vehicle coupled system with that of the conventional uncoupled system. Here, it is assumed that the vehicle (truck) is moving with a constant velocity of 16 m/s from  $x = 0$  to  $x = L$ . Results are obtained for different road surface roughness amplitude  $Y_R$ , and soil stiffness coefficient  $k$ . The road surface roughness amplitudes considered are 0.002 m (small), 0.025 m (medium) and 0.054 m (large). For each road surface roughness amplitude, the soil stiffness is varied as  $40.78 \times 10^4$  (small),  $40.78 \times 10^5$  (medium) and  $40.78 \times 10^6$  N/m/m (large). The following subsections describe the comparison of results (vehicle-body displacement, vehicle-wheel displacement and dynamic interaction force, as well as pavement displacement) for coupled and uncoupled systems under different road roughness amplitudes and different soil stiffness coefficients.

#### ***3.4.1 Effect of Coupling Action on Vehicle-Body Displacement***

Figure 3.21 shows the response of the vertical vehicle-body displacement at road surface roughness amplitude of  $Y_R = 0.002$  m and soil stiffness coefficient of  $k = 40.78 \times 10^4$  N/m/m. It can be seen that the maximum amplitude of vehicle-body displacement of coupled system is 40.7% greater than that of the conventional uncoupled system. It has also been found that for small road surface roughness amplitudes ( $Y_R = 0.002$  m) and soil stiffness coefficient of  $40.78 \times 10^5$  and  $40.78 \times 10^6$  N/m/m, the maximum amplitude of vehicle-body displacement is 13.4% and 1.59% greater than that of conventional uncoupled system, as shown in Figures 3.22

and 3.23, respectively. Thus for a small surface roughness amplitude, the effect of coupling action on vehicle-body response decreases with the increase in soil stiffness.

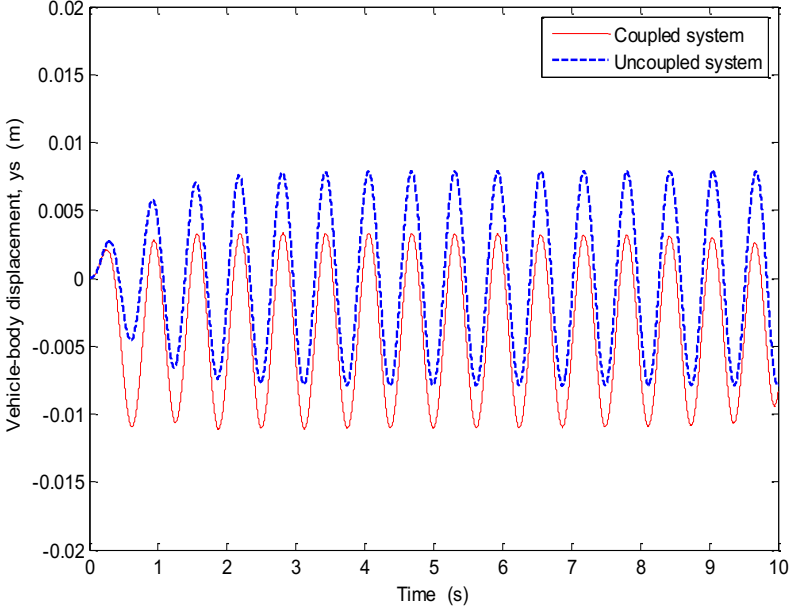


Figure 3.21 Vehicle-body response with  $Y_R = 0.002$  m and  $k = 40.78 \times 10^4$  N/m/m.

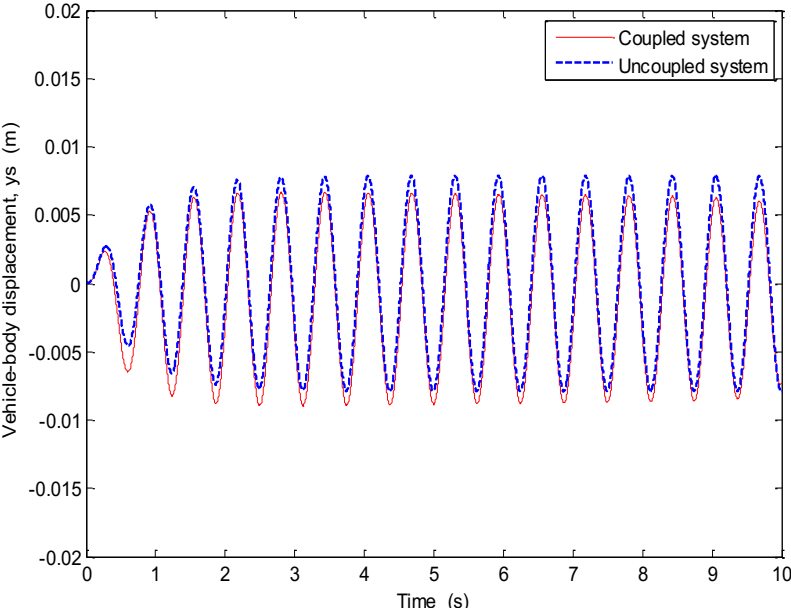


Figure 3.22 Vehicle-body response with  $Y_R = 0.002$  m and  $k = 40.78 \times 10^5$  N/m/m.

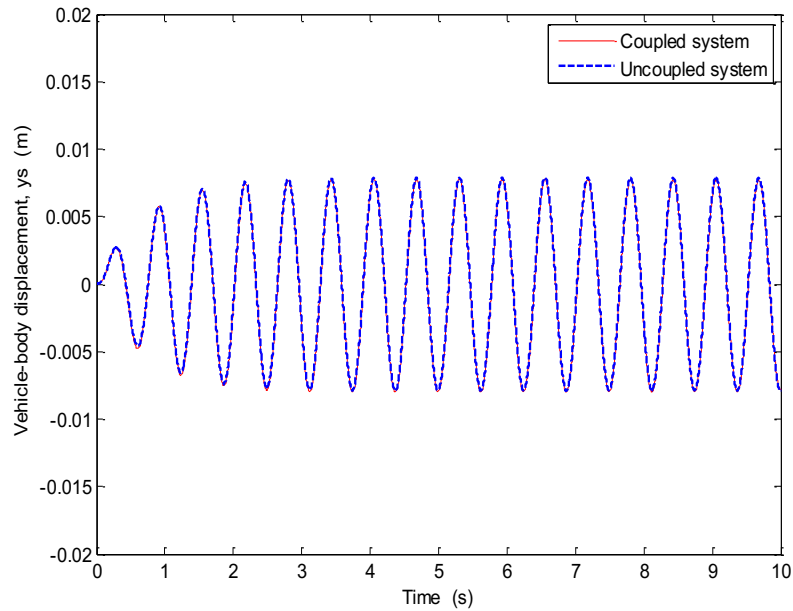


Figure 3.23 Vehicle-body response with  $Y_R = 0.002$  m and  $k = 40.78 \times 10^6$  N/m/m.

In Figures 3.24-3.26, the road surface roughness amplitude  $Y_R$  is chosen to be 0.025 m while the soil stiffness coefficient is increased from  $k = 40.78 \times 10^4$  N/m/m in Figure 3.24 to  $40.78 \times 10^5$  and  $40.78 \times 10^6$  N/m/m in Figures 3.25 and 3.26, respectively. Examination of results reveal that the maximum amplitude of vehicle-body displacement for coupled system is around 1.48% and 0.61% smaller than that of conventional system for small and medium stiffness coefficients, respectively, and it is slightly (0.13%) greater than that of conventional system for large stiffness coefficient. Thus similar to the small road roughness amplitude, for medium road surface roughness  $Y_R = 0.025$  m, the effect of coupling action on vehicle-body response decreases with the increase in soil stiffness.

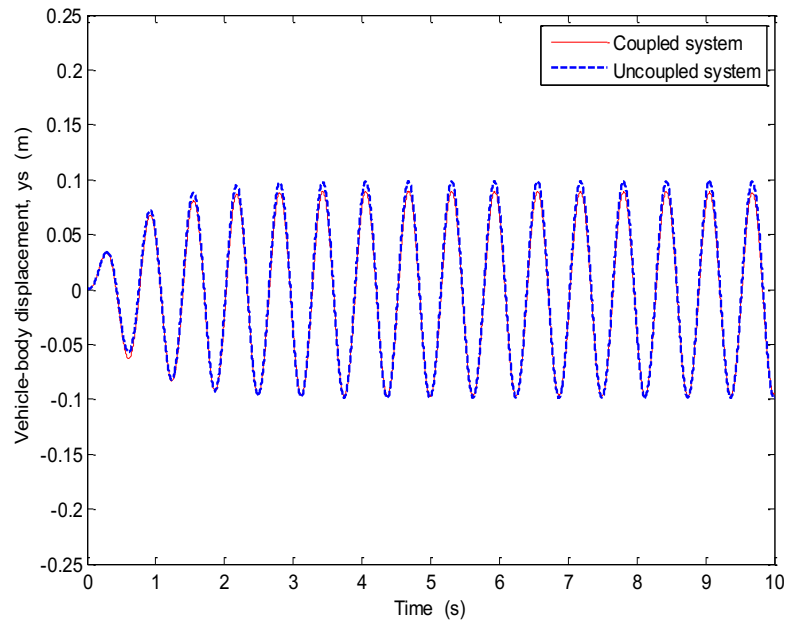


Figure 3.24 Vehicle-body response with  $Y_R = 0.025$  m and  $k = 40.78 \times 10^4$  N/m/m.

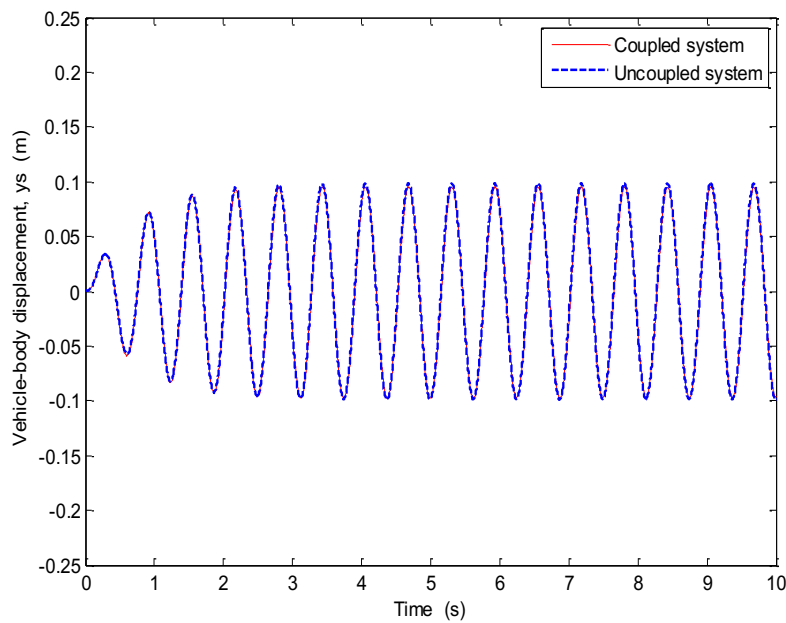


Figure 3.25 Vehicle-body response with  $Y_R = 0.025$  m and  $k = 40.78 \times 10^5$  N/m/m.

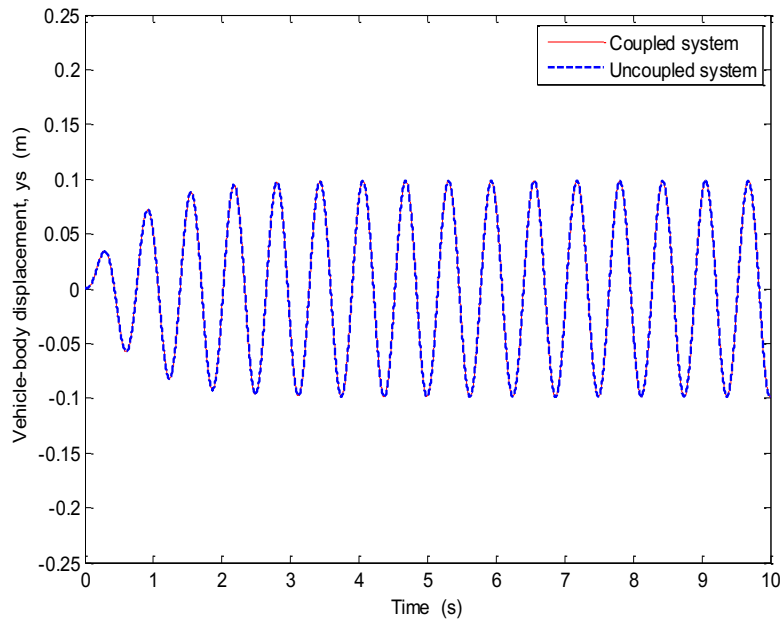


Figure 3.26 Vehicle-body response with  $Y_R = 0.025$  m and  $k = 40.78 \times 10^6$  N/m/m.

For the road surface roughness amplitude of  $Y_R = 0.054$  m, the maximum amplitude of vehicle-body displacement considering the coupling action becomes 3.42% and 1.20% smaller than that of conventional uncoupled system at soil stiffness coefficient of  $40.78 \times 10^4$  N/m/m and  $40.78 \times 10^5$  N/m/m, as shown in Figures 3.27 and 3.28, respectively. It has also been found that the maximum displacement of coupled system is increased slightly by 0.07% for a soil stiffness of  $40.78 \times 10^6$  N/m/m compared with that of conventional system as shown in Figure 3.29. This also again implies that the effect of coupling action on vehicle-body response decreases with the increase in soil stiffness for this level of road roughness amplitude. It is also observed that the effect of coupling action on the vehicle-body displacement decreases when the road surface roughness amplitude increases from 0.002 m to 0.025 m, and slightly increases once again at large road roughness amplitude.

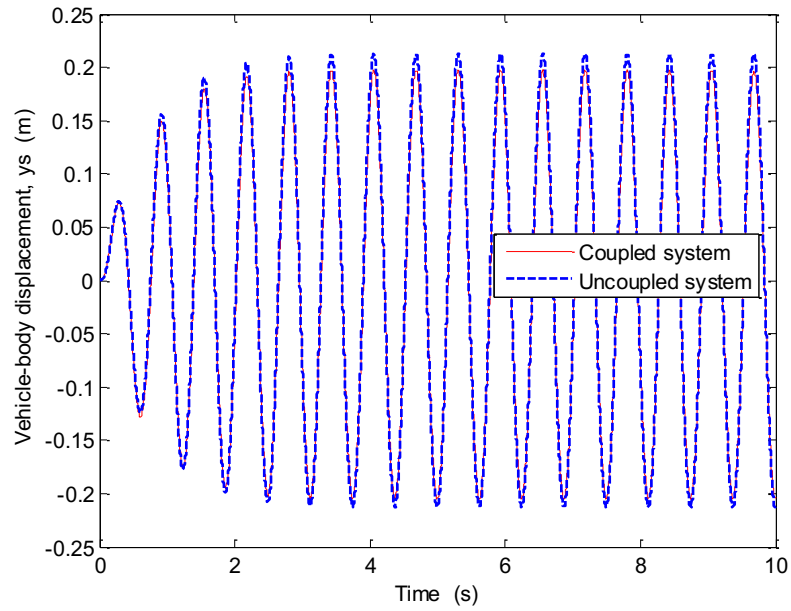


Figure 3.27 Vehicle-body response with  $Y_R = 0.054$  m and  $k = 40.78 \times 10^4$  N/m/m.

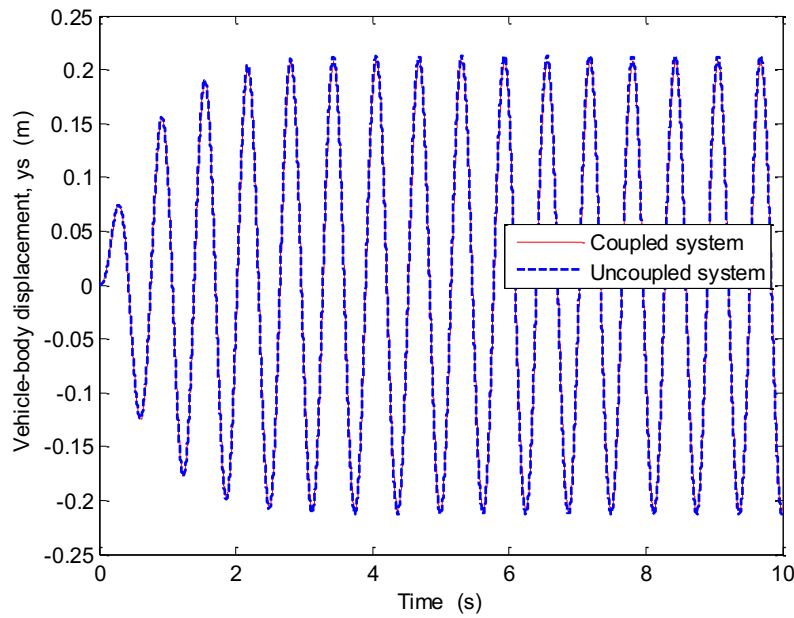


Figure 3.28 Vehicle-body response with  $Y_R = 0.054$  m and  $k = 40.78 \times 10^5$  N/m/m.

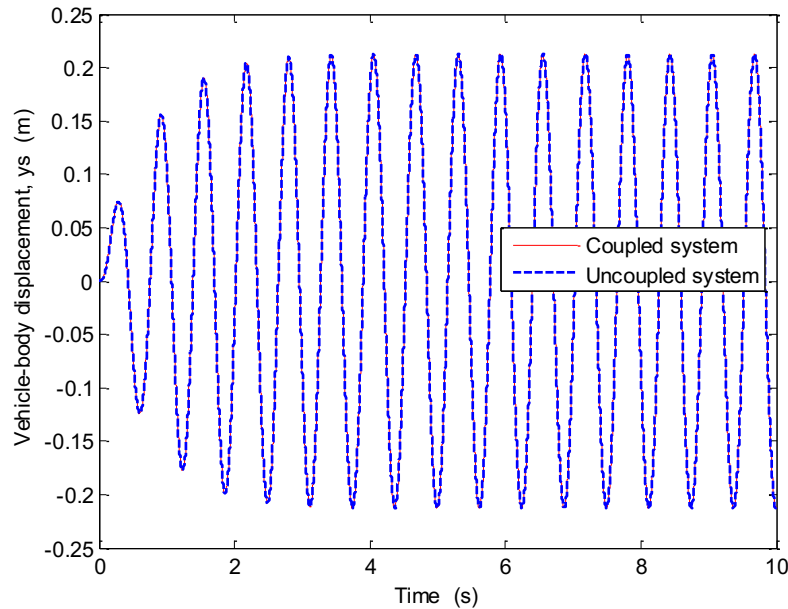


Figure 3.29 Vehicle-body response with  $Y_R = 0.054$  m and  $k = 40.78 \times 10^6$  N/m/m.

### 3.4.2 Effect of Coupling Action on Vehicle-Wheel Displacement

Figures 3.30-3.32 show vehicle-wheel displacement with road surface roughness amplitude of  $Y_R = 0.002$  m at different soil stiffness coefficients. As it can be seen the effect of coupling on the maximum vehicle-wheel displacement is more pronounced compared with that on the maximum vehicle-body displacement for small soil stiffness. Figure 3.30 shows that the maximum amplitude of vehicle-wheel displacement of coupled system is around 138% greater than that of conventional uncoupled system for small soil stiffness and it while reduces to 36.1% and 4% for medium and large soil stiffness coefficients as shown in Figure 3.31 and Figure 3.32, respectively. This confirms that for small surface roughness amplitude, the effect of coupling action on vehicle-wheel response also decreases with the increase in soil stiffness.

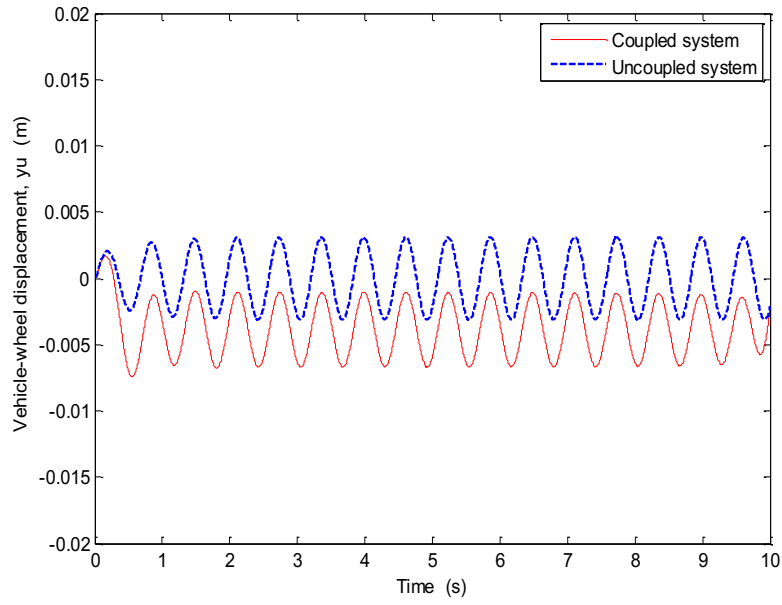


Figure 3.30 Vehicle-wheel response with  $Y_R = 0.002$  m and  $k = 40.78 \times 10^4$  N/m/m

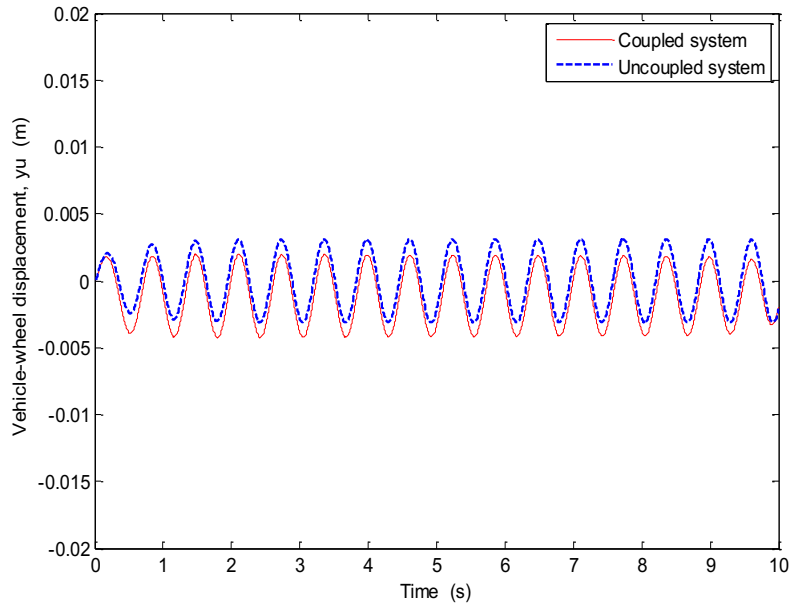


Figure 3.31 Vehicle-wheel response with  $Y_R = 0.002$  m and  $k = 40.78 \times 10^5$  N/m/m

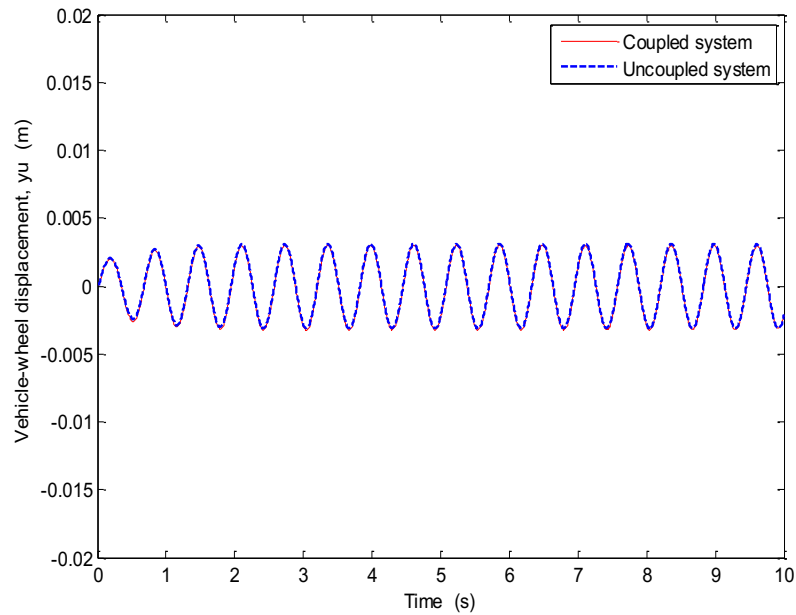


Figure 3.32 Vehicle-wheel response with  $Y_R = 0.002$  m and  $k = 40.78 \times 10^6$  N/m/m

In case of  $Y_R = 0.025$  m, Figures 3.33 and 3.34 show a decrease in the amplitude of vehicle-wheel displacement for coupled system by 4.4% at small soil stiffness. While the maximum amplitude increases slightly by 1.2% and 0.3%, respectively, for medium soil and large soil stiffness as shown in Figure 3.35. Therefore, for medium road surface roughness ( $Y_R = 0.025$  m), the effect of coupling action on vehicle-wheel response decreases with the increase in soil stiffness.

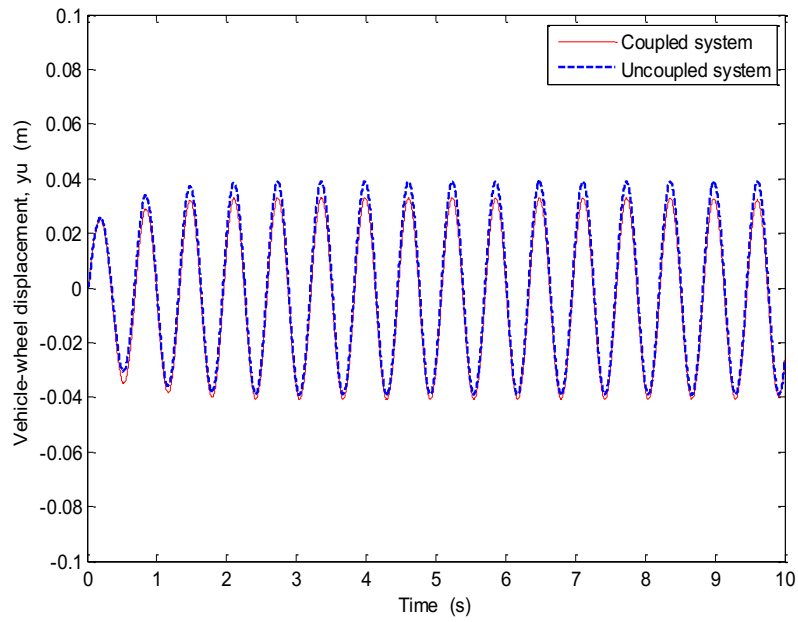


Figure 3.33 Vehicle-wheel response with  $Y_R = 0.025$  m and  $k = 40.78 \times 10^4$  N/m/m

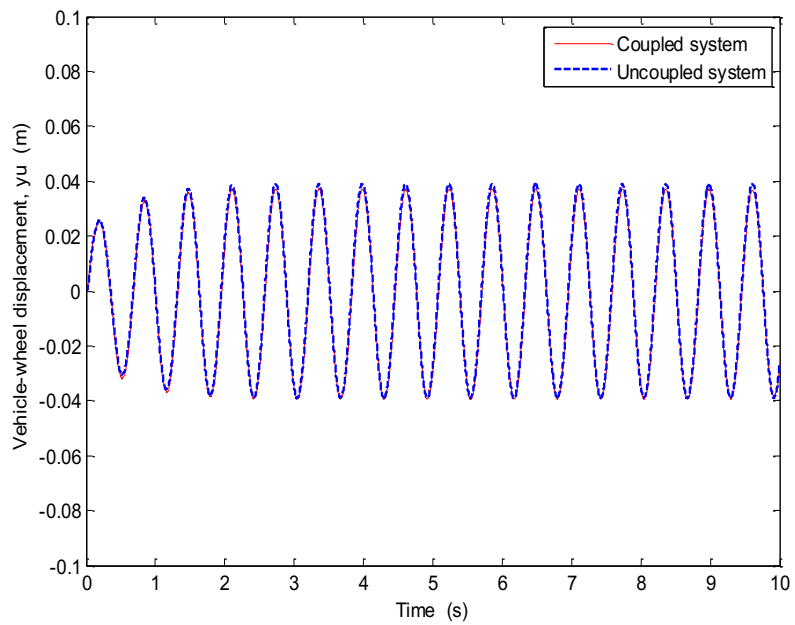


Figure 3.34 Vehicle-wheel response with  $Y_R = 0.025$  m and  $k = 40.78 \times 10^5$  N/m/m

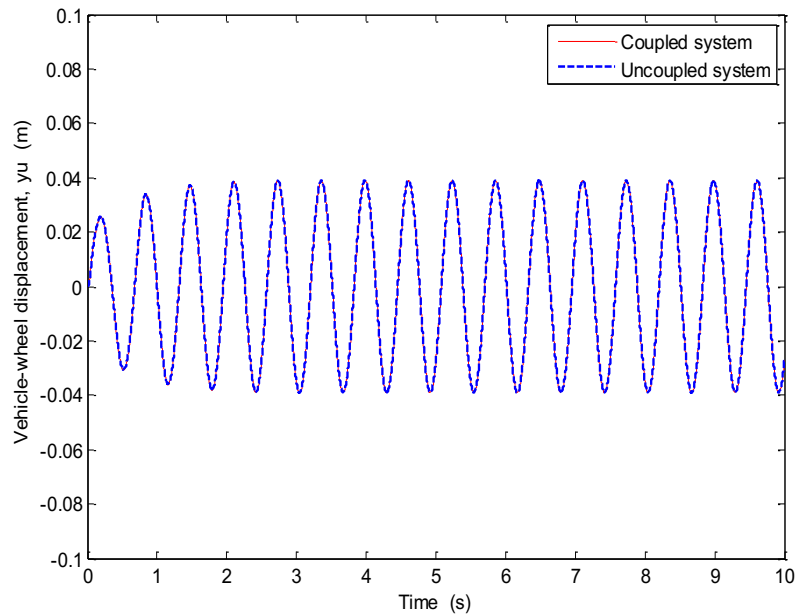


Figure 3.35 Vehicle-wheel response with  $Y_R = 0.025$  m and  $k = 40.78 \times 10^6 \text{N/m}^2$

Figure 3.36-3.38 present the vehicle-wheel response at different soil stiffness coefficients for road surface roughness amplitude of  $Y_R = 0.054$  m. Results show that maximum vehicle-wheel displacement for coupled system decreases by 0.65% and 0.33% compared with that of conventional system for small and medium soil stiffness coefficients, respectively, while it increases for large soil stiffness coefficient, which confirms again that the effect of coupling action on vehicle-wheel response decreases with the increase in soil stiffness at a large roughness of road surface ( $Y_R = 0.054$  m).

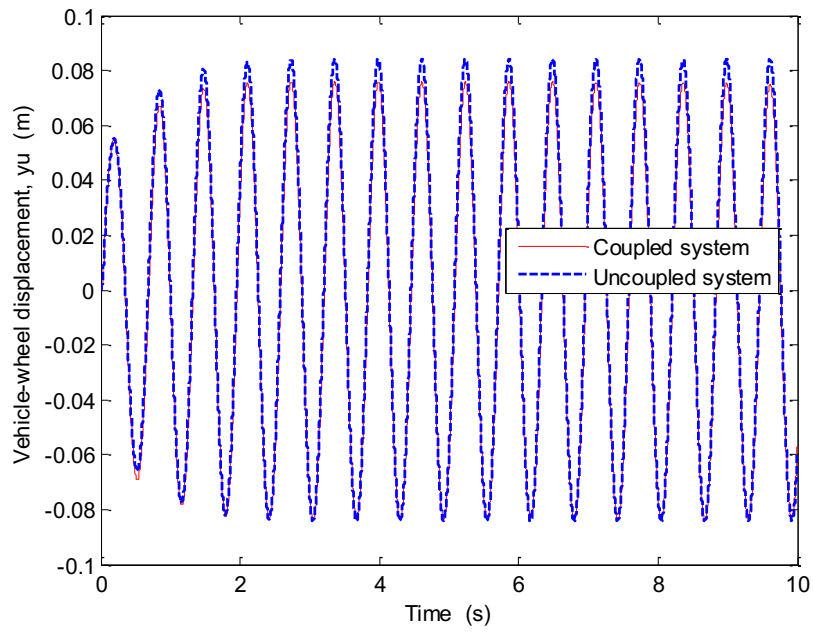


Figure 3.36 Vehicle-wheel response with  $Y_R = 0.054$  m and  $k = 40.78 \times 10^4$  N/m/m

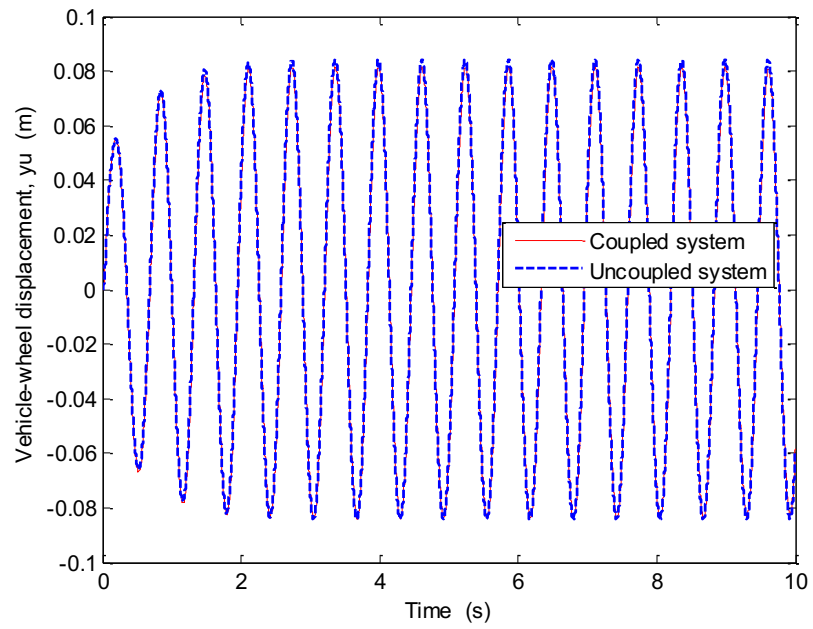


Figure 3.37 Vehicle-wheel response with  $Y_R = 0.054$  m and  $k = 40.78 \times 10^5$  N/m/m

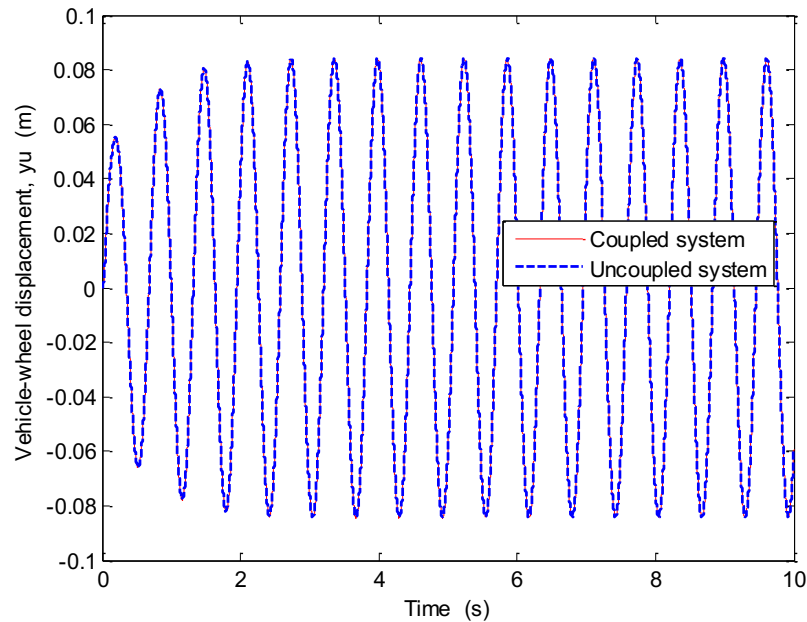


Figure 3.38 Vehicle-wheel response with  $Y_R = 0.054$  m and  $k = 40.78 \times 10^6$  N/m/m

### 3.4.3 Effect of Coupling Action on Dynamic Interaction Force

Figures 3.39-3.41 show interaction force response with  $Y_R = 0.002$  m at different soil stiffness coefficients. As it can be realized by considering coupling action the maximum interaction force amplitude reduces by 5% for small soil stiffness coefficient as shown in Figure 3.39. However it has been found that this amplitude reduces by 1.16%, and increases by 0.04% considering medium and large soil stiffness, as shown in Figures 3.40 and 3.41, respectively. Thus, for small surface roughness amplitude the effect of coupling action on the interaction force becomes smaller with increasing soil stiffness.

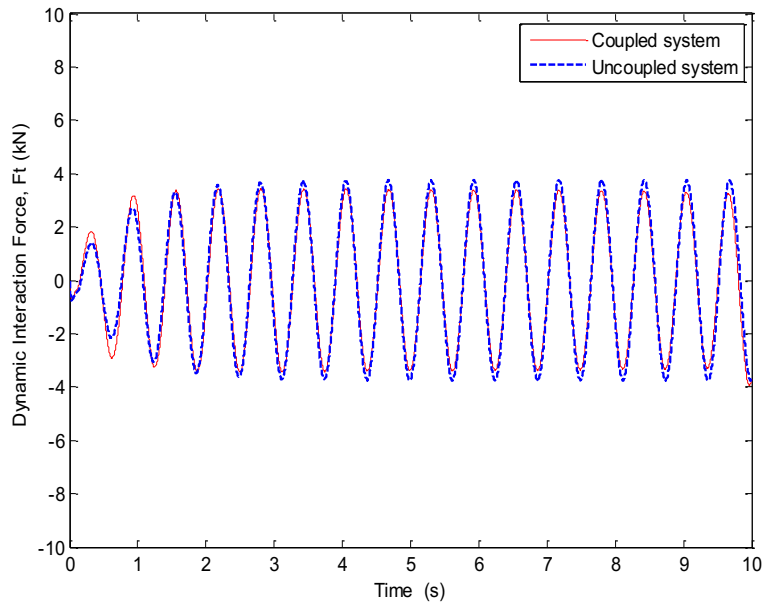


Figure 3.39 Dynamic response of interaction load with  $Y_R = 0.002$  m and  $k = 40.78 \times 10^4$  N/m/m

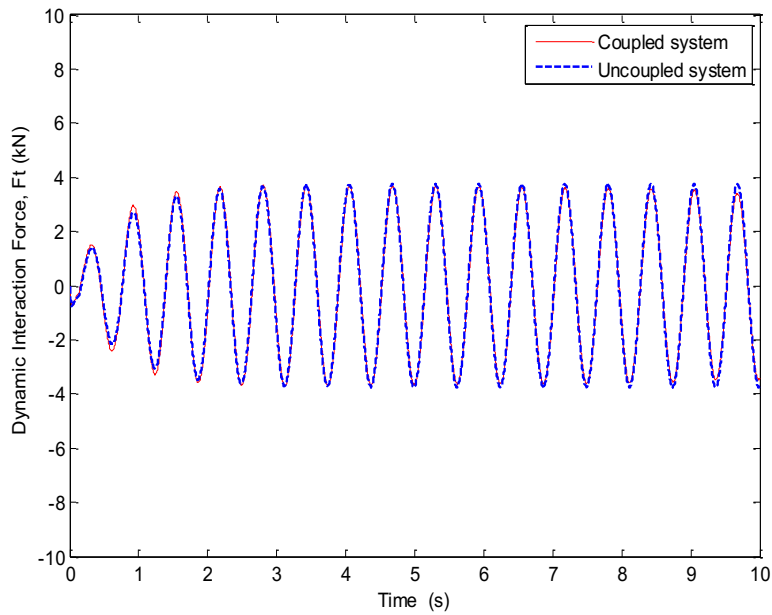


Figure 3.40 Dynamic response of interaction load with  $Y_R = 0.002$  m and  $k = 40.78 \times 10^5$  N/m/m

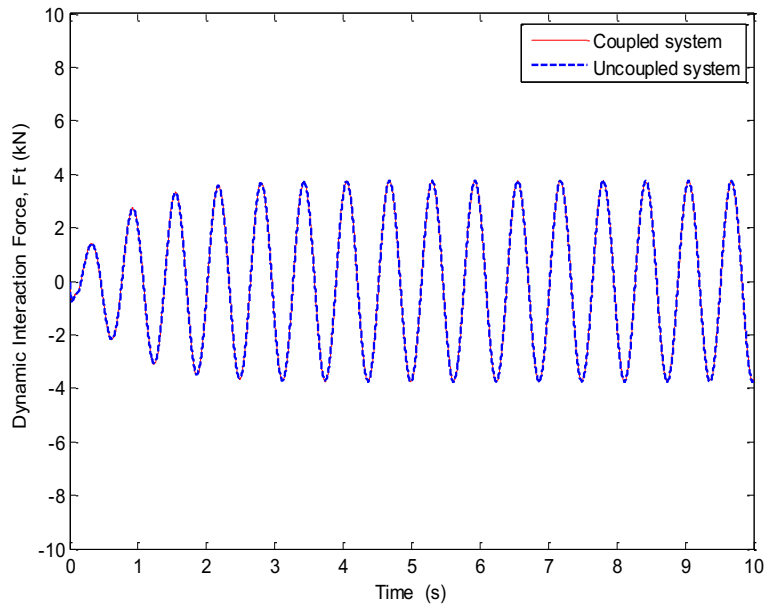


Figure 3.41 Dynamic response of interaction load with  $Y_R = 0.002$  m and  $k = 40.78 \times 10^6$  N/m/m

By increasing road surface roughness amplitude to  $Y_R = 0.025$  m the amplitude of dynamic interaction force for coupled system reduces by 3.5% and 1.7% considering small and medium soil stiffness coefficients, respectively, as shown in Figure 3.42 and Figure 3.43. However, it has been observed that the force amplitude increases slightly by 0.01% for large soil stiffness as shown in Figure 3.33. As a result, increasing road roughness amplitude leads to the decrease in the effect of coupling action on the interaction force.

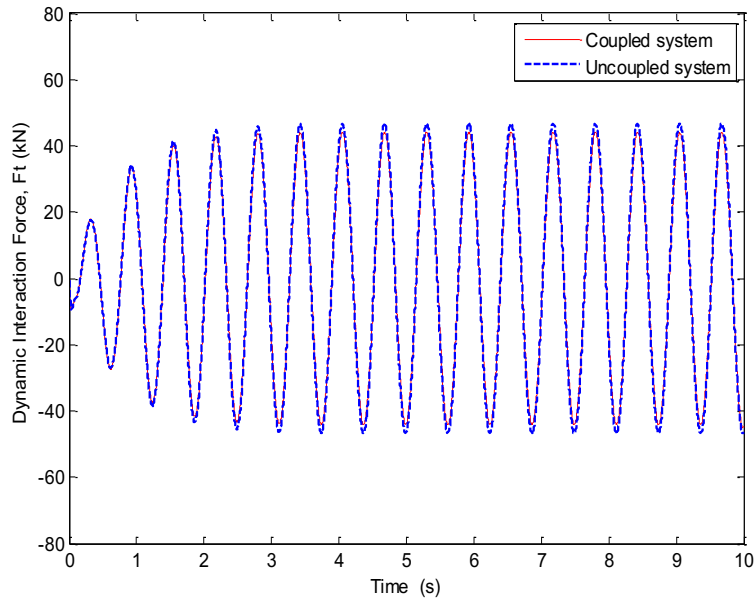


Figure 3.42 Dynamic response of interaction load with  $Y_R = 0.025$  m and  $k = 40.78 \times 10^4$  N/m/m

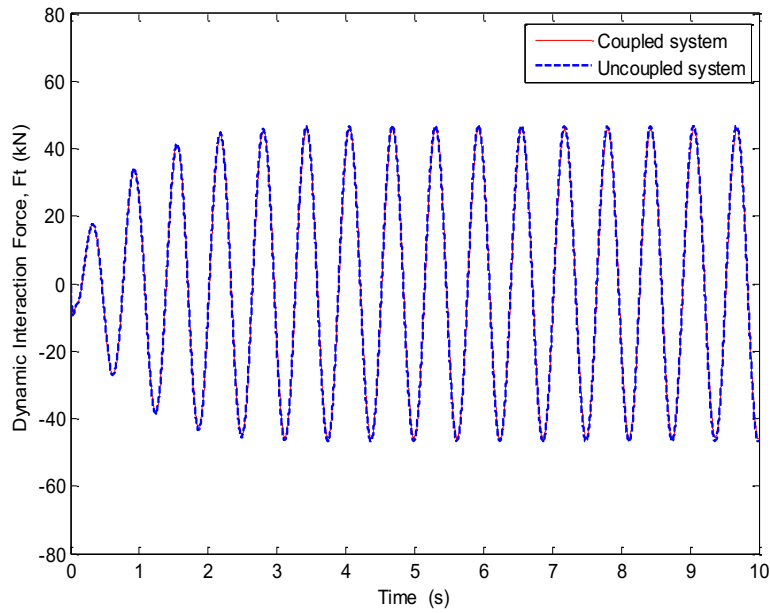


Figure 3.43 Dynamic response of interaction load with  $Y_R = 0.025$  m and  $k = 40.78 \times 10^5$  N/m/m

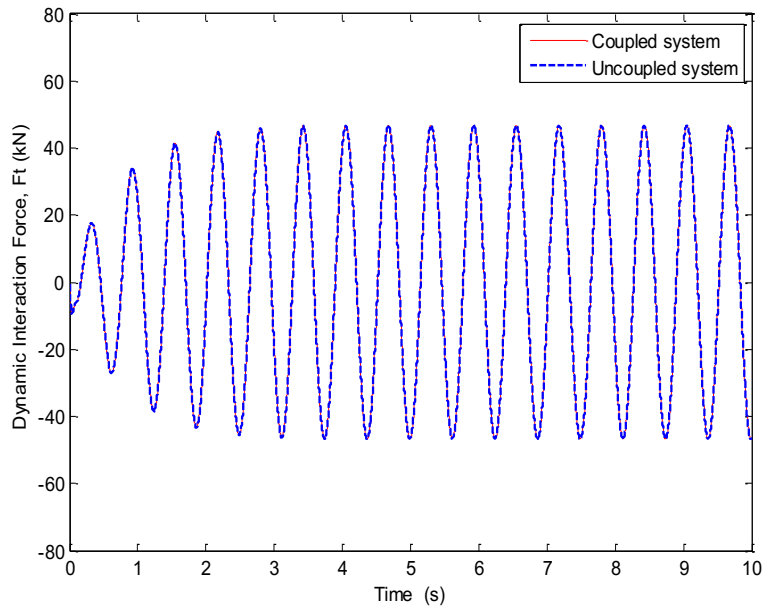


Figure 3.44 Dynamic response of interaction load with  $Y_R = 0.025$  m and  $k = 40.78 \times 10^6$  N/m/m

For road surface amplitude of  $Y_R = 0.054$  m, it is found that the force amplitude for coupled system is 3.7% and 1.4% smaller than that of conventional system for small and medium stiffness coefficient, respectively, as shown in Figures 3.45 and 3.46. While the force amplitude for coupled system becomes 0.01% greater compared with conventional system for large soil stiffness coefficient, as shown in Figure 3.47. Thus increasing the road surface amplitude from medium to large did not affect considerably on the coupling action.

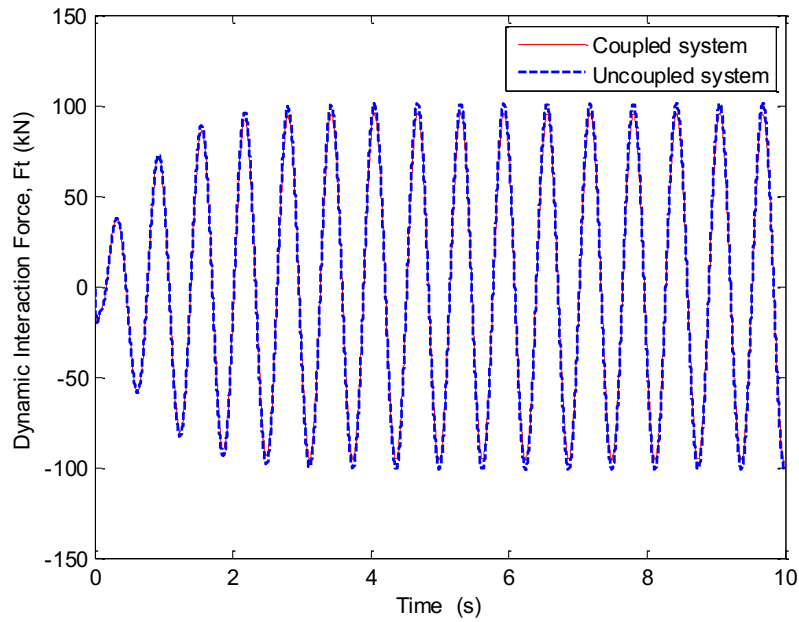


Figure 3.45 Dynamic response of interaction load with  $Y_R = 0.054$  m and  $k = 40.78 \times 10^4$  N/m/m

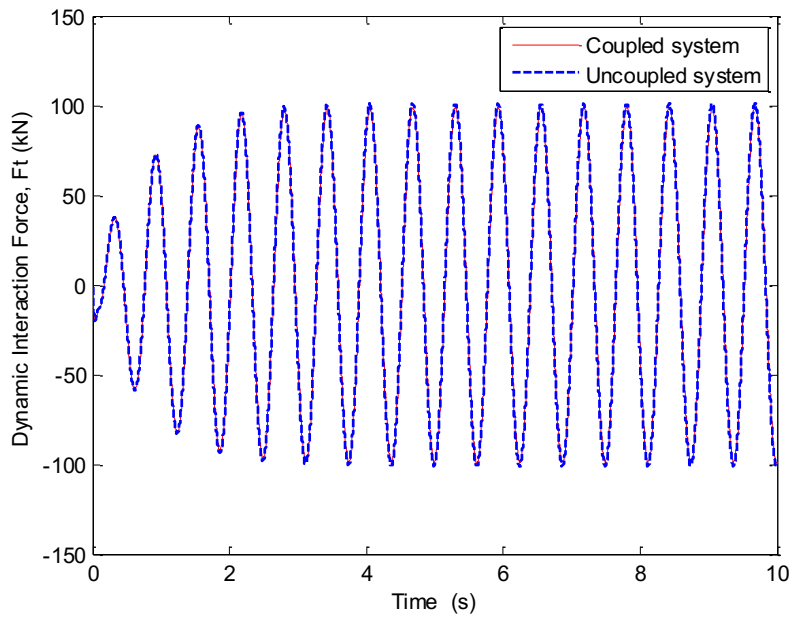


Figure 3.46 Dynamic response of interaction load with  $Y_R = 0.054$  m and  $k = 40.78 \times 10^5$  N/m/m

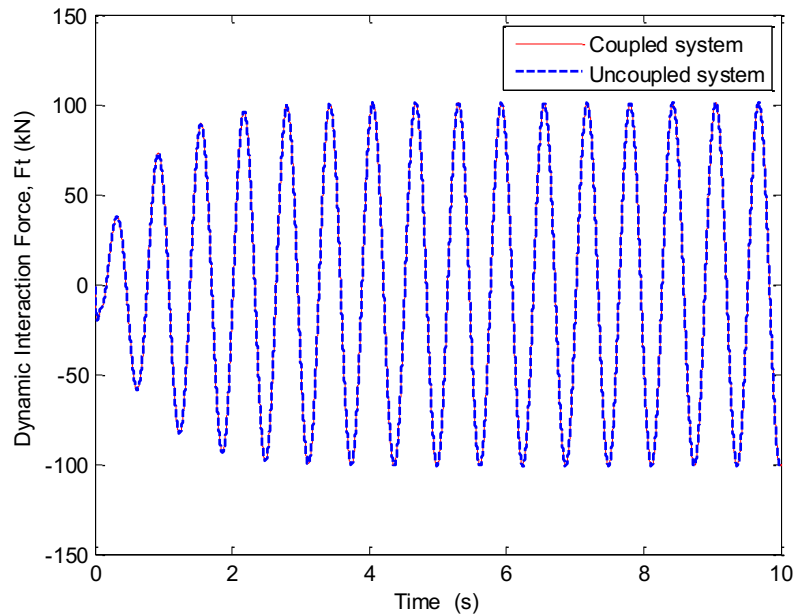


Figure 3.47 Dynamic response of interaction load with  $Y_R = 0.054$  m and  $k = 40.78 \times 10^6$  N/m/m

### 3.4.4 Effect of Coupling Action on Pavement Displacement

Figures 3.48-3.50 show the pavement displacement with  $Y_R = 0.002$  m at different soil stiffness coefficients. Results show that the pavement displacement amplitude decreases by 0.09% after considering the coupling action for small soil stiffness coefficient as shown in Figure 3.48. However for the pavement response in contrast to the vehicle response, the effect of coupling between the vehicle and pavement is more pronounced as the soil stiffness increases. For instance, by considering the coupling effect the amplitude of pavement displacement increases by 5.6% and 7.1% for the medium and large soil stiffness, respectively, as shown in Figure 3.49 and Figure 3.50. Thus, with increasing soil stiffness for small amplitude road roughness, the effect of coupling action on pavement displacement becomes greater.

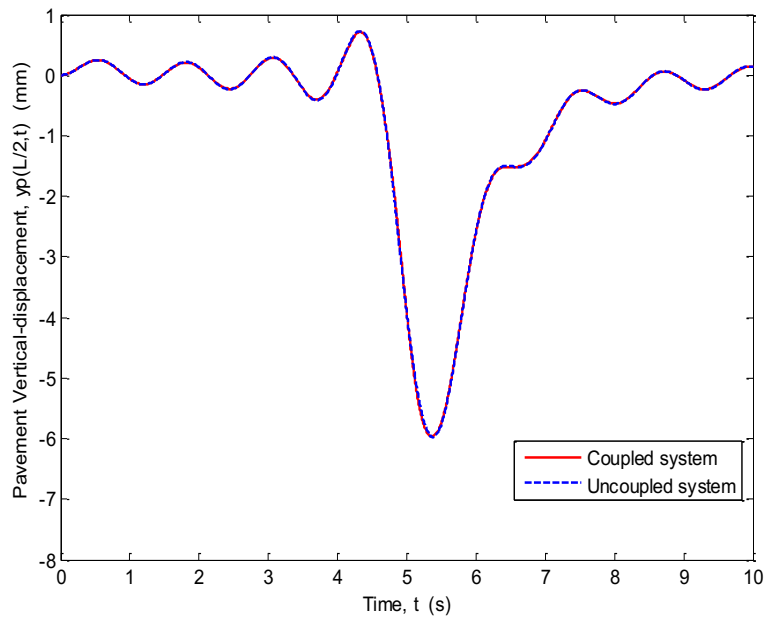


Figure 3.48 Pavement response with  $Y_R = 0.002$  m and  $k = 40.78 \times 10^4$  N/m/m

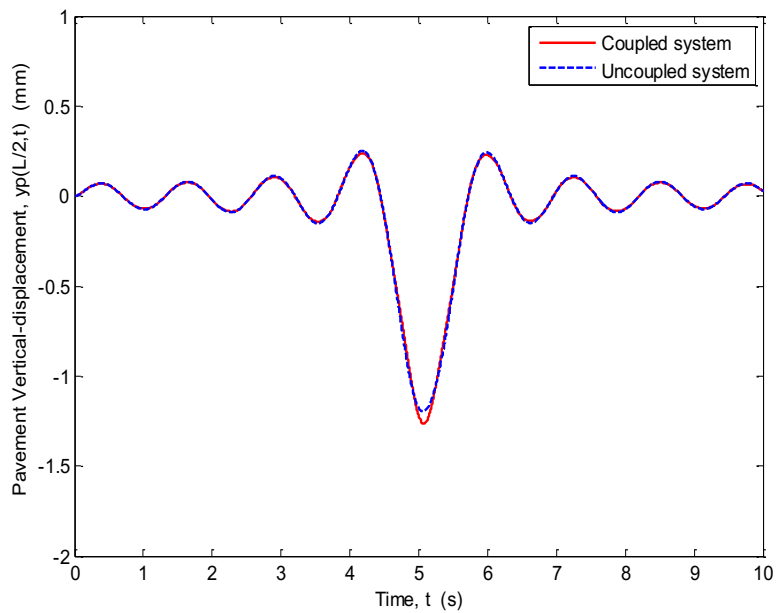


Figure 3.49 Pavement response with  $Y_R = 0.002$  m and  $k = 40.78 \times 10^5$  N/m/m

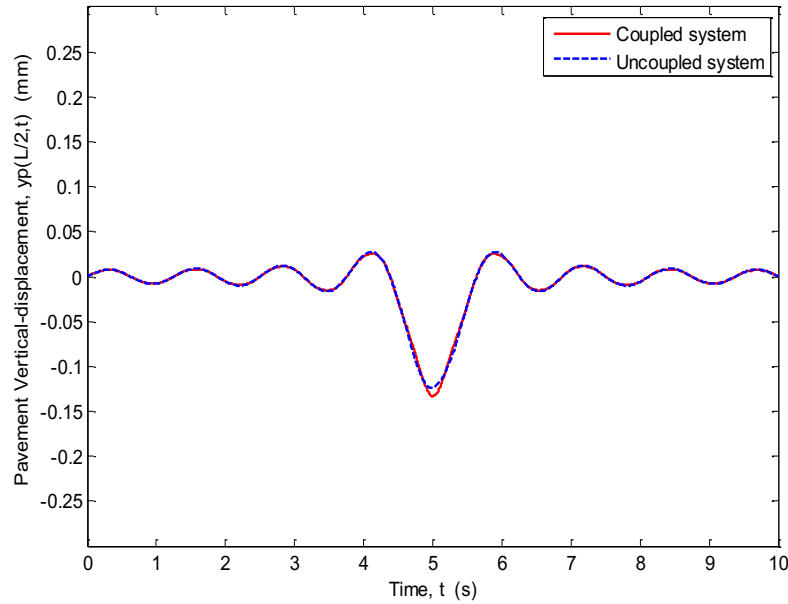


Figure 3.50 Pavement response with  $Y_R = 0.002$  m and  $k = 40.78 \times 10^6$  N/m/m

Similarly, figures 3.51-3.56 show the pavement response with road surface amplitude of  $Y_R = 0.025$  m and  $Y_R = 0.054$  m at different soil stiffness coefficients. The results indicate that the pavement displacement increases significantly with the increase in soil stiffness and road roughness considering the coupling action between the pavement and the vehicle. This implies that the coupling effect on the pavement response increases significantly with the increase in soil stiffness at rough surface amplitude.

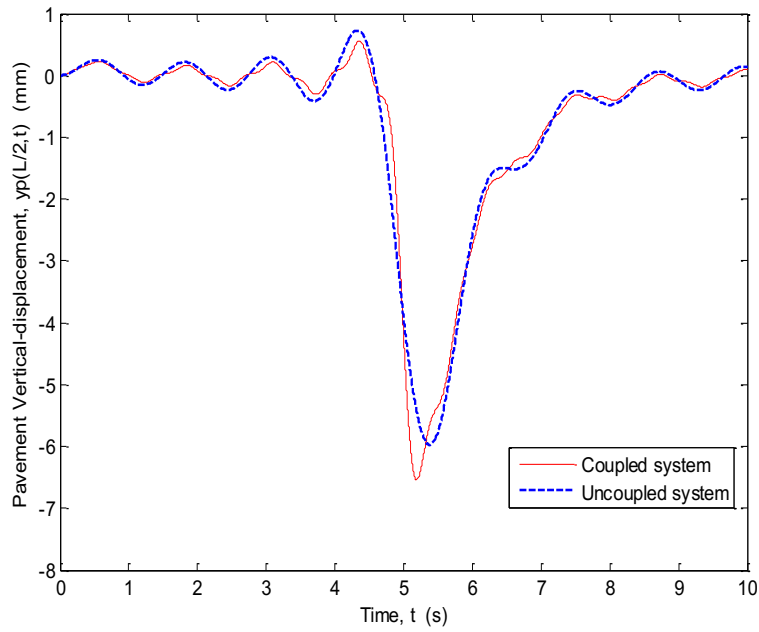


Figure 3.51 Pavement response with  $Y_R = 0.025$  m and  $k = 40.78 \times 10^4$  N/m/m

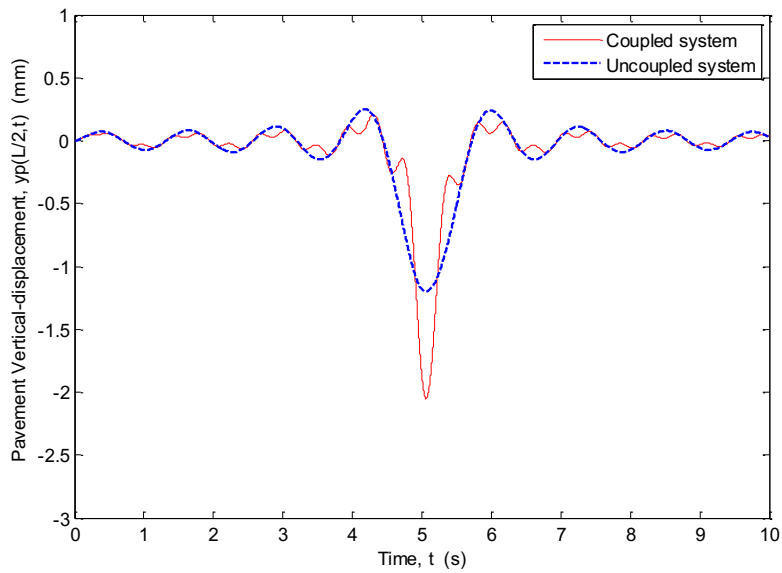


Figure 3.52 Pavement response with  $Y_R = 0.025$  m and  $k = 40.78 \times 10^5$  N/m/m

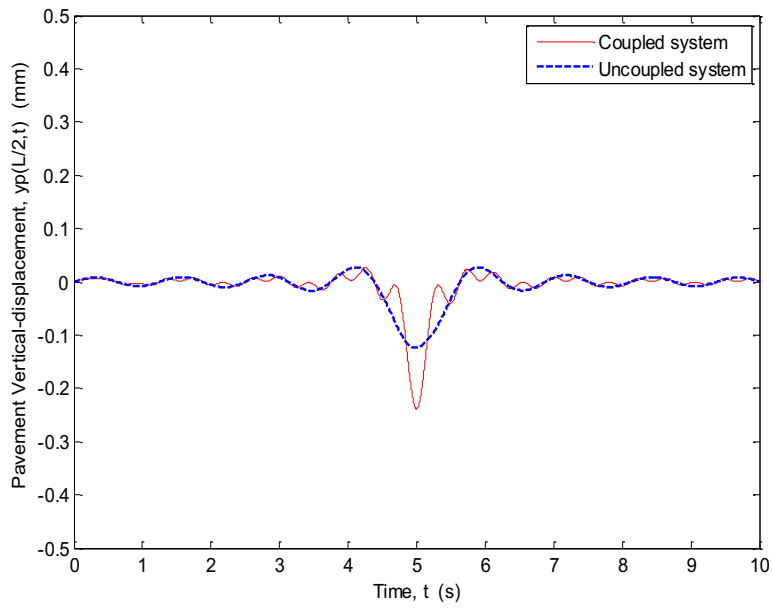


Figure 3.53 Pavement response with  $Y_R = 0.025$  m and  $k = 40.78 \times 10^6$  N/m/m

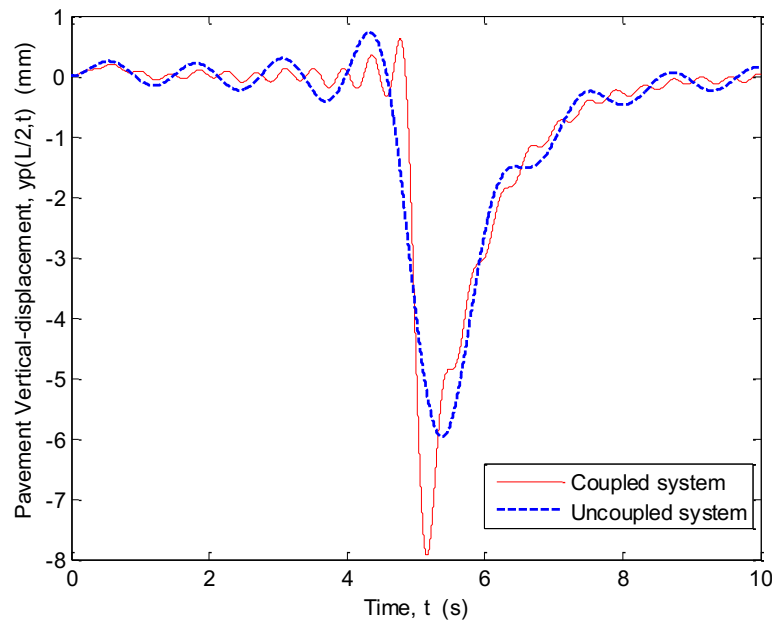


Figure 3.54 Pavement response with  $Y_R = 0.054$  m and  $k = 40.78 \times 10^4$  N/m/m

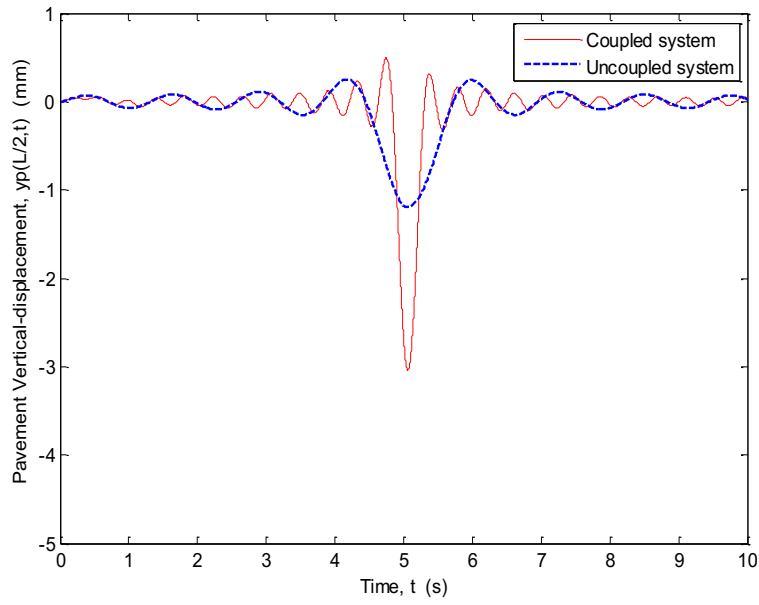


Figure 3.55 Pavement response with  $Y_R = 0.054$  m and  $k = 40.78 \times 10^5$  N/m/m

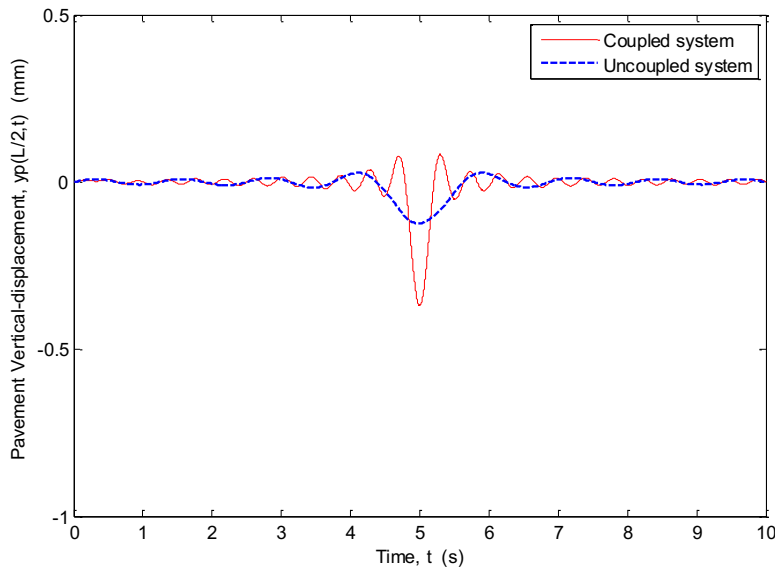


Figure 3.56 Pavement response with  $Y_R = 0.054$  m and  $k = 40.78 \times 10^6$  N/m/m

The results obtained in both analyses (coupled and uncoupled systems) for the pavement displacement results are summarized in Tables 3.11-3.14 for the sake of quantitative comparison.

Table 3.11 Variation in maximum vehicle-body displacement,  $V=16\text{m/s}$

$k$ (N/m/m)	$y_{s_{max}}$ (m)								
	$Y_R = 0.002$ m			$Y_R = 0.025$ m			$Y_R = 0.054$ m		
	Coupled	Uncoupled	%	Coupled	Uncoupled	%	Coupled	Uncoupled	%
$40.78 \times 10^4$	0.0111	0.0079	40.7	0.0970	0.0985	1.48	0.2055	0.2128	3.42
$40.78 \times 10^5$	0.0089	0.0079	13.4	0.0979	0.0985	0.61	0.2101	0.2128	1.20
$40.78 \times 10^6$	0.0080	0.0079	1.59	0.0986	0.0985	0.13	0.2129	0.2128	0.07

Table 3.12 Variation in maximum vehicle-wheel displacement,  $V=16\text{m/s}$

$k$ (N/m/m)	$y_{u_{max}}$ (m)								
	$Y_R = 0.002$ m			$Y_R = 0.025$ m			$Y_R = 0.054$ m		
	Coupled	Uncoupled	%	Coupled	Uncoupled	%	Coupled	Uncoupled	%
$40.78 \times 10^4$	0.0074	0.0031	138	0.0408	0.0390	4.4	0.0837	0.0843	0.65
$40.78 \times 10^5$	0.0042	0.0031	36.1	0.0395	0.0390	1.2	0.0840	0.0843	0.33
$40.78 \times 10^6$	0.0032	0.0031	4	0.0391	0.0390	0.3	0.0844	0.0843	0.17

Table 3.13 Variation in maximum interaction force,  $V=16\text{m/s}$

$k$ (N/m/m)	$F_{t_{max}}$ (kN)								
	$Y_R = 0.002$ m			$Y_R = 0.025$ m			$Y_R = 0.054$ m		
	Coupled	Uncoupled	%	Coupled	Uncoupled	%	Coupled	Uncoupled	%
$40.78 \times 10^4$	3.9273	3.7402	5	45.1328	46.7527	3.5	97.1992	100.98	3.7
$40.78 \times 10^5$	3.6965	3.7402	1.16	45.9625	46.7527	1.7	99.5606	100.98	1.4
$40.78 \times 10^6$	3.7417	3.7402	0.04	46.7588	46.7527	0.01	100.99	100.98	0.01

Table 3.14 Variation in maximum Pavement deflection at mid-span,  $V=16\text{m/s}$

$k$ (N/m/m)	$y_{pmax}$ (mm)								
	$Y_R = 0.002$ m			$Y_R = 0.025$ m			$Y_R = 0.054$ m		
	Coupled	Uncoupled	%	Coupled	Uncoupled	%	Coupled	Uncoupled	%
$40.78 \times 10^4$	5.9653	5.9708	0.09	6.5425	6.000	9.5	7.9369	5.9708	33
$40.78 \times 10^5$	1.2653	1.1976	5.6	2.0518	1.20	71.3	3.0449	1.1976	154
$40.78 \times 10^6$	0.1329	0.1241	7.1	0.2379	0.13	83	0.3703	0.1241	198

### 3.5 Summary

In this chapter, the coupled governing equations developed in Chapter 2 have been numerically solved using implicit Newmark time integration technique for the road surface roughness profile modeled as a sinusoidal function. The effect of coupling action on pavement and vehicle responses in both analyses (coupled and uncoupled systems) due to the variations in soil stiffness coefficient, roughness amplitude, speed and suspension damping is systematically investigated. The results reveal that the peak values of the coupled system responses occur at critical velocity around 16 m/s for the first peak and 82 m/s for the second peak which slightly increases with the increase in soil stiffness. Moreover, the coupled system responses decrease with the increase in suspension damping. Thus, tuning the suspension of the vehicle is one possible way to control and mitigate the response peak values. Furthermore, the pavement deflection reaches its maximum value at a location close to the position where the load is applied, and decreases farther away from the load. In addition, on smooth road and soft soil, the coupling action affects vehicle dynamics most significantly, while the effect of coupling action on pavement dynamics is very small. On rough road and hard soil the coupling action affects pavement dynamics most significantly, while the effect of coupling action on vehicle dynamics becomes smaller.

Therefore, the coupling action between pavement and a moving vehicle should not be neglected even in soft soil and smooth road.

# CHAPTER 4

## Pavement Response due to Random Excitation

### 4.1 Introduction

A more realistic representation of road surface roughness is to consider roughness as a random process. In this chapter the effects of different random roadsurface roughness and vehicle speed on the pavement response due to the passage of different types of vehicles (car, bus and truck) have been investigated considering the coupling action between the pavement and the vehicles. The road roughness profiles are generated based on ISO 8608 criterion considering three different road roughnesses: very good road, average road and very poor road.

### 4.2 Classification of Road Profiles

According to the ISO 8608, the different road surface roughness profiles based on their power spectral density (PSD) with reference spatial frequency of  $n_0 = 0.1(\text{cycles/m})$  is presented in Table 4.1. Eight classes of roads are specified ranging from class A, with small degree of roughness which represents a very good road, to class H with high degree of roughness which describes a very poor road [49].

Table 4.1 Road surface roughness profiles according to ISO 8608 [49]

Road Class	$S_g(n_0) \times 10^{-6} \text{ m}^3$		ISO Description
	Lower limit	Upper limit	
A	----	32	very good
B	32	128	good
C	128	512	average
D	512	2048	poor
E	2048	8192	very poor
F	8192	32768	----
G	32768	131072	----
H	131072	----	----

$n_0 = 0.1 \text{ cycles/m}$

The PSD of the roughness profile of road surface as a function of spatial frequency can be expressed as [83, 84]:

$$S_g(n) = S_g(n_0) \left(\frac{n}{n_0}\right)^{-2} \quad (4.1)$$

where

$n$  = spatial frequency/wave number (cycles/m).

$n_0$  = reference spatial frequency ( $n_0 = 0.1 \text{ cycles/m}$ ).

$S_g(n_0)$  = degree of road roughness ( $\text{m}^3$ ) at reference spatial frequency.

### 4.3 Generation of Road Profiles

Random road elevation profile can be described by a number of simple harmonic functions with different amplitudes [49, 85] as follows:

$$y_R(x) = \sum_{i=1}^{N_t} A_i \cos(2\pi i \Delta n x + \varphi_i) \quad (4.2)$$

where

$y_R(x)$  = road elevation/random road profile

$A_i$  = amplitudes of the harmonic excitation and can be defined by

$$A_i = \sqrt{2 S_g(n_i) \Delta n} \quad (4.3)$$

$S_g(n_i)$  = road PSD

$\Delta n$  = spatial frequency step, given by:

$$\Delta n = \frac{1}{L} \quad (4.4)$$

$\varphi_i$  = the phases which are treated as random variables based on the uniform distribution in the interval  $[0, 2\pi]$ .

The total number of sample points in pavement length is assumed to be  $N_t = 1000$

Sampling interval can be expressed as

$$B = \frac{L}{N_t} \quad (4.5)$$

Using Eq. (4.1), three ISO classes of road profile are considered [Class A with  $S_g(n_0) = 32 \times 10^{-6} \text{m}^3$ , Class C with  $S_g(n_0) = 320 \times 10^{-6} \text{m}^3$  and Class E with  $S_g(n_0) = 5120 \times 10^{-6} \text{m}^3$ ].

Figure 4.1 shows generated road surface roughness profile from very good road (ISO Class A, with  $\mp 20$  mm), to average road (ISO Class C, with  $\mp 70$  mm), and very poor road (ISO Class E, with  $\mp 280$  mm)

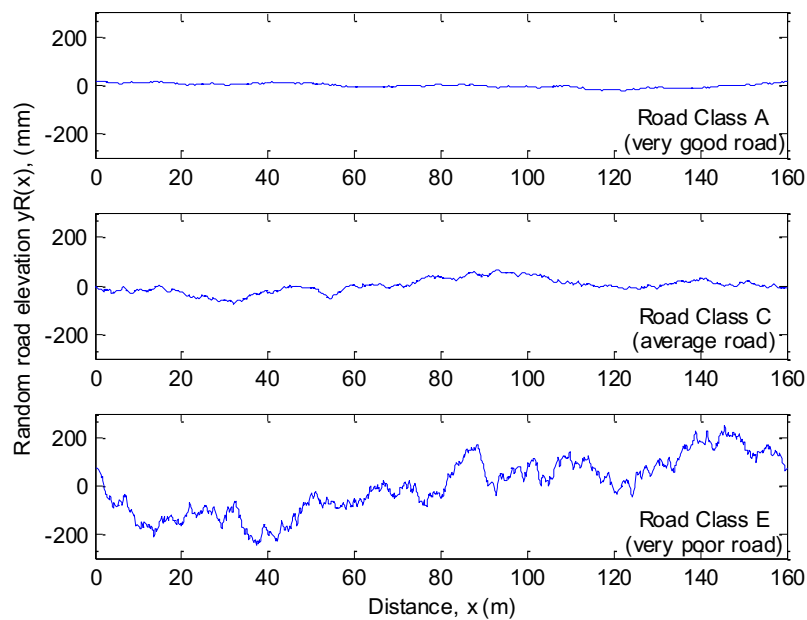


Figure 4.1 Random generated road profile for ISO Class A, C and E

#### 4.4 Effect of Road Roughness on Pavement Response due to Different Types of Vehicles

The simulation results for the pavement mid-span response  $y_p(L/2, t)$  generated by different vehicles at a speed of 16 m/s with variable ISO road profiles are presented in Figures 4.2-4.4, and the pavement peak values are provided in Table 4.3. It can be seen that for the same type of the vehicle (car, bus and truck), the maximum pavement displacement increases significantly with the increase in the degree of road roughness. For instance, the pavement peak generated by

the passage of a car is 0.0065 mm for road class A, and increases to 0.0193 mm for road class C which is approximately three times that of road class A, and for road class E, it is around four times that of road class C and is equal to 0.0764 mm. The pavement and vehicle parameters (for different configurations) are provided in Table 3.5 and 4.2, respectively.

Table 4.2 Numerical values of vehicle parameters [4, 28, 49 and 101]

Symbol	Physical quantity	Value		
		Car	Bus	Truck
$m_s$	Vehicle-body mass (Sprung mass), kg	417.6	4000	4500
$m_u$	Vehicle-wheel mass (Unsprung mass), kg	57.5	550	650
$K_s$	Suspension stiffness constant, kN/m	24.65	320	570
$K_t$	Tire stiffness constant, kN/m	200	1500	1700
$C_s$	Suspension damping constant, kN.s/m	2.287	10	21
$C_t$	Tire damping constant, kN.s/m	2	1.5	2
$V$	Vehicle speed, m/s		16	

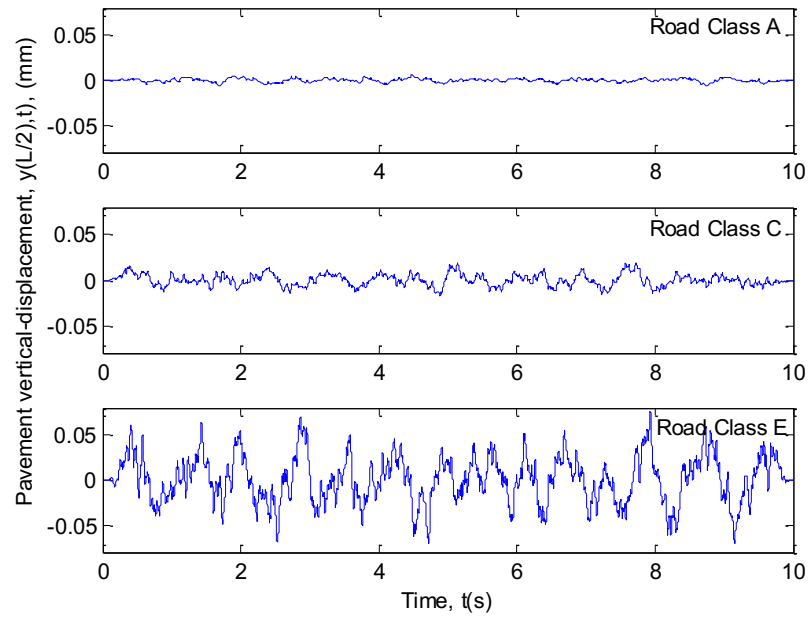


Figure 4.2 Pavement response due to the passage of a car at 16 m/s with different ISO road profiles

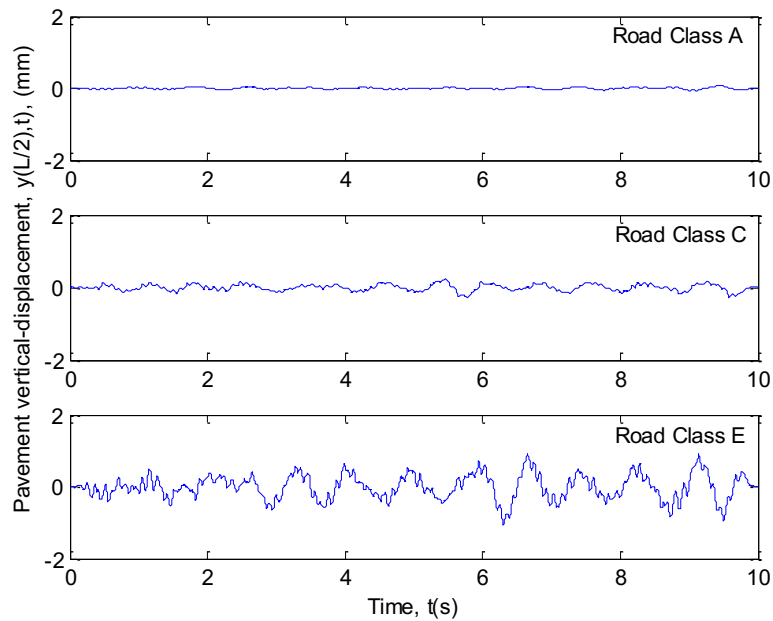


Figure 4.3 Pavement response due to the passage of a bus at 16 m/s with different ISO road profiles

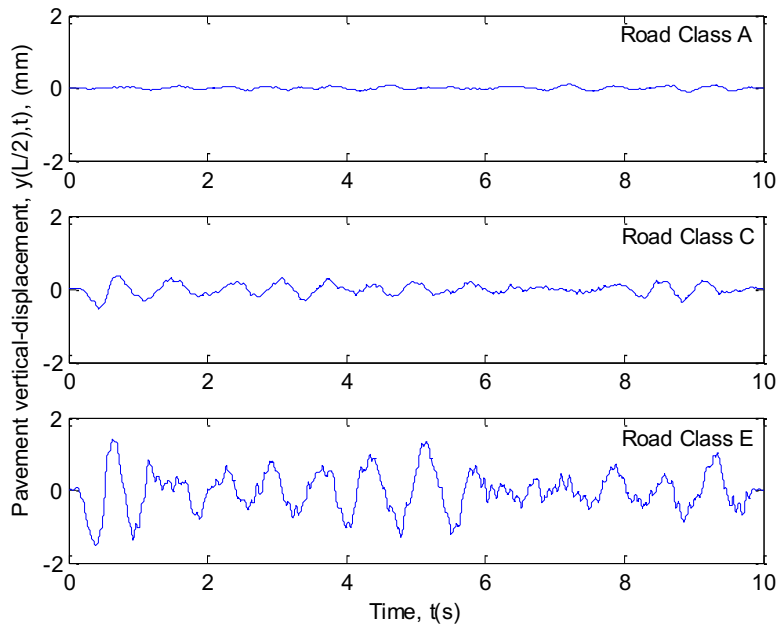


Figure 4.4 Pavement response due to the passage of a truck at 16 m/s with different ISO road profiles

The maximum pavement response values due to each type of considered vehicle at a speed of 16 m/s with variable ISO road profiles are presented in Table 4.3

Table 4.3 Maximum pavement response (mm) with different vehicles and different road profiles

ISO road profiles	Car	Bus	Truck
Class A	0.0065	0.0930	0.1156
Class C	0.0193	0.2751	0.5567
Class E	0.0764	1.0578	1.5156

### 4.5 Effect of Vehicle Speed on Pavement Response due to Different Types of Vehicles for ISO Road Profile Class C

Figures 4.2-4.4 show the pavement mid-span response  $y_p(L/2, t)$  generated by different vehicles at different speeds (10, 15, 20, 25 and 30 m/s) for ISO road profile class C. It can be seen for each vehicle type and the same road profile that the pavement displacement increases slightly with the increase in the vehicle speed (Table 4.4).

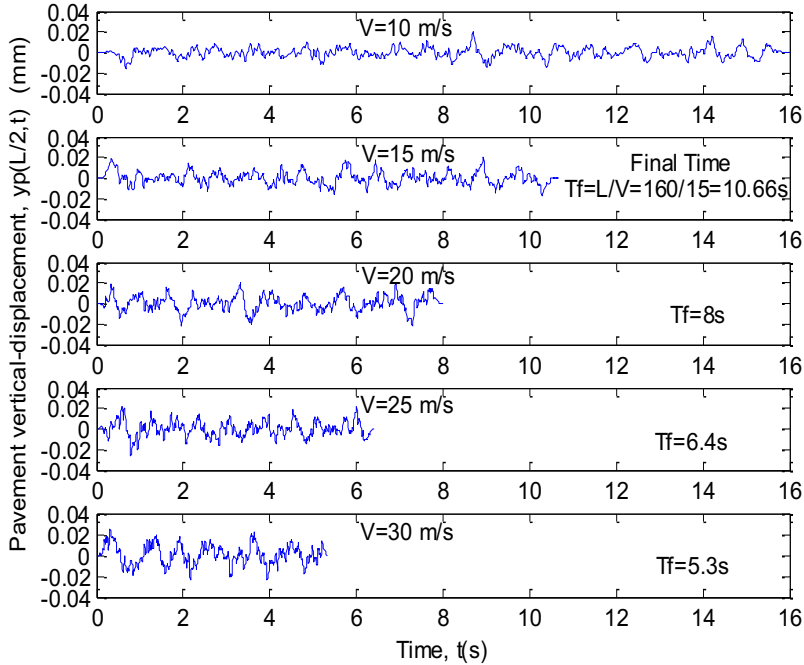


Figure 4.5 Pavement response due to the passage of a car with different speeds for ISO road profile class C

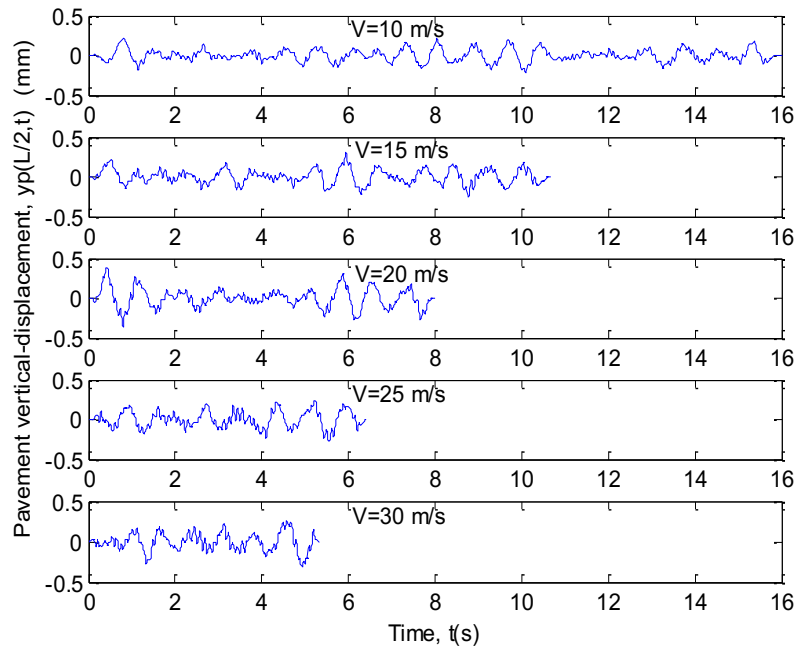


Figure 4.6 Pavement response due to the passage of a bus with different speeds for ISO road profile class C

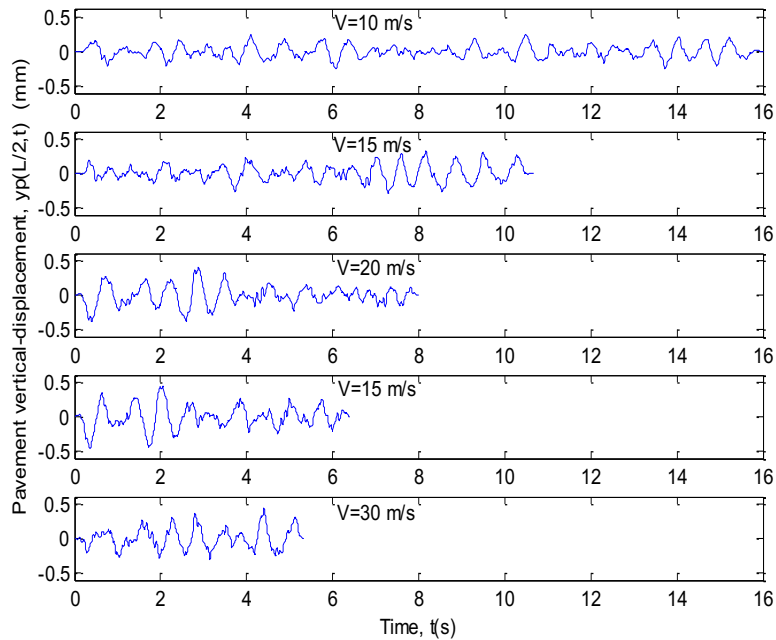


Figure 4.7 Pavement response due to the passage of a truck at different speeds for ISO road profile class C

The maximum pavement response values due to each type of vehicle at different speeds for ISO road profile class C are given in Table 4.4 for comparison.

Table 4.4 Maximum pavement response (mm) with different vehicles at different speeds for ISO road profile class C

Vehicle Speed (m/s)	Car	Bus	Truck
10	0.0197	0.2155	0.2493
15	0.0203	0.2629	0.3179
20	0.0221	0.3439	0.4047
25	0.0268	0.3739	0.4558
30	0.0251	0.2850	0.4305

#### **4.6 Effect of Vehicle Types on Pavement Response at Constant Speed for ISO Road Profile Class C**

In order to examine the effects of vehicle types (car, bus and truck) on pavement response a road profile class C has been selected with driving speeds of 10, 15, 20, 25 and 30 m/s (36, 54, 72, 90 and 108 km/h, respectively). Certain values of speed can determine resonance conditions where the natural frequencies for the vertical motion of the vehicle-body are located in a range of values between 6-25 rad/s (1 and 4 Hz), while the vehicle-wheel moves vertically faster and its natural frequency is approximately equal to 60 rad/s (10 Hz). Results are shown in Figures 4.8-4.11 for different vehicle speeds, and summarized in Table 4.5. It has been found that for the same degree of road roughness the effect of vehicle type on the pavement response at the same speed is more pronounced. For instance, at 15 m/s the maximum pavement displacement

generated by the passage of a car is 0.0228 mm, for a bus is 0.2005 mm approximately 9 times that of the car, and for the truck is around 0.5098 mm, about twice than that of the bus.

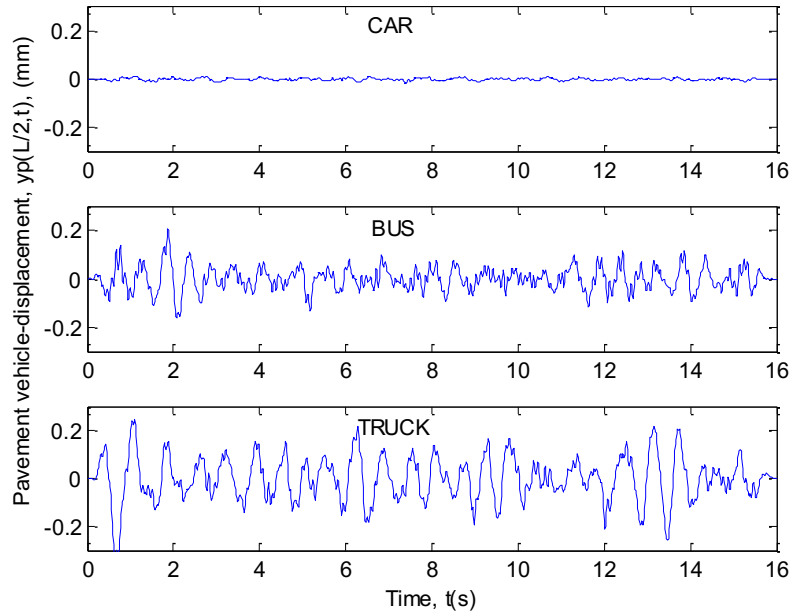


Figure 4.8 Pavement response due to different vehicles at 10 m/s for ISO road profile class C

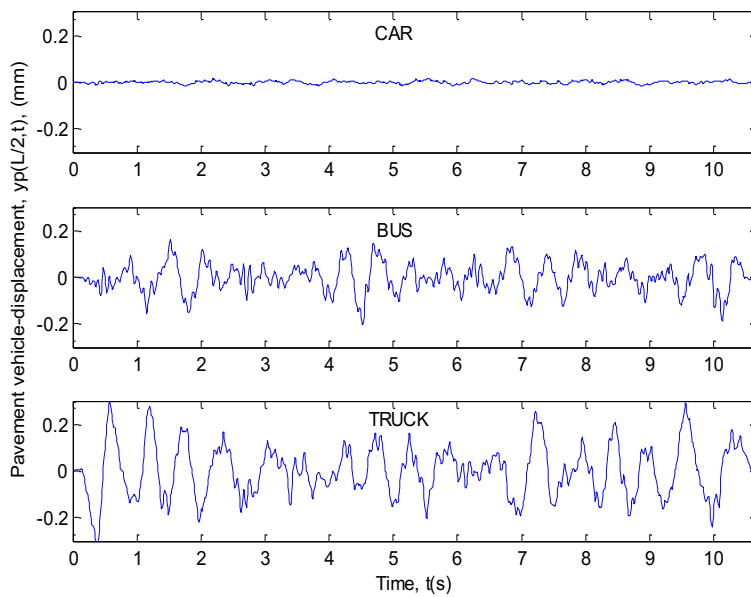


Figure 4.9 Pavement response due to different vehicles at 15 m/s for ISO road profile class C

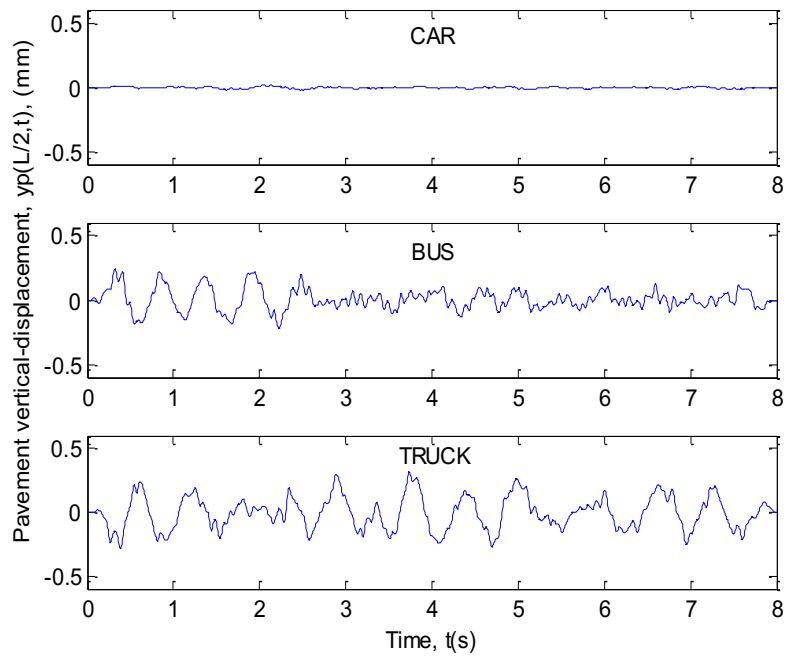


Figure 4.10 Pavement response due to different vehicles at 20 m/s for ISO road profile class C

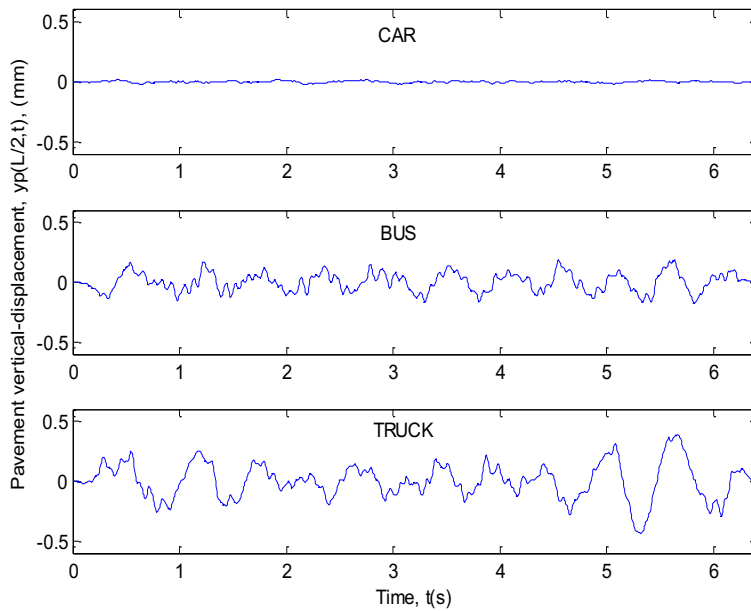


Figure 4.11 Pavement response due to different vehicles at 25 m/s for ISO road profile class C

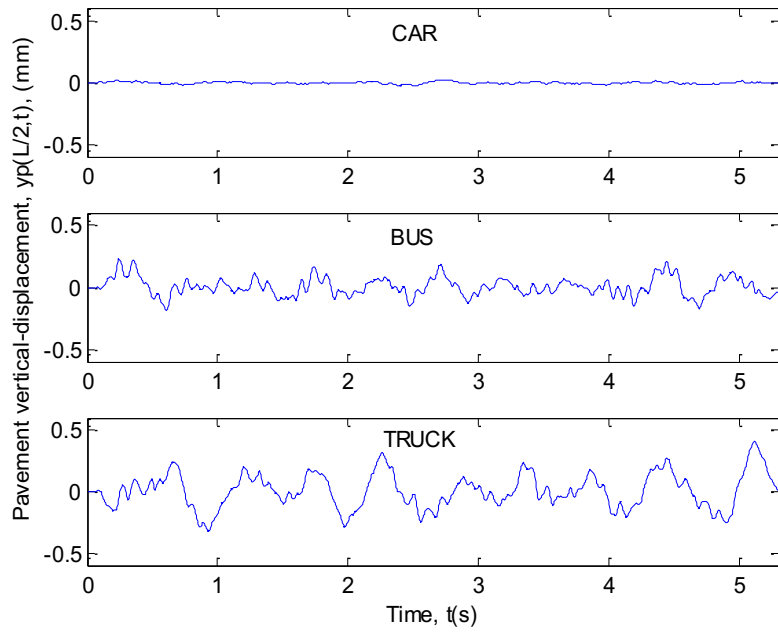


Figure 4.12 Pavement response due to different vehicles at 30 m/s for ISO road profile class C

Table 4.5 Peak response (mm) with different vehicles for ISO road profile class C

Vehicle Speed (m/s)	Car	Bus	Truck
10	0.0185	0.2072	0.3401
15	0.0228	0.2005	0.5098
20	0.0223	0.2399	0.3216
25	0.0218	0.1846	0.4395
30	0.0280	0.2307	0.4127

## **4.7 Summary**

In this chapter the passage of three types of vehicles (car, bus and truck) on random road surface roughness have been considered to investigate the dynamic behavior of the flexible pavement. Based on ISO 8608 standard, the random road roughness profiles are generated using three different classes of road roughness describing very good road (ISO Class A), average road (ISO Class C) and very poor road (ISO Class E). Effects of vehicle types, speed, and road surface roughness on the pavement response have been obtained considering the coupling action between the vehicle and the pavement. The results reveal that the effect of the vehicle type is significant and increases with the increase in road roughness. Moreover, the effect of vehicle speed is related to the degree of roughness, in other words the speed influence increases with the increase in road roughness and vice versa.

# CHAPTER 5

## Damage Model and Pavement Distress

### 5.1 Introduction

Distress in flexible pavements has been a problem due to the increase in road traffic and vehicle speeds and loads. One of the most important distress modes in the design and analysis of pavements is fatigue cracking. The fatigue cracking level of the pavement is determined by the stresses and strains produced in the pavement structure due to traffic loads. Despite the fact that there have been considerable efforts in recent years in fatigue performance evaluation and the design process of flexible pavements, there is still a need for further studies to overcome the difficulty in predicting fatigue cracking in terms of damage distribution considering the uncertainty associated with the input parameters of pavement life and traffic repetitions. In this chapter, a methodology has been developed for modeling pavement damage and predicting fatigue cracking of flexible pavements based on a combination of deterministic method and stochastic approach using Palmgren-Miner's hypothesis based on Poisson process to characterize the actual load of traffic arrivals. Four pavement damage models are presented for a case study to estimate the damage and predict fatigue cracking of the pavement surface layer: two proposed models (model 1 and model 2) are compared with two models (models 3 and 4) proposed by previous researchers. The solutions are obtained through numerical integration based on Gaussian quadrature method using a computer program developed in the Matlab environment.

## 5.2 Pavement Damage and Predicting Fatigue Cracking Formulations

According to the previous studies, the general fatigue damage equation used to predict fatigue cracking life of flexible pavements can be described as [86]:

$$Y = k_1 \left( \frac{1}{\varepsilon_t} \right)^{k_2} \left( \frac{1}{E} \right)^{k_3} \quad (5.1)$$

where

$Y$  = total number of load repetitions to cause failure.

$\varepsilon_t$  = maximum tensile strain at the bottom of asphalt layer ( $\varepsilon_t = 3.45 \times 10^{-4}$ ).

$E$  = Young's modulus of elasticity of asphalt layer ( $E = 3654.22$  MPa).

$k_j$  = laboratory material coefficient ( $j = 1, 2, 3$ )

The Asphalt Institute model [86] is adopted in this study including a correction factor that expresses the uncertainty in the calculation model ( $k_1 = 1.135 \times 10^{-3}$ ,  $k_2 = 3.291$  and  $k_3 = 0.854$ ).

Fatigue is considered as a damage accumulation process in which the material property deteriorates continuously under the application of loads. According to Palmgren-Miner's hypothesis, the damageindex can be expressed as:

$$D = \frac{X}{Y} \quad (5.2)$$

where

$D$  = Damageindex of fatigue cracking

$X$  = equivalent number of actual traffic load repetitions applied over the design period of the road section

Considering a traffic growth,  $X$  can be predicted as follows [87, 88, and 89]:

$$X = 365 A \times \left[ \frac{(1 + r_t)^{y_t} - 1}{r_t} \right] \times F_L \times L_f \quad (5.3)$$

where

$A$  = average annual commercial vehicle per day (250 cvpd).

$r_t$  = annual traffic growth rate ( $r_t = 0.07$ ).

$y_t$  = design period (one year).

$L_f$  = lateral distribution factor ( $L_f = 0.75$ ).

$F_L$  = used to convert the different vehicular loads into a common axle load ( $F_L = 2.33$ ).

The damage index  $D$  is considered as the ratio of two random variables  $X$  and  $Y$  whose joint probability function is defined as:

$$f_{X,Y}(x, y) = P(X = x, Y = y) \quad (5.4)$$

where  $x > 0, y > 0$ .  $f_{X,Y}(x, y)$  represents the probability that events  $X$  and  $Y$  occur at the same time.

Since the actual number of traffic load repetitions  $X$  is statistically independent of the traffic repetitions to cause failure  $Y$ , the joint probability of  $X$  and  $Y$  can be obtained by:

$$f_{X,Y}(x, y) = f_X(x) f_Y(y) \quad (5.5)$$

where  $f_X(x)$  and  $f_Y(y)$  are the probability density functions (PDF) of  $X$  and  $Y$ , respectively.

The cumulative distribution function (CDF) of the fatigue damage  $D$  is given by:

$$F_D(d) = P(D \leq d) = P\left(\frac{X}{Y} \leq d\right) = P(X \leq Yd) \quad (5.6)$$

Since  $X$  and  $Y$  are non-negative random variables, then CDF of  $D$  can be computed as follows:

$$F_D(d) = \int_0^{\infty} \int_0^{Yd} f_{X,Y}(x, y) dx dy = \int_0^{\infty} \int_0^{Yd} f_X(x) f_Y(y) dx dy \quad (5.7)$$

It is known that the PDF of  $D$  can be obtained by differentiating the CDF of  $D$  as:

$$f_D(d) = \frac{\partial F_D(d)}{\partial d} \quad (5.8)$$

$$f_D(d) = \int_0^{\infty} \left( \frac{\partial}{\partial d} \int_{x=0}^{Yd} f_X(x) dx \right) f_Y(y) dy \quad (5.9)$$

$$f_D(d) = \int_0^{\infty} y f_X(Yd) f_Y(y) dy = \int_0^{\infty} y f_{X,Y}(Yd, y) dy \quad (5.10)$$

According to Miner's law, fatigue cracking takes place when damage index  $D$  reaches or exceeds unity. Therefore, the fatigue cracking, FC, can be defined as the probability to have a damage index greater than 1. This can be mathematically expressed as:

$$FC = P(D > 1) = 1 - P(D \leq 1) \quad (5.11)$$

$$FC = \int_1^{\infty} f_D(d)dd = 1 - \int_0^1 f_D(d)dd \quad (5.12)$$

### 5.3 Pavement Damage Distribution Models

In order to evaluate the fatigue cracking as given by Eq. (5.12), the probability distribution of the damage index  $D$  is required which are generally unknown, although the majority of the previous research works [87, 88, 89 and 90] assumed that the pavement damage is either normally or lognormally distributed. In this study, two pavement damage models (*Models 1* and *2*) based on Poisson distribution to characterize the actual traffic load arrivals have been proposed and compared with previous assumed models (*Models 3* and *4*).

#### 5.3.1 Damage Model 1

The Poisson process is considered as one of the most counting processes used worldwide. It is usually used in cases of counting the occurrences of certain events that happen randomly at a certain rate. For example, the Poisson process might be a good model for representing the arrival of telephone calls per hour received by an office, the number of days school is closed due to snow during the winter, customer arrivals in a bank counter, or arrival of cars to a gas station, and arrival of customers to a convenience store [91, 92, and 93]. Therefore, considering the fact that the traffic load arrivals at a given point on the pavement occur independently of one another and as a counting process, a Poisson process model is a more realistic description of the vehicle traffic, that is  $X \sim \text{Pois}(\lambda_X)$ , and the corresponding probability mass function (PMF) of  $X$  can be expressed as follows:

$$f_X(x) = \frac{e^{-\lambda_x} \lambda_x^x}{x!} \quad (5.13)$$

where  $\lambda_x$  is the expected number of occurrences (mean).

Assuming that the mean is a large value, the Poisson distribution can be approximated by a normal distribution [94] with mean and variance as independent parameters defined as:

$$\lambda_x = \mu_x = \sigma_x^2 \quad (5.14)$$

where

$\mu_x$  = mean value of  $X$

$\sigma_x^2$  = variance of  $X$

The probability density function (PDF) of  $X$ , then, becomes

$$f_X(x) = \frac{1}{\sqrt{2\pi \lambda_x}} e^{-\frac{1}{2} \left( \frac{x-\lambda_x}{\sqrt{\lambda_x}} \right)^2} \quad (5.15)$$

Applying the logarithmic function to both sides of Eq. (5.1), yields:

$$\ln(Y) = \ln(k_1) - k_2 \ln(\varepsilon_t) - k_3 \ln(E) \quad (5.16)$$

which means that  $\ln(Y)$  is a normally distributed random variable due to the central limit theorem which states that the sampling distribution of the mean of any independent, random variable tends toward a normal distribution [95, 96], that is,  $\ln(Y) \sim N(\mu_{\ln Y}, \sigma_{\ln Y}^2)$ . Thus  $Y$  has a lognormal distribution  $Y \sim \ln N(\mu_Y, \sigma_Y^2)$  with PDF as:

$$f_Y(y) = \frac{1}{y \sigma_Y \sqrt{2\pi}} e^{-\frac{1}{2} \left( \frac{\ln y - \mu_Y}{\sigma_Y} \right)^2} \quad (5.17)$$

where the mean and variance of  $Y$  are

$$E(Y) = \mu_Y = e^{\mu_{\ln Y} + (\sigma_{\ln Y}^2/2)} \quad (5.18)$$

$$\text{Var}(Y) = \sigma_Y^2 = \left( e^{\sigma_{\ln Y}^2} - 1 \right) e^{2\mu_{\ln Y} + \sigma_{\ln Y}^2} \quad (5.19)$$

In the above, lognormal distribution parameters are given by

$$\sigma_{\ln Y}^2 = \ln \left( 1 + \frac{\sigma_Y^2}{\mu_Y^2} \right) \quad (5.20)$$

$$\mu_{\ln Y} = \ln \mu_Y - \frac{\sigma_{\ln Y}^2}{2} = \ln \mu_Y - \frac{1}{2} \ln \left( 1 + \frac{\sigma_Y^2}{\mu_Y^2} \right) \quad (5.21)$$

where

$\mu_{\ln Y}$  = mean value of  $\ln Y$

$\sigma_{\ln Y}^2$  = variance of  $\ln Y$

Then the resulting PDF of the pavement damage in this case can be written as:

$$f_D(d) = \int_0^{\infty} \frac{1}{2\pi \sigma_{\ln Y} \sqrt{\lambda_x}} e^{-\frac{1}{2} \left[ \left( \frac{yd - \lambda_x}{\sqrt{\lambda_x}} \right)^2 + \left( \frac{\ln y - \mu_Y}{\sigma_Y} \right)^2 \right]} dy \quad (5.22)$$

The cumulative distribution function of the pavement can be expressed as

$$F_D(d) = P(D \leq d) = \int_0^d f_D(d) dd \quad (5.23)$$

$$F_D(d) = \int_0^d \int_0^\infty \frac{1}{2\pi \sigma_Y \sqrt{\lambda_x}} e^{-\frac{1}{2} \left[ \left( \frac{yd - \lambda_x}{\sqrt{\lambda_x}} \right)^2 + \left( \frac{\ln y - \mu_Y}{\sigma_Y} \right)^2 \right]} dy dd \quad (5.24)$$

Finally the fatigue cracking can be predicted using Eq. (5.12) as:

$$FC = 1 - \int_0^1 \int_0^\infty \frac{1}{2\pi \sigma_Y \sqrt{\lambda_x}} e^{-\frac{1}{2} \left[ \left( \frac{yd - \lambda_x}{\sqrt{\lambda_x}} \right)^2 + \left( \frac{\ln y - \mu_Y}{\sigma_Y} \right)^2 \right]} dy dd \quad (5.25)$$

### 5.3.2 Damage Model 2

In this model,  $X$  is assumed to be a random variable that has a Poisson distribution  $X \sim \text{Pois}(\lambda_x)$ , and approximated by a normal distribution due to large mean, that is  $X \sim N(\lambda_x, \lambda_x)$ . Suppose  $Y$  follows a normal distribution, that is,  $Y \sim N(\mu_Y, \sigma_Y^2)$ . Then the resulting PDF of the pavement damage becomes:

$$f_D(d) = \int_0^\infty y \frac{1}{2\pi \sigma_Y \sqrt{\lambda_x}} e^{-\frac{1}{2} \left[ \left( \frac{yd - \lambda_x}{\sqrt{\lambda_x}} \right)^2 + \left( \frac{y - \mu_Y}{\sigma_Y} \right)^2 \right]} dy \quad (5.26)$$

According to Fieller [97] and Hinkley [98] the approximate form for such distribution (ratio of two normally distributed random variables) is given by the following expression:

$$f_D(d) = \frac{b(d) h(d)}{\sqrt{2\pi\lambda_x\sigma_y}a^3(d)} \left[ \Phi\left(\frac{b(d)}{a(d)}\right) - \Phi\left(-\frac{b(d)}{a(d)}\right) \right] + \frac{e^{-\frac{1}{2}c}}{\pi\sigma_y\sqrt{\lambda_x}a^2(d)} \quad (5.27)$$

where

$$a(d) = \sqrt{\frac{1}{\lambda_x}d^2 + \frac{1}{\sigma_y^2}} \quad (5.28)$$

$$b(d) = d + \frac{\mu_y}{\sigma_y^2} \quad (5.29)$$

$$c = \lambda_x + \frac{\mu_y^2}{\sigma_y^2} \quad (5.30)$$

$$h(d) = e^{\frac{b^2(d)-ca^2(d)}{2a^2(d)}} \quad (5.31)$$

The corresponding CDF can then be expressed as:

$$F_D(d) = \int_0^d \left[ \frac{b(d) h(d)}{\sqrt{2\pi\lambda_x\sigma_y}a^3(d)} \left[ \Phi\left(\frac{b(d)}{a(d)}\right) - \Phi\left(-\frac{b(d)}{a(d)}\right) \right] + \frac{e^{-\frac{1}{2}c}}{\pi\sigma_y\sqrt{\lambda_x}a^2(d)} \right] dd \quad (5.32)$$

Subsequently fatigue cracking can be obtained as:

$$FC = \int_1^\infty \left[ \frac{b(d) h(d)}{\sqrt{2\pi\lambda_x\sigma_y}a^3(d)} \left[ \Phi\left(\frac{b(d)}{a(d)}\right) - \Phi\left(-\frac{b(d)}{a(d)}\right) \right] + \frac{e^{-\frac{1}{2}c}}{\pi\sigma_y\sqrt{\lambda_x}a^2(d)} \right] dd \quad (5.33)$$

### 5.3.3 Damage Model 3

According to previous research the damage is assumed to follow a normal distribution,  $D \sim N(\mu_D, \sigma_D^2)$ , then its PDF, CDF and fatigue cracking, FC, respectively, can be expressed as

$$f_D(d) = \frac{1}{\sigma_D \sqrt{2\pi}} e^{-\frac{1}{2} \left( \frac{d - \mu_D}{\sigma_D} \right)^2} \quad (5.34)$$

$$F_D(d) = \int_{-\infty}^d \frac{1}{\sigma_D \sqrt{2\pi}} e^{-\frac{1}{2} \left( \frac{d - \mu_D}{\sigma_D} \right)^2} dd \quad (5.35)$$

$$FC = \Phi \left( \frac{\mu_D - 1}{\sigma_D} \right) = 1 - \Phi \left( \frac{1 - \mu_D}{\sigma_D} \right) \quad (5.36)$$

where

$\mu_D$  = mean value of  $D$ .

$\sigma_D$  = standard deviation of  $D$ .

$\Phi$  = CDF of the standard normal distribution, given by:

$$\Phi(u) = \int_{-\infty}^u \frac{1}{\sqrt{2\pi}} e^{-\frac{1}{2} \tau^2} d\tau \quad (5.37)$$

An approximate expression for damage mean value ( $\mu_D$ ) and damage variance ( $\sigma_D^2$ ) using Taylor series expansion can be obtained as [99]:

$$\mu_D = E(D) = E\left(\frac{X}{Y}\right) = \frac{E(X)}{E(Y)} \approx \frac{\mu_x}{\mu_y} \approx \frac{\lambda_x}{\mu_y} \quad (5.38)$$

and

$$\sigma_D^2 = \text{Var}(D) = \text{Var}\left(\frac{X}{Y}\right) \approx \frac{\text{Var}(X)}{\mu_y^2} + \frac{\mu_x^2 \text{Var}(Y)}{\mu_y^4} \approx \frac{\lambda_x}{\mu_y^2} + \frac{\lambda_x^2 \text{Var}(Y)}{\mu_y^4} \quad (5.39)$$

#### 5.3.4 Damage Model 4

In this model, the damage is assumed to have a lognormal distribution,  $\ln D \sim N(\mu_{\ln D}, \sigma_{\ln D}^2)$ , then the pavement damage PDF, CDF and the fatigue cracking, FC, respectively, can be expressed as:

$$f_D(d) = \frac{1}{d \sigma_{\ln D} \sqrt{2\pi}} e^{-\frac{1}{2} \left( \frac{\ln D - \mu_{\ln D}}{\sigma_{\ln D}} \right)^2} \quad (5.40)$$

$$F_D(d) = \int_0^d \frac{1}{d \sigma_{\ln D} \sqrt{2\pi}} e^{-\frac{1}{2} \left( \frac{\ln D - \mu_{\ln D}}{\sigma_{\ln D}} \right)^2} dd \quad (5.41)$$

$$\text{FC} = \Phi\left(\frac{\mu_{\ln D}}{\sigma_{\ln D}}\right) = 1 - \Phi\left(\frac{-\mu_{\ln D}}{\sigma_{\ln D}}\right) \quad (5.42)$$

here

$$\sigma_{\ln D}^2 = \ln\left(1 + \frac{\sigma_D^2}{\mu_D^2}\right) \quad (5.43)$$

and

$$\mu_{\ln D} = \ln \mu_D - \frac{\sigma_{\ln D}^2}{2} = \ln \mu_D - \frac{1}{2} \ln\left(1 + \frac{\sigma_D^2}{\mu_D^2}\right) \quad (5.44)$$

where

$\mu_{\ln D}$  = mean value of  $\ln D$

$\sigma_{\ln D}^2$  = variance of  $\ln D$

## 5.4 Numerical Results and Discussion

Here the integrals in the damage models are evaluated numerically based on the Gaussian quadrature method implemented using a computer program in the Matlab environment.

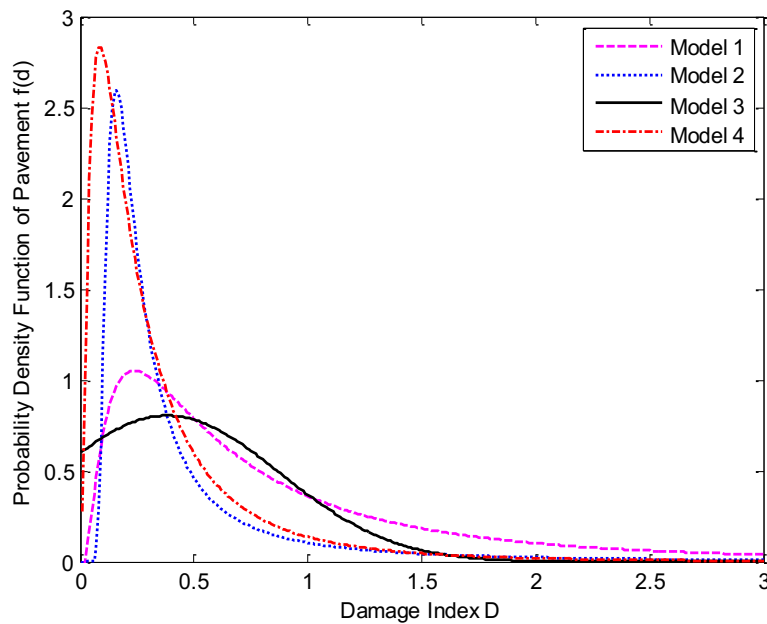


Figure 5.1 PDFs of pavement damage for different models

Figure 5.1 shows the PDFs of the pavement damage for different models discussed in Section 5.3. It can be seen that the PDF of model 2 and model 4 increase significantly with the increase in the damage index in the range between zero and the peak values of  $D$ , and then decrease sharply with the increase in the damage index, while the PDF of models 1 and 3 tend to decrease

gradually, when the damage index increase beyond the peak value. In addition, models 2 and 4 show a relatively narrow range distribution followed by model 3 compared with model 1 that shows a broad range distribution of pavement damage.

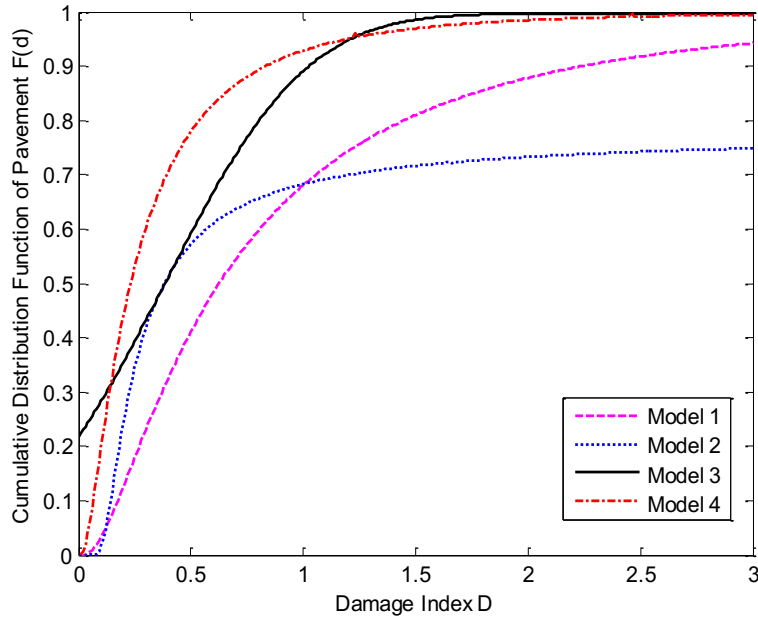


Figure 5.2 CDFs of pavement damage for different models

Figure 5.2 shows the cumulative distribution of pavement damage for different models, which represents the probability that  $D$  will take a value less than or equal to  $d$  ( $0 \leq d \leq \infty$ ). It is found that at  $D = 1$ , model 4 shows a highest CDF ( $F_D(1) = 0.9288$ ), and model 1 gives a lowest CDF ( $F_D(1) = 0.6812$ ), while CDF of models 2 and 3 are ( $F_D(1) = 0.6827$ ) and ( $F_D(1) = 0.8913$ ), respectively. Table 1 provides the fatigue crack index for different models: Thus, Model 1 shows a higher probability of occurrence of the fatigue cracking followed by models 2 and 3, while model 4 gives a lower expectation of fatigue cracking.

Table 5.1 Calculated fatigue cracking (FC) for different models

	Model 1	Model 2	Model 3	Model 4
FC	0.3187	0.3172	0.1035	0.0681

For a long design period (say 25 years) the expected fatigue cracking with time using proposed models is shown in Figure 5.3. It can be observed that the expected fatigue cracking using model 1 is higher than the other models in most periods.

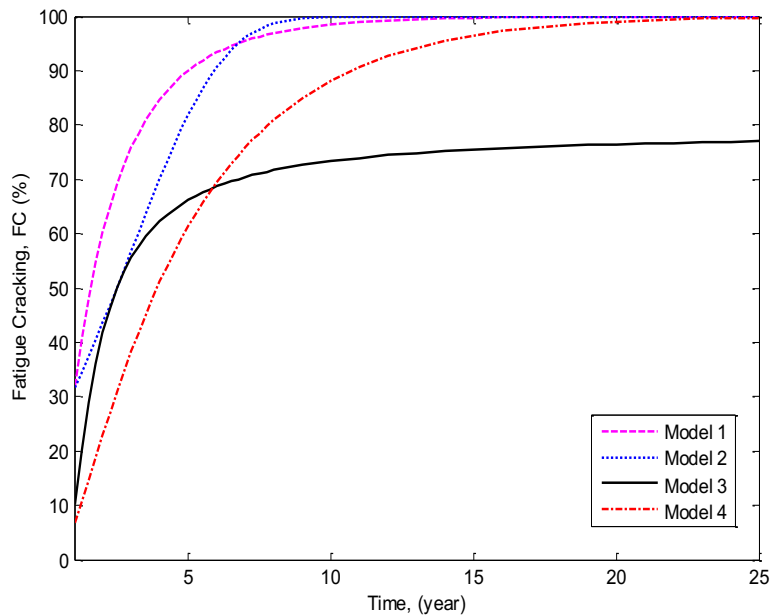


Figure 5.3 Fatigue cracking versus time for different models

The results reveal that the damage distribution is neither normal nor lognormal as the previous research works assumed. According to the derived model (Model 1) the damage follows a broad range distribution which represents the distribution of a ratio of two random variables  $X$  and  $Y$ , where  $X$  represents the actual traffic load repetitions which follows a Poisson distribution, and  $Y$  stands for the traffic repetitions to cause fatigue cracking which is lognormally distributed.

## 5.5 Summary

Predicting fatigue cracking and pavement damage, through four models is presented based on a mechanistic empirical approach using Asphalt Institute model and the probability distribution theory. The Palmgren-Miner's hypothesis is used to estimate the accumulation of damage for flexible pavement based on Poisson distribution to describe the arrival of traffic loads. The solutions are obtained through numerical integration based on Gaussian quadrature method. It is concluded that:

- (1) The damage distribution is neither normal nor lognormal.
- (2) The proposed model (model 1) has a broad range distribution of pavement damage.
- (3) Model 1 shows a highest expectation of fatigue cracking.
- (4) For a long design period, the expected fatigue cracking using model 1 is higher than the other models in most periods.

Thus, the damage distribution is neither normal nor lognormal as the previous research works assumed, and a better estimation of fatigue cracking in flexible pavements based on damage model can be carried out using model 1, in which the equivalent actual traffic load repetitions has a Poisson distribution, while the traffic repetitions to cause failure follows a lognormal distribution.

# CHAPTER 6

## Conclusions, Contributions, and Recommendation for Future Work

### 6.1 Dissertation Summary and Conclusions

In this thesis the dynamic behavior of a moving vehicle on flexible pavement is modeled and analysed considering the coupling action (interaction) between pavement and vehicle including the road surface roughness (harmonic/random) as internal excitation. Moreover, different damage models are presented and pavement distress in the form of fatigue cracking is predicted based on a combination of deterministic and probabilistic methods. In the first chapter, the concept of dynamic pavement-vehicle interaction (considering the coupling action) is reviewed. The development history of pavement life prediction using different methods is discussed. In chapter two, an integrated pavement and vehicle model is proposed to simulate the dynamic behaviour of a moving vehicle on flexible pavement considering the coupling action. In order to simulate the dynamic response of the moving vehicle, the vehicle is modeled as a Two-DOF quarter vehicle ride model while the flexible pavement is modeled as a simply supported finite Euler-Bernoulli beam of uniform cross section supported by a linear visco-elastic foundation using Pasternak model. The governing equations of motion of vehicle are obtained based on d'Alembert's principle. In order to reduce the complexity of the equations describing the pavement-foundation system, which depends on spatial and temporal variables, Galerkin method is applied to discretize the problem and to obtain a set of ordinary differential equations in the time domain. In chapter three, the direct integration Newmark-Beta approach based on linear

average acceleration method has been used to determine the response of the vibrating system numerically considering a sinusoidal road surface profile as the system input. A computer program is developed to acquire the response and the results are validated with previous research work and also compared with that of conventional uncoupled system. Moreover, the effects of vehicle speed, road roughness, soil stiffness and suspension damping on the responses are investigated. In Chapter four, the random road surface profile is considered as internal excitation to the system. The road surface profile is generated based on ISO 8608 criterion considering three different ISO classes of pavement roughness (very good road, average road and very poor road). The effects of road surface roughness and vehicle speed on the pavement response due to the passage of different types of vehicles (car, bus and truck) are then analyzed. In order to model the pavement damage and predict the pavement distress in the form of fatigue cracking, chapter five provides a methodology based on a combination of deterministic method with stochastic approach using Palmgren-Miner's hypothesis, and Poisson process to characterize the traffic loads. By integrating the findings derived from the previous chapters, it can be concluded that:

1. Poisson distribution for the traffic arrivals has been found to be a meaningful mathematical model for the actual traffic repetitions.
2. In the absence of any other pavement damage estimation model, the Palmgren-Miner's hypothesis provides realistic estimation for the pavement damage.
3. Pavement damage distribution is neither normal nor lognormal as some previous research assumed. Pavement fatigue cracking can be predicted based on a pavement damage model that has a broad range distribution in which the traffic arrivals at a given

point on the road has Poisson distribution, while the traffic repetitions to failure follows lognormal distribution.

4. Present study highlights the importance of the coupling action in the analysis of either vehicle dynamics or pavement dynamics. The effect of coupling action on vehicle dynamics is more pronounced for soft and smooth roads, for example the vertical vehicle-body displacement of the coupled system is approximately 41% greater than that of the uncoupled system. While the effect of coupling action on pavement dynamics is very small (only 0.1% of difference). On rough road and hard soil the coupling action affects pavement dynamics most significantly. As a result, coupling action between the vehicle and the pavement should not be neglected even in soft soil and smooth roads.
5. The maximum pavement deflection occurs at a location close to where the vehicular load is applied and decreases farther away from the load, for example when the vehicle arrived to the mid-span (80 m) the pavement deflection is 3.009 mm, while the maximum pavement deflection (3.041mm) occurs at the location 79.28 m.
6. Vehicle system coupled to the pavement provided results that are better than the traditional uncoupled system. For instance, the vertical vehicle-body displacement and the transverse mid-span pavement deflection are, respectively, 14% and 6% greater than those of the uncoupled system for a good road.
7. The response of flexible pavement due to moving vehicular load depends primarily on the road surface roughness and only to a much lesser effect on the increase in vehicle speed. For the same type of the vehicle, the pavement response increases significantly

with the increase in road roughness. For instance, the pavement response generated by the passage of a car (at 16 m/s) is 0.0065 mm for very good road (Class A), and increases to 0.0193 mm for average road (Class C) which is approximately three times that of road class A, and for a very poor road (Class E) is around four times that of road class C and equal to 0.0764 mm.

8. The flexible pavement vibration response depends on the vehicle type. For instance, at vehicle speed of 16 m/s the pavement response generated by the passage of a car is 0.0228 mm, for a bus is 0.2005 mm approximately 9 times that of the car, and for the truck is around 0.5098 mm, about three times that of the bus.

## **6.2 Contributions**

This thesis presents a comprehensive study of pavement and vehicle interaction system as well as pavement damage and fatigue cracking prediction. The thesis contributions are summarized as follows:

1. A 17-DOF pavement vehicle coupled model is proposed based on the interaction generated between the moving vehicle and the surface of the pavement. In this model, vehicle vibrations and dynamic nature of flexible pavement with road surface roughness are considered.
2. A parametric study is carried out to compare the pavement-vehicle coupled system with the conventional uncoupled system that shows that the coupling action between the

pavement and vehicle should not be neglected in analyzing both vehicle and pavement dynamics.

3. Traffic load arrivals at a given point on the pavement are modeled using Poisson process model.
4. Mechanistic-Empirical method and Stochastic approach are used together to model the pavement damage using Palmgren-Miner's law based on Poisson process to characterize the actual traffic load of repetitions.
5. Based on damage distribution model, pavement distress in the form of fatigue cracking is predicted to define the pavement performance.

### **6.3 Recommendations for Future Work**

While this work can be considered as a major step to better understand the effect of coupling action between the flexible pavement and the moving vehicle, and also to predict fatigue cracking in the pavement, the following future research works are suggested to further advance the state-of-the art in this field:

- For heavy vehicle, nonlinear suspension with asymmetric damping and progressively hardening spring (air spring) with unidirectional tire spring should be considered in order to balancing between ride quality and minimum pavement load.
- Some parameters such as rainfall, snow, moisture, and temperature changes can play an important role in both vehicle and pavement dynamics and they should be included in the analysis.

- The pavement stiffness modulus and the strain are considered deterministic parameters in the proposed damage distribution model. Due to the uncertainty and variability of these parameters, they can be considered as random variables that follow a certain distribution.

## BIBLIOGRAPHY

- [1] Sawant, V. A., Patil, V. A., and Deb, K., "Effect of Vehicle-Pavement Interaction on Dynamic Response of Rigid Pavements." *Geo-mechanics and Geo-engineering*, 2011, 31-39.
- [2] Lu, Z., and Yao, H., "Effects of The Dynamic Vehicle-Road Interaction on The Pavement Vibration Due to Road Traffic." *Journal of Vibro-engineering*, 15(3), 2013, 1291-1301.
- [3] Hunt, P. D., and Bunker, J. M., "Analysis of Unbound Granular Pavement Deterioration for Use in Asset Management Modelling: A Literature Review." *State of Queensland (Department of Main Roads)* 2001.
- [4] Yang, S., Li, S., and Lu, Y., "Investigation on Dynamical Interaction Between a Heavy Vehicle and Road Pavement." *Vehicle System Dynamics*, 48(8), 2010, 923-944.
- [5] Yi, K., and Hedrick, J.K., "Active and Semi-Active Heavy Truck Suspensions to Reduce Pavement Damage." *Society of Automotive Engineers (SAE 892486)*, 1989, 588-595.
- [6] Potter, T. E. C., Cebon, D., and Cole, D. J., "Assessing The Relative Road Damaging Potential Of HGVs." *Road Transport Technology*, 1995, 75-81.
- [7] Sun, L., "Optimum Design of Road-Friendly Vehicle Suspension Systems Subjected to Rough Pavement Surfaces." *Applied Mathematical Modeling*, 26(5), 2002, 635-652.
- [8] Salama, H. K., Chatti, K., and Lyles, R. W., "Effect of Heavy Multiple Axle Trucks on Flexible Pavement Damage Using In-Service Pavement Performance Data." *Journal of Transportation Engineering*, 132(10), 2006, 763-770.
- [9] Sun, L., and Luo, F., "Nonstationary Dynamic Pavement Loads Generated by

- Vehicles Traveling at Varying Speed." *Journal of Transportation Engineering*, 133(4), 2007, 252-263.
- [10] Sun, L., Cai, X. and Yang, J., "Genetic Algorithm-based Optimum Vehicle Suspension Design Using Minimum Dynamic Pavement Load as A Design Criterion." *Journal of Sound and Vibration*, 301 (1), 2007, 18-27.
- [11] Ihsan, S. I., Faris, W. F., and Ahmadian, M., "Analysis of Control Policies and Dynamic Response of a Q-car 2-DOF Semi Active System." *Shock and Vibration*, 15(5), 2008, 573-582.
- [12] Bogsjö, K., and Rychlik, I., "Vehicle Fatigue Damage Caused By Road Irregularities." *Fatigue and Fracture of Engineering Materials and Structures*, 32(5), 2009, 391-402.
- [13] Patel, C. B., Gohil, P. P., and Borhade, B., "Modeling and Vibration Analysis of a Road Profile Measuring System." *International Journal of Automotive and Mechanical Engineering (IJAME)*, 1 (1), 2010, 13-28.
- [14] Cao, D., Song, X., and Ahmadian, M., "Editors' Perspectives: Road Vehicle Suspension Design, Dynamics, and Control." *Vehicle System Dynamics*, 49(1-2), 2011, 3-28.
- [15] Suzuki, T., and Takahashi, M., "Semi-Active Suspension Control Considering Lateral Vehicle Dynamics due to Road Input." *In ASME 5th Annual Dynamic Systems and Control Conference joint with the JSME 11<sup>th</sup> Motion and Vibration Conference*, 2012, 549-554.
- [16] Collop, A.C., and Cebon, D., "Parametric Study of Factors Affecting Flexible-Pavement Performance." *Journal of Transportation Engineering*, 121 (6), 1995, 485-494.
- [17] Kim, S. M., and Roesset, J. M., "Moving Loads on A Plate on Elastic

- Foundation." *Journal of Engineering Mechanics*, 124(9), 1998, 1010-1017.
- [18] Lin, J. H., and Weng, C. C., "Analytical Study of Probable Peak Vehicle Load on Rigid Pavement." *Journal of Transportation Engineering*, 127(6), 2001, 471-476
- [19] Huang, M. H., and Thambiratnam, D. P., "Dynamic Response of Plates on Elastic Foundation to Moving Loads." *Journal of Engineering Mechanics*, 128 (9), 2002, 1016-1022.
- [20] Kim, S. M., and McCullough, B. F., "Dynamic Response of Plate on Viscous Winkler Foundation to Moving Loads of Varying Amplitude." *Engineering Structures*, 25 (9), 2003, 1179-1188.
- [21] Kargarnovin, M. H., and Younesian, D., "Dynamics of Timoshenko Beams on Pasternak Foundation Under Moving Load." *Mechanics Research Communications*, 31(6), 2004, 713-723.
- [22] Sun, L., "Dynamics of Plate Generated by Moving Harmonic Loads." *Journal of Applied mechanics*, 72(5), 2005, 772-777.
- [23] Mallik, A. K., Chandra, S., and Singh, A. B., "Steady-state Response of An Elastically Supported Infinite Beam to A Moving Load." *Journal of Sound and Vibration*, 291(3), 2006, 1148-1169.
- [24] Kettil, P., Lenhof, B., Runesson, K., and Wiberg, N. E., "Simulation of Inelastic Deformation in Road Structures Due to Cyclic Mechanical and Thermal Loads." *Computers and Structures*, 85(1), 2007, 59-70.
- [25] Papagiannakis, A. T., and Gujarathi, M. S., "A Roughness Model Describing Heavy Vehicle-pavement Interaction." *Washington State Transportation Commission Final Research Report (No. WA-RD 372.1)*, 1995.
- [26] Wu, C. P., and Shen, P. A., "Dynamic Analysis of Concrete Pavements Subjected to Moving Loads." *Journal of Transportation Engineering*, 122(5), 1996, 367-373.

- [27] Mamlouk, M. S., "General Outlook of Pavement and Vehicle Dynamics." *Journal of Transportation Engineering*, 123(6), 1997, 515–517.
- [28] Sun, L., and Deng, X., "Predicting Vertical Dynamic Loads Caused by Vehicle-pavement Interaction." *Journal of Transportation Engineering*, 124(5), 1998, 470-478.
- [29] Rutka, A., and Sapragonas, J., "The Role of A Tire in Vehicle and Road Interaction." *Transport*, 17(2), 2002, 39-45.
- [30] Lombaert, G., and Degrande, G., "The Experimental Validation of A Numerical Model For The Prediction of The Vibrations in The Free Field Produced by Road Traffic." *Journal of Sound and Vibration*, 262(2), 2003, 309-331.
- [31] Nassif, H. H., and Liu, M., "Analytical Modeling of Bridge-Road-Vehicle Dynamic Interaction System." *Journal of Vibration and Control*, 10(2), 2004, 215-241.
- [32] Papagiannakis, A. T., Zelelew, H. M., and Muhunthan, B., "A wavelet Interpretation of Vehicle-pavement Interaction." *International Journal of Pavement Engineering*, 8(3), 2007, 245-252.
- [33] Sawant, V., "Dynamic Analysis of Rigid Pavement with Vehicle-pavement Interaction." *International Journal of Pavement Engineering*, 10(1), 2009, 63-72.
- [34] Shi, X. M., and Cai, C. S., "Simulation of Dynamic Effects of Vehicles on Pavement Using a 3D Interaction Model." *Journal of Transportation Engineering*, 135(10), 2009, 736-744.
- [35] Xia, K. M., "A Finite Element Model for Tire/Pavement Interaction: Application to Predicting Pavement Damage." *International Journal of Pavement Research and Technology*, 3(3), 2010, 135-141.
- [36] Taheri, A., OBrien, E. J., and Collop, A. C., "Pavement Damage Model Incorporating Vehicle Dynamics and A 3D Pavement Surface." *International*

*Journal of Pavement Engineering*, 13(4), 2012, 374-383.

- [37] Wang, G., Roque, R., and Morian, D., "Effects of Surface Rutting on Near-Surface Pavement Responses Based on a Two-Dimensional Axle-Tire-Pavement Interaction Finite-Element Model." *Journal of Materials In Civil Engineering*, 24(11), 2012, 1388-1395.
- [38] Cao, P., Zhou, C., Feng, D., Zhao, Y., & Huang, B., "A 3D Direct Vehicle-Pavement Coupling Dynamic Model and Its Application on Analysis of Asphalt Pavement Dynamic Response." *Mathematical Problems in Engineering*, 2013, 1-8.
- [39] Patil, V. A., Sawant, V. A., and Deb, K., "2-D Finite Element Analysis of Rigid Pavement Considering Dynamic Vehicle-pavement Interaction Effects." *Applied Mathematical Modelling*, 37(3), 2013, 1282-1294.
- [40] Patil, V. A., Sawant, V. A., and Deb, K., "3D Finite-Element Dynamic Analysis of Rigid Pavement Using Infinite Elements." *International Journal of Geomechanics*, 13(5), 2013, 533-544.
- [41] Liu, Y., and You, Z. P., "Fundamental Study on Pavement-Wheel Interaction Forces through Discrete Element Simulation." *International Journal of Pavement Research and Technology*, 6(6), 2013, 689-695.
- [42] Ding, H., Yang, Y., Chen, L. Q., and Yang, S. P., "Vibration of Vehicle-pavement Coupled System Based on A Timoshenko Beam on A Nonlinear Foundation." *Journal of Sound and Vibration*, 333(24), 2014, 6623-6636.
- [43] Rouillard, V., Bruscella, B., and Sek, M., "Classification of Road Surface Profiles." *Journal of Transportation Engineering*, 126 (1), 2000, 41-45.
- [44] Waechter, M., Riess, F., Kantz, H., and Peinke, J., "Stochastic Analysis of Surface Roughness." *EPL (Europhysics Letters)*, 64 (5), 2003, 579.
- [45] Fujikawa, T., Koike, H., Oshino, Y., and Tachibana, H., "Definition of Road

- Roughness Parameters for Tire Vibration Noise Control." *Applied Acoustics*, 66 (5), 2005, 501-512.
- [46] González, A., O'brien, E. J., Li, Y. Y., and Cashell, K., "The Use of Vehicle Acceleration Measurements to Estimate Road Roughness." *Vehicle System Dynamics*, 46 (6), 2008, 483-499.
- [47] Ngwangwa, H. M., Heyns, P. S., Labuschagne, F. J. J., and Kululanga, G. K., "Reconstruction of Road Defects and Road Roughness Classification Using Vehicle Responses With Artificial Neural Networks Simulation." *Journal of Terramechanics*, 47 (2), 2010, 97-111.
- [48] Bogsjö, K., Podgórski, K., and Rychlik, I., "Models For Road Surface Roughness." *Vehicle System Dynamics*, 50 (5), 2012, 725-747.
- [49] Agostinacchio, M., Ciampa, D., and Olita, S., "The Vibrations Induced by Surface Irregularities in Road Pavements—a Matlab® Approach." *European Transport Research Review*, 6 (3), 2013, 267-275.
- [50] Liu, X., Wang, H., Shan, Y., and He, T., "Construction of Road Roughness in Left and Right Wheel Paths Based on PSD and Coherence Function." *Mechanical Systems and Signal Processing*, 60, 2015, 668-677.
- [51] Erlingsson, S., "Failure modes in pavements." *KTH AF2903 Road Construction and MaintenanceAF2903 Road Construction and Maintenance*, 2013.
- [52] Guo, R., and Prozzi, J. A., "Prediction of In-Service Fatigue Life of Flexible Pavements Based on Accelerated Pavement Testing." *Journal of Testing and Evaluation*, 37(5), 2009, 449-453.
- [53] Anonymous, "Pavement distress survey manual." *Oregon Department of Transportation Pavement Services Unit*, 2010
- [54] Wang, Y., Mahboub, K. C., and Hancher, D. E., "Survival Analysis of Fatigue

- Cracking for Flexible Pavements Based on Long-term Pavement Performance Data." *Journal of transportation engineering*, 131(8), 2005, 608-616.
- [55] Priest, A. L., and Timm, D. H., "Methodology and Calibration of Fatigue Transfer Functions for Mechanistic-Empirical Flexible Pavement Design." *No. NCAT Report*, 06-03, 2006.
- [56] Kim, Y. R., and Park, H. J., "Investigation of Primary Causes of Fatigue Cracking in Asphalt Pavement in North Carolina." *Research and development*, North Carolina State University, Project 2010-01, 2015.
- [57] Moreno-Navarro, F., and Rubio-Gámez, M. C., "A Review of Fatigue Damage in Bituminous Mixtures: Understanding The Phenomenon From A New Perspective." *Construction and Building Materials*, 113, 2016, 927-938.
- [58] Guercio, M. C., Mehta, Y., and McCarthy, L. M., "Evaluation of Fatigue Cracking Performance of Asphalt Mixtures Under Heavy Static and Dynamic Aircraft Loads." *Construction and Building Materials*, 95, 2015, 813-819.
- [59] Ambassa, Z., Allou, F., Petit, C., and Eko, R. M., "Top-Down and Bottom-Up Fatigue Cracking of Bituminous Pavements Subjected to Tangential Moving Loads." *7th RILEM international conference on cracking in pavements*. Springer Netherlands, 2012, 675-685.
- [60] Lytton, R. L., "Concepts of Pavement Performance Prediction and Modeling." *Proc., 2nd North American Conference on Managing Pavements*,(2), 1987.
- [61] Ferreira, A., Picado-Santos, L. D., Wu, Z., and Flintsch, G., "Selection of Pavement Performance Models for Use in The Portuguese PMS." *International Journal of Pavement Engineering*, 12 (1), 2011, 87-97.
- [62] Schwartz, C. W., and Carvalho, R. L., "Evaluation of Mechanistic-Empirical Design Procedure." *Final report, MDSHA Project No. SP0077B41, Maryland*, 2, 2007.

- [63] Li, Z., "A Probabilistic and Adaptive Approach to Modeling Performance of Pavement Infrastructure." *Diss. University of Texas at Austin*, 2005.
- [64] El-Basyouny, M., and Matthew W., "Part 2: Flexible Pavements: Calibration of Alligator Fatigue Cracking Model for 2002 Design Guide." *Transportation Research Record: Journal of the Transportation Research Board* 1919, 2005, 76-86.
- [65] Read, J. M., "Fatigue Cracking of Bituminous Paving Mixtures." *Diss. University of Nottingham*, 1996.
- [66] Pokorski, P., Radziszewski, P., and Sarnowski, M., "Fatigue Life of Asphalt Pavements on Bridge Decks." *Procedia Engineering*, 153, 2016, 556-562.
- [67] Chua, K. H., Der Kiureghian, A., and Monismith, C. L., "Stochastic Model for Pavement Design." *Journal of transportation engineering*, 118 (6), 1992, 769-786.
- [68] Uzan, J., Zollinger, D. G., and Lytton, R. L., "The Texas flexible pavement systems mechanistic-empirical model." FHWA/TX- 91/455-1. Texas Transportation Institute, College Station, 1990.
- [69] Golabi, K., Kulkarni, R. B., and Way, G. B., "A Statewide Pavement Management System." *Interfaces*, 12 (6), 1982, 5-21.
- [70] Madanat, S., Bulusu, S., and Mahmoud, A., "Estimation of Infrastructure Distress Initiation and Progression Models." *Journal of Infrastructure Systems*, 1 (3), 1995, 146-150.
- [71] Li, N., Xie, W. C., and Haas, R., "Reliability-based Processing of Markov Chains for Modeling Pavement Network Deterioration." *Transportation Research Record: Journal of the Transportation Research Board* 1524, 1996, 203-213.
- [72] Mishalani, R. G., and Madanat, S. M., "Computation of Infrastructure Transition Probabilities Using Stochastic Duration Models." *Journal of Infrastructure systems*, 8 (4), 2002, 139-148.

- [73] Retherford, J., and McDonald, M., "Reliability Methods Applicable to Mechanistic-empirical Pavement Design Method." *Transportation Research Record: Journal of the Transportation Research Board* 2154, 2010, 130-137.
- [74] Ferreira, A., Picado-Santos, L. D., Wu, Z., and Flintsch, G., "Selection of Pavement Performance Models for Use in The Portuguese PMS." *International Journal of Pavement Engineering*, 12(1), 2011, 87-97.
- [75] Ahmed, A. K. W., "Ground Transportation System." *Encyclopedia of Vibration*, ISBN 0-12-227085-1, Academic Press, London, UK, 2001, 603-620.
- [76] Jahromi, A. F., Bhat, R. B., and Xie, W. F., " Robust Control of Passenger Cars With Semi-Active Suspension System Using Magnetorheological Shock Absorber." In *Proc. of the Canadian Society for Mechanical Engineering (CSME) International Congress 2014*.
- [77] Basic Civil Engineering, <http://www.basiccivilengineering.com/2015/04/comparison-between-flexible-pavement.html>, visited March, 2016.
- [78] Zhaohua, F., and Cook, R. D., "Beam elements on two-parameter elastic foundations." *Journal of Engineering Mechanics*, 109 (6), 1983, 1390-1402.
- [79] Akbarian, M., "Model Based Pavement-vehicle Interaction Simulation for Life Cycle Assessment of Pavements." *Diss. Massachusetts Institute of Technology*, 2012.
- [80] Bathe, K. J., and Wilson, E. L., "Stability and accuracy analysis of direct integration methods." *Earthquake Engineering and Structural Dynamics*, 1(3), 1972, 283-291.
- [81] Gavin, H., "Numerical integration for structural dynamics." *Department of Civil and Environmental Engineering, Duke University, Durham, NC*, 2001
- [82] Senalp, A. D., Arikoglu, A., Ozkol, I., and Dogan, V. Z., "Dynamic Response of a Finite Length Euler-Bernoulli Beam on Linear and Nonlinear Visco-elastic Foundations to a Concentrated Moving Force." *Journal of Mechanical Science and*

*Technology*, 24 (10), 2010, 1957-1961.

- [83] Lundström, J., "Road Roughness Estimation Using Available Vehicle Sensors." 2009.
- [84] Andren, P., "Power Spectral Density Approximations of Longitudinal Road Profiles." *International Journal of Vehicle Design*, 40 (1-3), 2005, 2-14.
- [85] Park, S., Popov, A. A., and Cole, D. J., "Influence of Soil Deformation on Off-road Heavy Vehicle Suspension Vibration." *Journal of Terramechanics*, 41 (1), 2004, 41-68.
- [86] Dilip, D. M., Ravi, P., and Babu, G. S., "System Reliability Analysis of Flexible Pavements." *Journal of Transportation Engineering*, 139 (10), 2013, 1001-1009.
- [87] Kalita, K., and Rajbongshi, P., "Variability Characterization of Input Parameters in Pavement Performance Evaluation." *Road Materials and Pavement Design*, 16 (1), 2015, 172-185.
- [88] Maji, A., and Das, A., "Reliability Considerations of Bituminous Pavement Design by Mechanistic-Empirical Approach." *International Journal of Pavement Engineering*, 9 (1), 2008, 19-31.
- [89] Thongram, S., and Rajbongshi, P., "Probability and Reliability Aspects in Pavement Engineering." *National Institute of Technology Silchar*, 2016
- [90] Kim, H.B. and Buch, N., "Reliability-based pavement design model accounting for inherent variability of design parameters." *Transportation Research Board*, 82nd Annual Meeting, Washington DC, 2003.
- [91] Miller, I., and Freund, J. E., "*Probability and Statistics for Engineers.*" 2<sup>nd</sup> edition, Prentice-Hall, 1977.
- [92] Walpole, R. E, and Myers, R. H., "Probability and Statistics for Engineers and Scientists." 4th edition, Macmillan, 1989.

- [93] Bhat, R. B., "Random Vibrations." lecture notes, ENGR 7331, Concordia University, delivered July 2016.
- [94] Griffin, T. F., "Distribution of The Ratio of Two Poisson Random Variables." *Diss. Texas Tech University*, 1992.
- [95] Kallianpur, G., Krishnaiah, P. R., and Ghosh, J. K., "A proof of the central limit theorem motivated by the Cramér-Rao inequality." *Statistics and probability: essays in honor of CR Rao*, 1982, 141.
- [96] The Central Limit Theorem, <http://www.math.uah.edu/stat/sample/CLT.html>, visited January, 2017.
- [97] Fieller, E. C., "The Distribution of The Index in A Normal Bivariate Population" *Biometrika*, 1932, 428-440.
- [98] Hinkley, D. V., "On The Ratio of Two Correlated Normal Random Variables." *Biometrika*, 56 (3), 1969, 635-639.
- [99] Van Kempen, G. M. P., and Van Vliet, L. J., "Mean and Variance of Ratio Estimators Used in Fluorescence Ratio Imaging." *Cytometry Part A*, 39 (4), 2000, 300-305.
- [100] Uzzal, R. U. A., Bhat, R. B., and Ahmed, W., "Dynamic Response of A Beam Subjected to Moving Load and Moving Mass Supported by Pasternak Foundation." *Shock and Vibration*, 19 (2), 2012, 205-220.
- [101] Ahmed, A. K. W., "Vehicle Dynamics." lecture notes, MECH 6751, Concordia University, delivered January 2014.

**APPENDIX I The Non-dimensional Form of The Dynamic Interaction Force**  
**Considering The Coupling Action for The LTI System**

$$F_t = c_t(\dot{y}_u - \dot{y}_R - \dot{y}_p) + k_t(y_u - y_R - y_p) \quad (I.1)$$

Let

$$\begin{aligned} y_u &= Y_u e^{j(\omega t - \phi_u)} = \bar{Y}_u e^{j\omega t} \\ \dot{y}_u &= j Y_u \omega e^{j(\omega t - \phi_u)} = j \bar{Y}_u \omega e^{j\omega t} \\ y_p &= Y_p e^{j(\omega t - \phi_p)} = \bar{Y}_p e^{j\omega t} \\ \dot{y}_p &= j Y_p \omega e^{j(\omega t - \phi_p)} = j \bar{Y}_p \omega e^{j\omega t} \end{aligned} \quad (I.2)$$

$$y_R = Y_R e^{j\omega t}$$

$$\dot{y}_R = j Y_R \omega e^{j\omega t}$$

Substituting Eqs. (I.2) into Eq. (I.1), yields:

$$F_t = [(k_t + j c_t \omega) \bar{Y}_u - (k_t + j c_t \omega) Y_R - (k_t + j c_t \omega) \bar{Y}_p] e^{j\omega t} \quad (I.3)$$

Let

$$F_{t_0} = (k_t + j c_t \omega) \bar{Y}_u - (k_t + j c_t \omega) Y_R - (k_t + j c_t \omega) \bar{Y}_p \quad (I.4)$$

$$F_{t_0} = (k_t + j c_t \omega) (\bar{Y}_u - \bar{Y}_p - Y_R)$$

Dividing both sides of Eq. (I.4) by  $k_t Y_R$ , yields:

$$\frac{F_{t_0}}{k_t Y_R} = \left[ 1 + j \left( \frac{c_t}{k_t} \right) \omega \right] \left( \frac{\bar{Y}_u}{Y_R} - \frac{\bar{Y}_p}{Y_R} - 1 \right) \quad (I.5)$$

## APPENDIX II CDF of A Random Variable of Normal/Lognormal Distribution

1-The PDF of a random variable  $X$  with normal distribution,  $X \sim N(\mu_X, \sigma_X^2)$ , can be expressed as follows:

$$f_X(x) = \frac{1}{\sigma_X \sqrt{2\pi}} e^{-\frac{1}{2} \left( \frac{x - \mu_X}{\sigma_X} \right)^2} \quad (\text{II.1})$$

The CDF of  $X$  can be obtained by:

$$F_X(x) = \int_{-\infty}^x \frac{1}{\sigma_X \sqrt{2\pi}} e^{-\frac{1}{2} \left( \frac{y - \mu_X}{\sigma_X} \right)^2} dy \quad (\text{II.2})$$

Let

$$u = \frac{y - \mu_X}{\sigma_X} \quad (\text{II.3})$$

Then

$$\frac{du}{dy} = \frac{1}{\sigma_X} \quad (\text{II.4})$$

$$dy = \sigma_X du$$

$$y \rightarrow -\infty, \quad u \rightarrow -\infty$$

$$y \rightarrow x, \quad u \rightarrow \frac{x - \mu_X}{\sigma_X}$$

Eq. (II.2) becomes:

$$F_X(x) = \int_{-\infty}^{\frac{x - \mu_X}{\sigma_X}} \frac{1}{\sqrt{2\pi}} e^{-\frac{1}{2} u^2} du \quad (\text{II.5})$$

Finally,

$$F_X(x) = \frac{1}{2} \left[ 1 + \operatorname{erf} \left( \frac{x - \mu_X}{\sigma_X \sqrt{2}} \right) \right] = \Phi \left( \frac{x - \mu_X}{\sigma_X} \right) \quad (\text{II.6})$$

2-The PDF of a random variable  $X$  with lognormal distribution,  $\ln X \sim N(\mu_{\ln X}, \sigma_{\ln X}^2)$ , can be expressed as follows:

$$f_X(x) = \frac{1}{x \sigma_{\ln X} \sqrt{2\pi}} e^{-\frac{1}{2} \left( \frac{\ln x - \mu_{\ln X}}{\sigma_{\ln X}} \right)^2} \quad (\text{II.7})$$

The CDF of  $X$  can be obtained by:

$$F_X(x) = \int_0^x \frac{1}{y \sigma_{\ln X} \sqrt{2\pi}} e^{-\frac{1}{2} \left( \frac{\ln y - \mu_{\ln X}}{\sigma_{\ln X}} \right)^2} dy \quad (\text{II.8})$$

Let

$$u = \frac{\ln y - \mu_{\ln X}}{\sigma_{\ln X}} \quad (\text{II.9})$$

Then

$$\frac{du}{dy} = \frac{1}{y \sigma_{\ln X}} \quad (\text{II.10})$$

$$dy = y \sigma_{\ln X} du$$

$$y \rightarrow 0, \quad u \rightarrow -\infty$$

$$y \rightarrow x, \quad u \rightarrow \frac{\ln x - \mu_{\ln X}}{\sigma_{\ln X}}$$

Eq. (II.8) becomes:

$$F_X(x) = \int_{-\infty}^{\frac{\ln x - \mu_{\ln X}}{\sigma_{\ln X}}} \frac{1}{\sqrt{2\pi}} e^{-\frac{1}{2} u^2} du \quad (\text{II.11})$$

Finally,

$$F_X(x) = \frac{1}{2} \left[ 1 + \operatorname{erf} \left( \frac{\ln x - \mu_{\ln X}}{\sigma_{\ln X} \sqrt{2}} \right) \right] = \Phi \left( \frac{\ln x - \mu_{\ln X}}{\sigma_{\ln X}} \right) \quad (\text{II.12})$$

### APPENDIX III CDF and PDF of A Ratio of Two Random Variables

Let  $X$  and  $Y$  be independent random variables having the respective PDF's  $f_X(x)$  and  $f_Y(y)$ .

Then the CDF of a ratio  $D = \frac{X}{Y}$  can be computed as follows:

$$F_D(d) = P(D \leq d) = P\left(\frac{X}{Y} \leq d\right) = P\left(\frac{X}{Y} \leq d, Y < 0\right) + P\left(\frac{X}{Y} \leq d, Y > 0\right) \quad (\text{III.1})$$

Then

$$F_D(d) = P(X \geq Yd, Y < 0) + P(X \leq Yd, Y > 0) \quad (\text{III.2})$$

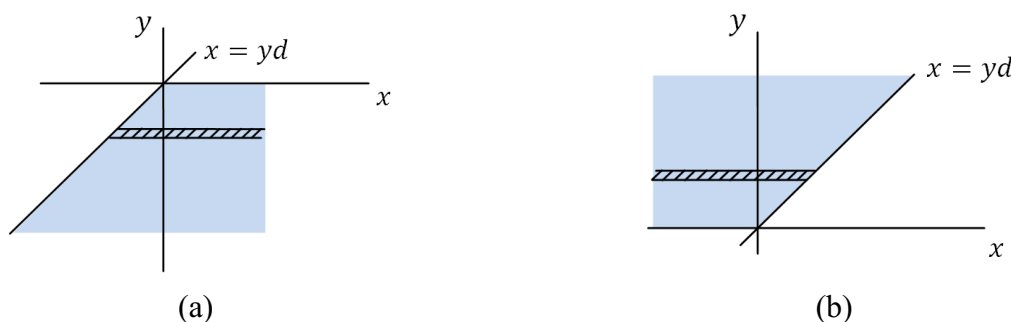


Figure III.1 The areas corresponding to the Eq. (III.2): (a) area corresponding to the first right term; (b) area corresponding to the second right term

$$F_D(d) = \int_{-\infty}^0 \left[ \int_{yd}^{\infty} f_X(x) dx \right] f_Y(y) dy + \int_0^{\infty} \left[ \int_{-\infty}^{yd} f_X(x) dx \right] f_Y(y) dy \quad (\text{III.3})$$

The PDF of  $D$  can be obtained by differentiating  $F_D(d)$

$$f_D(d) = \frac{d}{dd} F_D(d)$$

$$f_D(d) = \int_{-\infty}^0 [-yf_X(yd)]f_Y(y)dy + \int_0^{\infty} [yf_X(yd)]f_Y(y)dy = \int_{-\infty}^{\infty} |y|f_X(yd)f_Y(y)dy \quad (\text{III.3})$$

In this study  $X$  and  $Y$  are non-negative random variables, then the area of integration is reduced to that shown in Figure III.2. This gives:

$$f_D(d) = \int_0^{\infty} [yf_X(yd)]f_Y(y)dy \quad (\text{III.3})$$

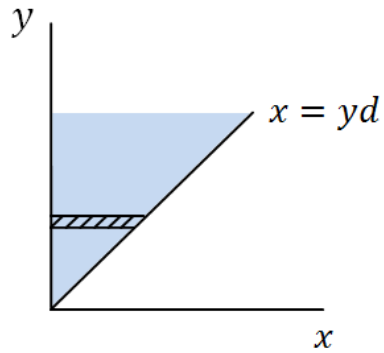


Figure III.2 The areas corresponding to the Eq. (III.3)